



Centre for Sensors, Instruments and
Systems Development
UNIVERSITAT POLITECNICA DE CATALUNYA
Shaping light to your needs

DOCTORAL THESIS

FOR OBTAINING THE DOCTORAL DEGREE
IN THE FIELD OF OPTICAL ENGINEERING FROM THE
TECHNICAL UNIVERSITY OF CATALONIA
UPC-BARCELONATECH
TERRASSA FACULTY OF OPTICS AND OPTOMETRY FOOT

OPTICAL AND VISUAL CHARACTERIZATION OF MULTIFOCAL CONTACT LENSES AND MULTIFOCAL INTRAOCULAR LENSES

Author:

Anna GINER TORT

Thesis Directors:

Dr. Jaume PUJOL RAMO
Dr. Montserrat ARJONA CARBONELL

Tribunal members:

Dr. Josep ARASA
Dr. Josep GÜELL
Dr. José FERNÁNDEZ DORADO

Presented in Terrassa, 2018

SUPERVISOR'S CERTIFICATE

Dr. **Jaume Pujol Ramo**, profesor at the Universitat Politècnica de Catalunya (UPC), and Dr. **Montserrat Arjona Carbonell**, professor at the Universitat Politècnica de Catalunya (UPC)

CERTIFY

that the work reported in the thesis entitled

Optical and viual characterization of multifocal contact lenses and multifocal intraocular lenses

which is submitted by Anna Giner Tort in fulfillment of the requirements for the degree of Doctor by the Universitat Politècnica de Catalunya (UPC) has been carried out under our supervision within the framework of the PhD program in Optical Engineering of the same university.

Jaume Pujol Ramo

Montserrat Arjona Carbonell

Terrassa, 2018

Terrassa, 2018

Acknowledgements

I suppose that every PhD student that has arrived at this point feels the same that I am feeling right now. My hands are trembling and my brain is trying to remember each person that deserves to appear in this modest and sincere acknowledgements. I don't know if my words will be enough to express how thankful I am, but let me try using their own languages.

Primer de tot, gràcies al Jaume i a la Montserrat per confiar en mi per portar a terme aquesta tesi i per fer-me arribar a aquest meravellós punt.

I also want to say thank you to Prof. Atchison to bring the opportunity to work in his group and meet amazing people as Dr. Suheimat. You and Australia changed me for good and I will never forget it.

Dono infinites gràcies a les dues persones que van fer possible que jo formés part d'aquest món, als meus pares, Roge i Eli. Papa, em sap molt de greu que no hagi pogut arribar a llegir aquestes paraules, però, sé que ens vas deixar estant tranquil de saber que sóc conscient de que no he pogut tenir millors mestres de la vida que tu i la mama i de que, encara que no hi siguis present en cos, sempre m'acompanyes en esperit i pensament. Mama, només dir-te que no et puc demanar res més, que no canviïs mai i que em segueixis recordant que la vida s'ha de gaudir i sempre caminar endavant.

A tu, Laia, per ser el meu referent, per ensenyar-me el que vol dir sacrificar-se i lluitar per aconseguir el que un vol, per posar-me la capa protectora de germana gran, per fer-me viure el primer concert, la primera discoteca, i per infinitat de coses més, gràcies. Gràcies també al Kinin, per cuidar-la i fer-la somriure com mai.

Per descomptat, gràcies a la meva parella, Raúl, per ser aquella llum perenne que em dona escalfor i m'il·lumina la vida, fins hi tot, quan al voltant només hi ha foscor. Sense tu, clarament, no hagués arribat mai a acabar aquesta etapa.

Vull fer també un especial agraïment, a dos angelets de la guarda de la meva tesi que m'han ensenyat el camí quan jo creia que ja no en quedava. Mikel, Pepe, no hay palabras...

Tampoc em puc oblidar de donar les gràcies a tota la meva família (Maria, Ramón, Juan, Remedios, Isabel, Angela, Josefa, Diego, Antonia, Arsenio, Juan, Julio, Nico, Lidia, Pere, Marga, Juanjo, Nadia, David, Noemi, Cris, Àngel, Héctor, Xavi, Marc, Genís, Anna,

Adrián, Alejandro, Irene, i, també, Montse, Emilio, Anaïs) per ser com sou i ensenyar-me que som un equip imparable.

Gràcies també a sa meva família menorquina (Pilar, Pili, Juanma, Nacho i Ariadna) per cuidar-me, col·locar-me i fer-me sentir una més des del primer moment que vaig trepitjar Menorca.

I ara, li toca el torn a aquelles persones que no són família oficialment, però que per un, és la família escollida. Tots els que em coneixeu, sabeu de bon tros que no puc despersonalitzar una cosa tant important com els agraïments de la meva tesi doctoral, així que aquí van:

- Marina, Laura, Irene, Julis y Mireia: Gracias por hacerme sentir lo que significa la palabra amistad y por no dejar que ni el tiempo ni la distancia nos haga dejar de sentirla.
- Patri, Iván, Cisco y Dani: que lo que la óptica unió, lo siga uniendo la aventura de la vida. Con vosotros, todo se ve más nítido...
- Esther, Cristina, Alfonso, Selena, Lorena, Alberto, Francisco y las pequeñas Marina y Vega: creo que desde que empezó mi tesis, os he dicho que este GRACIAS va para vosotros, y sé que, no hace falta que diga nada más...
- Mis gimnastas (Tamara, Carla, Sara y Jessi): Pip! El montaje empezó y nunca más acabó! Gracias por estar siempre ahí!
- Rosa, Cristina Cusidó , Júlia , Xavi, Fernando, Ferran, Sergio, Meritxell, Jaume Castellà, Fermín, Jordi, Maite, Reza, Jorge, i tota la resta de persones que fan que tingui un molt bon record del CD6.
- Javi, Mateu, Cris, Joan, Lara J., Guiem, Marina, Lara, Sandra, Cris F., David, Maria F., Alberto, Deivid, Maria M., Ana, Maria C., Débora i Antonio: gràcies per obrir-me les portes, per les nits de jocs, per les acampades, per les hores de pàdel i per tots els somriures que m'heu creat!

Per últim, simplement afegir un gràcies a cada una de les persones que s'han creuat, en algun moment, a la meva vida i m'ha fet aprendre alguna cosa nova, que ha fet que avui sigui la persona que sóc!

Contents

| | |
|---|------------|
| Table of contents | III |
| List of figures | VI |
| List of tables | VII |
| 1 Introduction and aims | 1 |
| 2 State of Art | 5 |
| 2.1 Multifocal Correction Systems for Presbyopia | 5 |
| 2.1.1 Alternating Vision Multifocal Systems | 5 |
| 2.1.1.1 Bifocal and Trifocal Lenses | 5 |
| 2.1.1.2 Progressive Lenses | 5 |
| 2.1.1.3 GP Alternating Bifocal Contact Lenses | 6 |
| 2.1.2 Simultaneous Vision Multifocal Systems | 7 |
| 2.1.2.1 Multifocal Intraocular Lenses | 7 |
| 2.1.2.2 Simultaneous Vision Multifocal Contact Lenses | 11 |
| 2.2 Characterization of Simultaneous Multifocal Vision Systems | 12 |
| 2.2.1 Assessment of visual quality | 12 |
| 2.2.1.1 Evaluation of the visual quality after an implantation of a MIOL or an adaptation of a MCL | 12 |
| 2.2.1.2 Evaluation of the visual quality before an implantation of a MIOL | 15 |
| 2.2.2 Assessment of optical quality | 19 |
| 2.2.2.1 Simple-pass systems | 20 |
| 2.2.2.2 Double-pass systems | 23 |
| 2.2.2.3 Aberrometers | 26 |
| 3 Suitability to perform objective measurements in users of multifocal contact lenses (MCLs) | 29 |
| 3.1 Methods | 29 |
| 3.1.1 Subjects | 29 |
| 3.1.2 Multifocal contact lenses | 30 |
| 3.1.3 Autorefractor | 30 |
| 3.1.4 Measurement protocol | 30 |
| 3.1.5 Data analysis | 31 |
| 3.2 Results | 31 |
| 3.3 Conclusions | 34 |
| 4 Visual quality performance of multifocal intraocular lenses (MIOLs) before surgical implantation | 37 |
| 4.1 Preliminary clinical study to assess visual quality of MIOLs before its surgical implantation | 38 |
| 4.1.1 Methods | 38 |
| 4.1.1.1 Patients | 38 |
| 4.1.1.2 Multifocal Intraocular Lens (MIOL) | 38 |
| 4.1.1.3 Measurement protocol | 39 |

CONTENTS

| | | |
|----------|---|------------|
| 4.1.2 | Results | 39 |
| 4.1.3 | Conclusions | 40 |
| 4.2 | Visual quality performance of different MIOs by means of a simulated implantation | 41 |
| 4.2.1 | Intraocular lenses | 41 |
| 4.2.2 | Measurement protocol | 41 |
| 4.2.3 | Results | 41 |
| 4.2.4 | Conclusions | 44 |
| 4.3 | Visual performance comparison between new prototype of a multifocal intraocular lens and a commercial one. | 44 |
| 4.3.1 | Intraocular lenses | 45 |
| 4.3.2 | Patients | 45 |
| 4.3.3 | Measurement protocol | 45 |
| 4.3.4 | Results | 45 |
| 4.3.5 | Conclusions | 46 |
| 5 | Open-field double-pass system with asymmetric focus (DPAF) | 47 |
| 5.1 | Opto-mechanical design and assembled prototype | 47 |
| 5.2 | Control and analysis software | 49 |
| 5.2.1 | Control interface | 49 |
| 5.2.2 | Analysis interface | 51 |
| 5.3 | System's validation | 53 |
| 5.3.1 | Characterization of electro-optical lenses (EOLs) | 53 |
| 5.3.2 | Validation of the laser power | 54 |
| 5.3.3 | Optical validation of the DPAF | 55 |
| 5.3.4 | Validation of the through-focus measurements | 55 |
| 5.3.4.1 | Methods | 56 |
| 5.3.4.2 | Results | 57 |
| 5.3.4.3 | Conclusions | 58 |
| 6 | Objective evaluation of the optical quality of patients implanted with multifocal intraocular lenses by means of DPAF: Preliminary study | 61 |
| 6.1 | Assessment of the optical quality of patients implanted with a multifocal intraocular lens | 61 |
| 6.1.1 | Patients | 61 |
| 6.1.2 | Multifocal Intraocular Lens | 61 |
| 6.1.3 | Measurement protocol | 61 |
| 6.1.4 | Results | 62 |
| 6.1.5 | Conclusions | 66 |
| 7 | Conclusions and future work | 67 |
| A | Appendix 1: Design of the Double-Pass System with Asymmetric Focus (DPAF) | 69 |
| A.1 | First Pass | 69 |
| A.2 | Second Pass | 71 |
| A.3 | Complete system | 72 |
| A | Appendix 2: Data sheets | 75 |
| A | Appendix 3: Interferometry Project Report | 101 |
| A.1 | Introduction | 101 |
| A.2 | Methods | 102 |
| A.2.1 | Experimental Set-Up: Configuration 1 | 102 |
| A.2.2 | Experimental Set-Up: Configuration 2 | 103 |
| A.2.3 | Experimental Set-Up: Configuration 3 | 103 |
| A.2.4 | Modified Lotmar Interferometer | 105 |
| A.2.4.1 | Participants and Measurement Conditions | 106 |
| A.3 | Results | 107 |

CONTENTS

| | |
|--------------------------|------------|
| A.4 Discussion | 107 |
| Bibliography | 109 |

List of Figures

| | | |
|--------|---|----|
| 1.0.1 | Visual path and its components (Source: [2]). | 1 |
| 1.0.2 | Accommodated and no-accommodated crystalline lens (Source: [5]) | 1 |
| 1.0.3 | Comparison of an eye without and with cataract (Source: [11]) | 2 |
| 2.1.1 | Schemes of a bifocal (a) and a trifocal (b) lenses (Source: [22]). | 5 |
| 2.1.2 | Image of a commercial progressive lens (a) (Source: [25]) and the different vision zones that this kind of lenses have (b) (Source: [26]). | 6 |
| 2.1.3 | Design of Menicon Z Executive GP Lens (Menicon S.L.) (a) (Source: [28]), and an image of the adaptation of BIAS-BICON lens (Conoptica) (b) (Source: [29]). | 6 |
| 2.1.4 | Simulation of the differences that a monofocal correction and a simultaneous vision multifocal correction provide to the users (Source: [31]). | 7 |
| 2.1.5 | Tecnis ZM 900 Scheme (Source: [33]). | 8 |
| 2.1.6 | Comparison of the foci that a monofocal IOL, a MIOL and the new generation Tecnis®Symfony create (Source: [37]). | 8 |
| 2.1.7 | Examples of one rotational symmetric refractive MIOL (a) (Source: [39]) and one of a non-symmetric refractive MIOL (b) (Source: [40]). | 9 |
| 2.1.8 | Optical design of the Precizon Presbyopic MIOL (Source: [41]). | 9 |
| 2.1.9 | ReStor SA60D3 (Alcon Laboratories) (Source: [42]). | 10 |
| 2.1.10 | ACUVUE®OASYS®for Presbyopia Design (Source: [47]) | 11 |
| 2.1.11 | Air Optix®AQUA Multifocal (Alcon®Vision Care) design (Source: [48]) | 12 |
| 2.2.1 | Examples of standardized VA charts (Sources: [50, 51]). | 13 |
| 2.2.2 | Example of two different tests to measure CS (Sources: [55, 56]). | 14 |
| 2.2.3 | Images of stereoacuity tests and its complements to perform them (Sources: [59, 60, 61, 62]). | 15 |
| 2.2.4 | Schematic diagram of the simultaneous vision system. (Source: [16]) | 16 |
| 2.2.5 | Schematic diagram of the upgraded simultaneous vision system. (Source: [67]) | 16 |
| 2.2.6 | Scheme of the optical design of AOVS where PPM is a liquid crystal programmable phase modulator and HS is a Hartmann-Shack wavefront corrector. First image (a) represents the optical path of an objective measurement. In contrast, image (b) shows the subjective measurement path.(Source: [17]). | 17 |
| 2.2.7 | Image of the current version of VAO (Source: [73]) | 18 |
| 2.2.8 | Schematic diagram of the VioBioLab AO II system with the different channels in its final configuration (Source: [18]). | 18 |
| 2.2.9 | Image of the instrument (Source: [77]). | 19 |
| 2.2.10 | Results of the two methods of measurement of the diffractive Tecnis ZM900 MIOL (Source: [84]). | 21 |
| 2.2.11 | Design of the optical bench set-up (Source: [87]). | 21 |
| 2.2.12 | OPAL Vector System Scheme (Source: [89]). | 22 |
| 2.2.13 | Images of OptiSpheric®IOL (TRIOPTICS, GmbH., Germany) (Source: [92]). | 22 |
| 2.2.14 | Scheme of a basic double-pass system (Source: [100]). | 23 |
| 2.2.15 | DP commercial instrument (Source: [81, 102]). | 25 |
| 2.2.16 | MTF cut-off results along the through-focus with a diffractive MIOL (Restor (black filled points)) and a monofocal IOL (IQ(red empty points)) (Asterisks indicates statistic significant differences between MIOLs)(Source: [21]). | 26 |
| 2.2.17 | Simulation of the principles of HS technique (Source: [110]). | 26 |
| 2.2.18 | Examples of one experimental (a) and one commercialized HS aberrometer (b) | |

LIST OF FIGURES

| | | |
|--------|--|----|
| | (Source: [111, 113]). | 27 |
| 2.2.19 | Scanning over pupil aperture. Example of a set of entrance points (Source: [117]). | 28 |
| 3.2.1 | Correlation plot of the SE results between objective and subjective over-refraction with MCL (a); Bland and Altman plot of the SE with the mean difference and the confidence limits (CL) comparing the objective and the subjective over-refraction (b). | 33 |
| 3.2.2 | Correlation plot of J_0 and J_{45} results between objective and subjective over-refraction with MCL (a); Bland and Altman plot of J_0 and J_{45} with the mean difference and the confidence limits (CL) comparing the objective and subjective over-refractions (b). | 34 |
| 4.0.1 | Optical design of VirtIOL and its elements: vision test (1); mirror (2); artificial eye (3); MIOL submerged in saline solution (4); lens (5); mirrors (6 and 7); aperture of the pupil (8); lenses (9 and 10); cold mirror (11); IR LED (12); mirror (13); pupil's camera (14); pupil's display (15); patient's eye (16). | 37 |
| 4.0.2 | Image of VirtIOL while the patient is observing a vision test through the inserted MIOL. | 38 |
| 4.1.1 | Visual acuity differences between first and second session for the BDCVA (Best Distance Corrected Visual Acuity) and BDCNVA (Best Distance Corrected Near Visual Acuity). | 39 |
| 4.1.2 | Mean contrast sensitivity differences curve between first and second session for BDCVA (Best Distance Corrected Visual Acuity). | 40 |
| 4.2.1 | Visual acuity results for the through-focus for all lenses with natural pupils in high luminance conditions and 100% of contrast. | 42 |
| 4.2.2 | Mean absolute difference of VA [$\log\text{MAR}$] between central position and decentered positions from the optical axis [mm] of each MIOL. | 43 |
| 4.2.3 | Visual Acuity [$\log\text{MAR}$] at far and near vision of the MPlus (MP) and the NDIOL-CF (ND) MIOLs for each angle to study the rotational effect. | 43 |
| 4.3.1 | Mean defocus curves, representing the visual acuity (VA) in decimal units [decimal] against the accommodative stimulation in diopters [D]. | 46 |
| 5.1.1 | Optical System Design composed for laser, EP (entrance pupil), EOL1 (electro-optical lens 1), M1 (mirror 1), BS (beam splitter), L1 (lens 1), HM (hot mirror), DC (dichroic filter), Pupil's Camera, EOL2 (electro-optical lens 2), M2 (mirror 2), Afocal System (L2 (lens 2) and L3 (lens 3)), M3 (mirror 3), ExP (exit pupil), Camera Lens and DP Camera (double-pass camera). | 48 |
| 5.1.2 | Image of the DPAF prototype assembled in our laboratory. | 49 |
| 5.2.1 | Image of the graphical interface of the control part. | 50 |
| 5.2.2 | Image of the graphical interface of the analysis part. | 52 |
| 5.2.3 | Image of the centered drop-down menu to choose the image or curve that can be shown in the graphical areas. | 52 |
| 5.3.1 | Characterization of the focal length of both EOLs based on the level of current. | 53 |
| 5.3.2 | Power correction range based on the current level of each EOL. | 54 |
| 5.3.3 | Graphic representation of the MTF of the system (solid line) and the MTF limited by diffraction (dashed line) that were used to do the optical validation. | 55 |
| 5.3.4 | Double-pass images of a non-concentric refractive MIOL (Power = +20.00D / Addition = +2.75D). The power indicated in the images is the value of the accommodative stimuli per each one. | 57 |
| 5.3.5 | Double-pass images of the concentric diffractive MIOL (AcrySof®IQ ReSTOR®SN6AD1) (Power = +21.00D / Addition = +3.00D). The power indicated in the images is the value of the accommodative stimuli per each one. | 57 |
| 5.3.6 | (a) MTF cut-off values of the diffractive and the refractive MIOL along the through-focus; (b) Strehl ratio values of the diffractive and the refractive MIOL along the through-focus. | 58 |
| 6.1.1 | DP images of a through-focus from $-4D$ to $+1.5D$ in steps of $0.50D$ | 62 |

LIST OF FIGURES

| | | |
|-------|---|-----|
| 6.1.2 | MTFs of each step of the mean through-focus from $-4D$ to $+1.5D$ in steps of $0.50D$. The black curve is the MTF only limited by diffraction (DIF). | 63 |
| 6.1.3 | SR values for each patient on the left and mean SR values including SD on the right. | 64 |
| 6.1.4 | Cut-Off frequency values for each patient on the left and mean Cut-Off values including SD on the right. | 64 |
| 6.1.5 | LogMAR VA values for each patient on the left and mean logMAR VA values including SD on the right. | 65 |
| 6.1.6 | Normalized mean values for SR, Cut-Off and $1/VA$ are included. SR values are in pink, Cut-Off in green and $1/VA$ in blue. | 65 |
| | | |
| A.1.1 | Caption of the shaded model lay-out of the non-sequential mode: (1) laser, (2) collimator, (3) EOL 1, (4) M1, (5) BS, (6) VL, (7) HM, (8) DC and (9) Eye. | 69 |
| A.1.2 | Representation of the MTF of the simulated system and the one only limited by diffraction on the left (a). Simulation of the retinal image on the right (b) | 70 |
| A.2.1 | Caption of the shaded model lay-out of the non-sequential mode: (1) eye, (2) DC, (3) HM (4) VL, (5) BS, (6) EOL 2, (7) M2, (8) Afocal System, (9) M3 and (10) Lens od the DP camera. | 71 |
| A.2.2 | Representation of the MTF of the simulated system and the one only limited by diffraction on the left (a). PSF curve in 3 dimensions on the right (b) | 72 |
| A.3.1 | Caption of the shaded model lay-out of the non-sequential mode of the whole system: (1) laser, (2) collimator, (3) EOL 1, (4) M1, (5) BS, (6) VL, (7) HM, (8) DC, (9) Eye, (10) EOL 2, (11) M2, (12) Afocal System, (13) M3 and (14) Lens od the DP camera. | 73 |
| | | |
| A.1.1 | A drawing of a section through the human eye with a schematic enlargement of the retina (Source: [146]). | 101 |
| A.2.1 | Configuration 1; Laser (1), Circular Apertures (2), Dove Prism (3), FBS (5), Achromatic Doublet (6), Eye (7), Camera Lens (8) and Camera (9). | 102 |
| A.2.2 | Circular apertures. | 103 |
| A.2.3 | Configuration 2; Laser (1), Circular Apertures (2), Dove Prism (3), Divergent lens (4), Cube beamsplitter (5), Achromatic Doublet (6), Eye (7), Camera Lens (8) and Camera (9). | 104 |
| A.2.4 | First part of configuration 3; Beam expander (1), flat beamsplitter (2), mirror 1 (3), mirror 2 (4) and mirror 3 (5). | 104 |
| A.2.5 | Image of the new illumination system composed by the optical fiber of the laser and the achromatic doublet. | 105 |
| A.2.6 | Modified Lotmar interferometer; Illumination system (1), cube beamsplitter (2), camera lens (telecentric) + camera (3), beam trap (4). | 106 |
| A.3.1 | Retinal plane image of configuration 1. | 107 |
| A.3.2 | Retinal plane image of configuration 3. | 107 |
| A.3.3 | Images of the retina plane of the model eye (<i>Exposuretime</i> = 240ms; <i>LaserPower</i> = 8.03mW) | 108 |
| A.3.4 | Images of the retina plane of the no-dilated right eye of the 31 years old participant (<i>Exposuretime</i> = 570ms; <i>LaserPower</i> = 8.03mW) [Images had been modified in Photoshop]. | 108 |
| A.3.5 | Images of the retina plane of the dilated right eye of the 22 years old participant (<i>Exposuretime</i> = 130ms (a) and 230ms (b); <i>LaserPower</i> = 8.03mW) [Images had been modified in Photoshop]. | 108 |

List of Tables

| | | |
|-------|---|----|
| 3.2.1 | Mean subjective and objective refractive errors with and without MCL in terms of SE , J_0 and J_{45} . The mean difference \pm SD (D) and range (D) are shown. (Values are in dioptries (D)). | 32 |
| 3.2.2 | Comparison between objective and subjective refraction with and without MCL. The mean difference \pm SD (D), Pearson's correlation coefficients and their significance and the paired sample t test significance are shown. | 32 |
| 4.2.1 | Far Visual Acuity (FVA) and Near Visual Acuity (NVA) in LogMAR units for each contrast level (100%, 25% and 10%) in high luminance conditions. | 42 |

1. Introduction and aims

Vision is presented and universally accepted as the most precious of the human senses. It is also considered one of the most complex, given that it is the result of different processes linked by each other (Figure 1.0.1). Vision is structured in three main parts: the optical system (eye), the photo-sensor (eye's retina), and the data processor (brain) [1]. If one of them is affected by any disease or dysfunction, vision will be terrible or even nonexistent.



Figure 1.0.1: Visual path and its components (Source: [2]).

One of the most common dysfunction is presbyopia. It is an age-related disorder that is undergone by all the population since their mid-late-40s. It consists in the loss of the ability to focus near objects [3]. This capacity of the eye is performed by the deformation of the crystalline lens (Figure 1.0.2) and it is called accommodation [4]. Actually, accommodation is being reduced throughout life until it is completely lost. But, this loss is only named presbyopia when the near objects can not be focused.

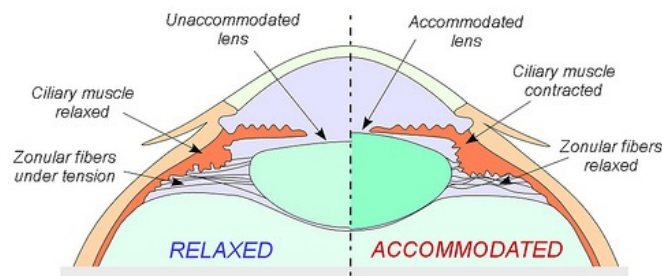


Figure 1.0.2: Accommodated and no-accommodated crystalline lens (Source: [5])

Regarding the fact that all the population is affected by presbyopia, a huge number of possible corrections of it can be easily found. On one hand, there are temporary corrections, as progressive spectacle lenses [6] or multifocal contact lenses [7]. On the other hand, permanent corrections as multifocal intraocular lenses, multifocal corneal ablation, accommodating intraocular lenses,

monovision systems, or scleral modifications are also applied to correct presbyopia [8].

Another age-related dysfunction is cataract. Cataract is the opacification of the crystalline lens and decreases the quality of the visual function (Figure 1.0.3). Consequently, it is one of the leading visual impairments in adults over 60 years old, affecting the half of the adults aged between 75-85 years old [9]. The only possible solution for cataract is the extraction of the opacified fibers of the crystalline lens and the replacement of them with an intraocular lens by surgery. If this surgery is not done the cataract causes blindness by a complete opacification of the crystalline lens. Currently, the WHO (World Health Organization) still considers cataract as the first cause of permanent visual impairments in all areas of the world, except for developed countries where cataract surgeries are performed everyday [10].

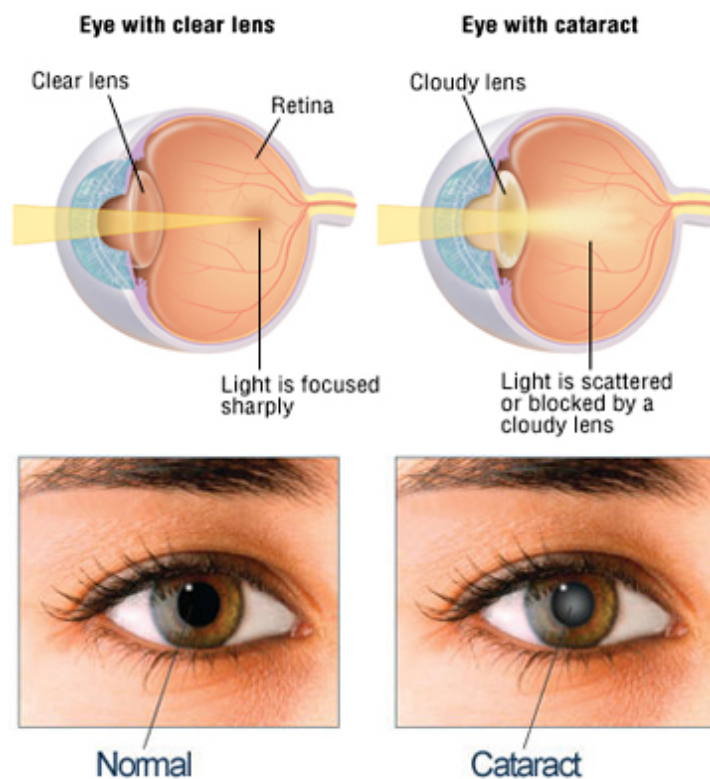


Figure 1.0.3: Comparison of an eye without and with cataract (Source: [11])

Due to the fact that all the patients affected by an age-related cataract are also affected by presbyopia, it is totally understandable that the most chosen permanent presbyopia correction to replace the opacified fibers of the crystalline lens is the multifocal intraocular lens. This way, only one surgery is needed to solve both age-related dysfunctions.

Usually, young presbyopes choose a temporary correction as a first option to correct presbyopia. Although, a part of them select one of the permanent corrections, once they are affected also by cataract.

Some presbyopia corrections are based on the simultaneous vision principle, as, for example, multifocal contact or intraocular lenses. This means that there is a superposition of one focused image with defocused images on the retina [12]. The optical design of these kind of lenses is very complex. Consequently, its characterization is also difficult.

When these lenses were launched into the market, it was only possible to characterize optical quality before the implantation or the adaptation of them (characterization *in vitro*) [13] and the visual quality after the surgery or the clinical adaptation was performed (characterization *in vivo*) [14, 15]. At present and thanks to the technological advances, different new commercial instruments that are able to perform characterization *in vivo* of the visual quality before the implantation or the adaptation of simultaneous vision lenses. They are based on the simulation of the vision that these lenses give to the implanted eye. Visual quality that the patient would have if he were implanted with one of them can be evaluated by using these instruments [16, 17, 18, 19]. Some experimental prototypes and commercial aberrometers or double-pass systems have used to perform an optical quality characterization *in vivo*, but some issues have been reported [20, 21].

Taking into account all this information, the main goal of this thesis is the design and the assembly of a new open-field double-pass system with asymmetric focus that is suitable to characterize *in vivo* optical quality in patients implanted or adapted with multifocal intraocular or contact lenses. In order to be able to achieve this goal, the following stages were performed along this project:

1. **Review of presbyopia corrections and the characterization of them.** An analysis of the literature about this issue was performed. A first study to prove the suitability of an auto-refractometer to perform a over-refraction with multifocal contact lenses wearers was accomplished.
2. **Verification of the suitability of one commercial simulator.** A study with the commercial simulator VirtIOL (10Lens S.L.) was achieved to prove the suitability of this instrument to perform a visual characterization *in vivo* before surgical implantation of a multifocal intraocular lens.
3. **Design of the double-pass system with asymmetric focus.** A first idea of the optical design was introduced in an optical simulator. Then, the simulation was analyzed and adjusted with the selected commercial elements until the result was the expected.
4. **Assembly of the double-pass system with asymmetric focus.** After getting all the selected optical elements, a customized mechanical supports were created to assemble the new open-field double-pass system with asymmetric focus.
5. **Programming of the softwares.** Two softwares were programmed for this new prototype. The first one controls all the hardware of the system to obtain the double-pass images that are needed. The second one processes the images and calculates all the parameters that indicate the optical quality of the measured eye.
6. **Validation of the new prototype.** In order to prove the suitability of the system to perform an analysis of the optical quality of the eye implanted with a multifocal intraocular lens, two different studies were performed:
 - (a) **Optical characterization *in vitro* with a model eye.** Two different multifocal intraocular lenses were introduced in the customized model eye.
 - (b) **Optical characterization with eyes implanted with multifocal intraocular lenses.** The new prototype analyzed eight left eyes implanted with a multifocal intraocular lens.

This manuscript is structured in eight chapters including this one. Chapter 2 presents the state of art of the different topics that are included in this thesis: corrections for presbyopia and the characterization of them.

Chapter 3 describes the published study that was done to assess the use of an auto-refractometer to perform an over-refraction in patients adapted with a multifocal contact lens.

Chapter 4 shows two different studies that evaluated the function of the commercial simulator named VirtIOL (10Lens S.L.). It was concluded that VirtIOL can be a useful tool to decide which lens is the better option per each patient before the surgery.

Chapter 5 presents the new open-field double-pass system with asymmetric focus. This one is the main chapter of this thesis. It is divided in three distinguished parts: design of the opto-mechanical system, assembly and programming of the software, and validation of the whole system.

Chapter 6 includes the results of a clinical study where patients implanted with MIOLs were objectively measured by means of the new double-pass system with asymmetric focus.

Chapter 7 includes the conclusions of this work.

Finally, references and appendices are presented. Appendix 1 shows a little summary of the design process of the new open-field double-pass system. Appendix 2 has all the data sheets of the main elements used in the double-pass system. To finish, Appendix 3 includes the work carried out in the Queensland University of Technology supervised by Prof. Atchison.

2. State of Art

The description of all the different existing multifocal correction systems for presbyopia and methods to evaluate them are included in this chapter.

2.1 Multifocal Correction Systems for Presbyopia

There are many ways to classify the different multifocal correction systems for presbyopia that are used currently by presbyopes. One of these ways is which is presented here and that classify the correction systems in two groups: alternating vision multifocal systems and simultaneous vision multifocal systems.

2.1.1 Alternating Vision Multifocal Systems

Multifocal corrections are classified as an alternating vision system when it is only arriving light from one focal zone of the system on retina's plane. Due to this, these systems are based on the natural eyes' movements to change focus from distance objects to the nearest ones. The main examples of this group are bifocal, trifocal and progressive spectacle lenses, and gas-permeable (GP) alternating bifocal contact lenses.

2.1.1.1 Bifocal and Trifocal Lenses

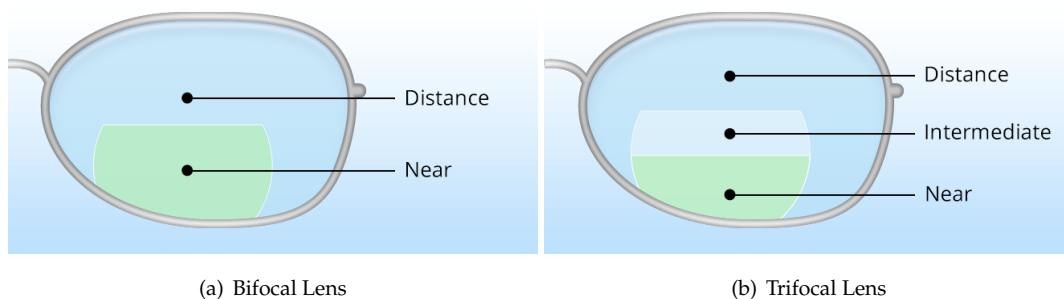


Figure 2.1.1: Schemes of a bifocal (a) and a trifocal (b) lenses (Source: [22]).

Bifocal and trifocal lenses offer two and three zones, respectively, of fixed-focus vision separated by a visible discontinuity [23]. In this case the change of one focused vision to another is abrupt. As a consequence, the user's vision jumps from distance or intermediate vision to near vision, and vice versa (Figure 2.1.1).

2.1.1.2 Progressive Lenses

Owen Aves patented the first progressive addition lens in 1907 [24]. The main advantage of these lenses is the fact that have a soft transition between the different vision distances that the user

needs in each situation. This means that they have a gradual increase of power following the sight path followed by eyes to change their focus from a distance vision to intermediate and to near vision [6]. Another advantage of these lenses is the non-visible focus change due to the smooth transition among focus (Figure 2.1.2 (a)).

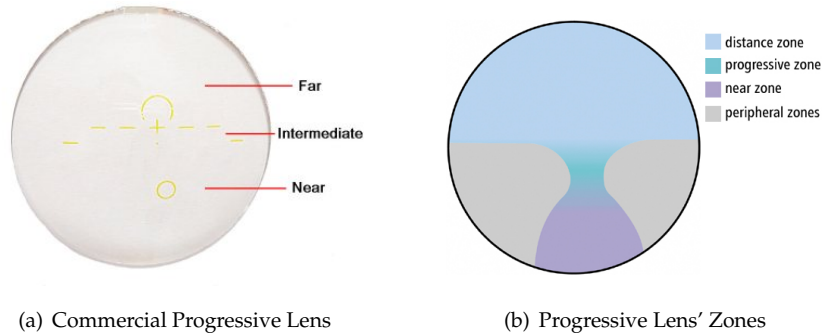


Figure 2.1.2: Image of a commercial progressive lens (a) (Source: [25]) and the different vision zones that this kind of lenses have (b) (Source: [26]).

Lots of improvements are been added to progressive lenses, since the company Essel created the first commercialized progressive lens in 1959. All the improvements have been focused on the reduction of the intrinsic lateral aberrations that the increase of the power has (Figure 2.1.2 (b)).

Nowadays, the most innovative progressive lens is based on the Free-Form technology. This technology creates a customized progressive lenses per each user, in order to adapt their visual needs as best as possible. These lenses exist thanks to the technological advances that are been introduced in the manufacturing processes in the last 10 years [27].

2.1.1.3 GP Alternating Bifocal Contact Lenses

One of the main characteristics of the GP contact lenses is the several millimeters that they are able to move on the cornea. Due to this fact, is it possible to have an alternating vision contact lens. The designs are based on a segmented bifocal lens with a truncation at the bottom of the lens (Figure 2.1.3). Consequently, when the lens is rested in the inferior eyelid, the lens comes up and the user is viewing through the near vision zone. Nevertheless, Ames et al. demonstrated that the translation movement of these lenses was not enough to have a real alternating vision [30].

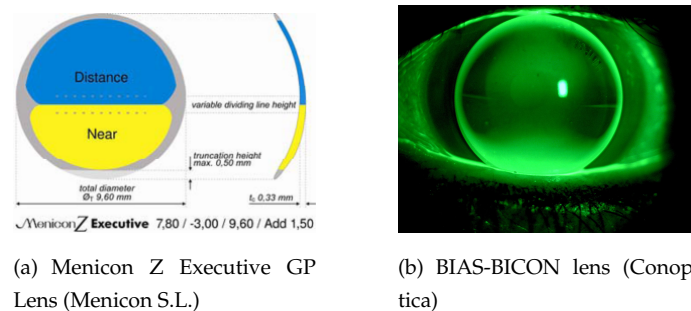


Figure 2.1.3: Design of Menicon Z Executive GP Lens (Menicon S.L.) (a) (Source: [28]), and an image of the adaptation of BIAS-BICON lens (Conoptica) (b) (Source: [29]).

Actually, they have a mixed function between alternating and simultaneous vision (Figure 2.1.3).

Examples of available GP alternating bifocal lenses are: Menicon Z Executive (Menicon Espana S.L.) and all the group of BIAS-BICON family (Conoptica S.L.). BIAS-BICON family is composed by 6 different designs and each design is available in four different materials.

2.1.2 Simultaneous Vision Multifocal Systems



Figure 2.1.4: Simulation of the differences that a monofocal correction and a simultaneous vision multifocal correction provide to the users (Source: [31]).

A system is a simultaneous vision multifocal system when the light is passing through all the different foci of it simultaneously [12]. Thus, a user of this kind of systems is receiving all the focus vision at the same time on the retina. For example, if the user is focusing a distance object receives the image of this object well-focused meanwhile is receiving an out of focus images of the intermediate and near objects that are situated in his field of view (Figure 2.1.4). Multifocal Intraocular Lenses (MIOLs) and Soft Multifocal Contact Lenses (MCLs) are included in this group.

2.1.2.1 Multifocal Intraocular Lenses

MIOLs became popular in the first decade of XXI century. These lenses introduced the possibility of no wear glasses, even after a cataract extraction surgery. This issue would be able to represent a huge increase of the user's convenience, but, due to the complex designs of these lenses, different details can affect the optical and visual quality of them. As a consequence, different improvements have been introduced in their designs.

Taking into account the optics principal that their designs are based on, we can theoretically classify the MIOLs as: diffractive, refractive or hybrid [32].

Diffractive Multifocal Intraocular Lenses

Diffractive lenses are based on the optical principles of diffraction what creates different and independent focal points thanks to constructive interferences [34]. In order to be able to get the different foci, the lens has a large number of concentric rings with little sharp edges (Figure 2.1.5). Each ring diffract the light in a different way creating the different focal points that correspond to the different vision distances that people normally use.

2.1. MULTIFOCAL CORRECTION SYSTEMS FOR PRESBYOPIA

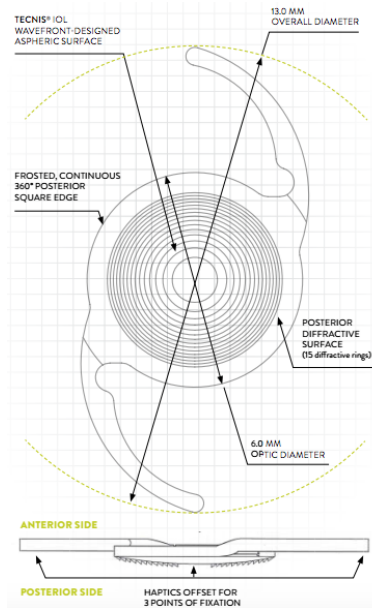


Figure 2.1.5: Tecnis ZM 900 Scheme (Source: [33]).

The advantage of the diffractive MIOLs is that they are not as pupil-dependent as the refractive ones. Although, the distribution of the light energy is asymmetric among the foci. They are also very prone to create halos and glares to the user of them [35].

Examples of available diffractive MIOLs are: Acri.Twin (Acri.Tech/ Carl Zeiss Meditec, Inc), Acriva Reviol (VSY Biotechnology), MS6125 (Dr.Schmidt Intraocular Linsen, GmbH), OptiVis (Aaren®Scientific), FineVision (Physiol s.a.), Tecnis®ZM900 (Abbott Medical Optics) (Figure 2.1.5) [36].

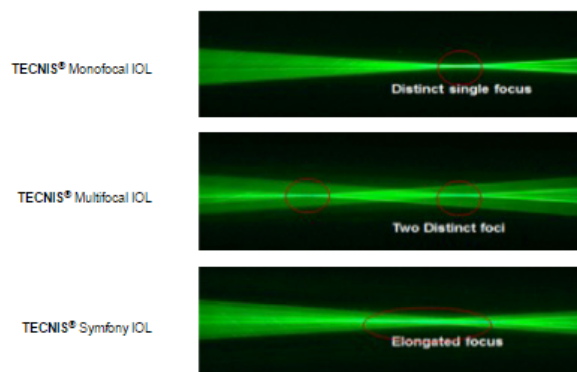


Figure 2.1.6: Comparison of the foci that a monofocal IOL, a MIOL and the new generation Tecnis®Symphony create (Source: [37]).

A new generation of a diffractive lens has recently approved by the U.S.FDA (United States Food and Drug Administration) [38]. It is called Tecnis®Symphony and it has been developed by Abbott Laboratories (USA). This new generation lens is defined as an “Extended Range of Vision IOL” what means that it does not provide two or more different foci, but instead it provides an extended focus (Figure 2.1.6).

The first clinical study performed by Abbott Laboratories, conclude that Tecnis®Symfony provide the implanted patients with a very good distance and intermediate vision (LogMAR VA = 0.0) and a quite good near vision (LogMAR VA = 0.3). The most important advantages of this lens are; that it has a level of glares and halos comparable to a monofocal IOL and the contrast enhancement due to the new achromatic technology correction.

Refractive Multifocal Intraocular Lenses

In this case the lenses have different rotational symmetric or non-symmetric zones with different value of curvature radius. Thus, each zone has a different dioptric power corresponding to the different distance vision for the implanted eye (Figure 2.1.7).

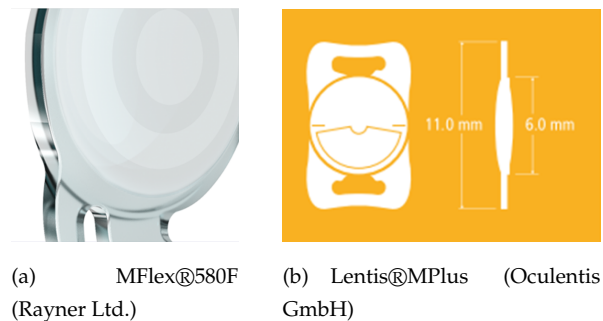


Figure 2.1.7: Examples of one rotational symmetric refractive MIOL (a) (Source: [39]) and one of a non-symmetric refractive MIOL (b) (Source: [40]).

In contrast with the diffractive MIOLs, refractive MIOLs creates less halos and glares but they are more pupil dependent. They are very sensitive to centered errors [35]. Several numbers of this kind of lenses have aspheric surfaces to reduce these problems as much as possible.

Examples of available refractive MIOLs are: Array SA40N (Abbott Medical Optics), Lentis®MPlus (Oculentis GmbH), MFlex®580F (Rayner Ltd.) [36].

In recent weeks, OPHTEC B.V. (Groningen, Netherland) obtained the CE-Mark for its new MIOL Precizon Presbyopic.



Figure 2.1.8: Optical design of the Precizon Presbyopic MIOL (Source: [41]).

This MIOL presents an innovative optical design patented as Continuous Transitional Focus (CTF). This technology offers a full range of vision and, due to the CTF's transitional zones (Figure 2.1.8), a smooth, continuous transition from near to infinity vision is achieved. consequently, CTF ensures a more “forgiving” lens that enables surgeons to treat a wider range of presbyopic patients with a higher degree of confidence [41]. OPHTEC declares that Precizon Presbyopic is able to forgive larger degrees of lens tilt and decentration. It is considered that the misalignmet tolerance reduces photic phenomena and that the CTF optic is less dependent on pupil size under all lighting conditions.

CD6 was involved in the design process and the optical validation of this lens. Details of this collaboration are explained in chapters 4 and 5.

Hybrid Multifocal Intraocular Lenses

Just like their own name indicates, these lenses combine refractive zones with diffractive zones to decrease the problems that an only diffractive or refractive MIOL have (Figure 2.1.9). This complex combinations try to reduce the halos and glares of the diffractive designs and the pupil-dependency of the refractive ones [32]. Nevertheless, it has not been possible to completely remove the different problems.

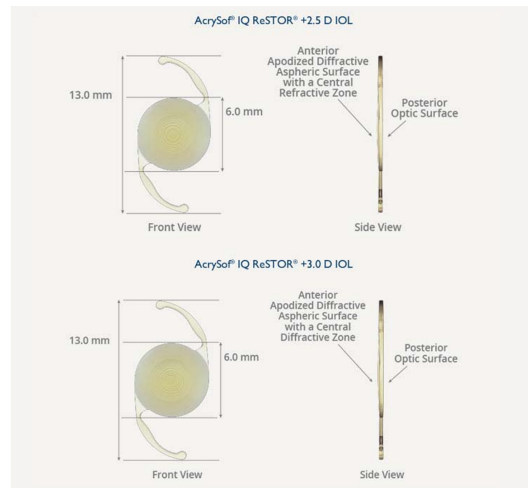


Figure 2.1.9: ReStor SA60D3 (Alcon Laboratories) (Source: [42]).

Examples of available hybrid MIOLs are: AcriLISA 366D (Carl Zeiss Medical, Inc.), ReStor SA60D3 (Alcon Laboratories), ReZoom NXG1 (Abbott Medical Optics) [36].

A review of several clinical studies about hybrid MIOLs was published in 2010 by Madrid-Costa *et al.* [43]. They concluded that hybrid MIOLs provide a satisfactory full range of vision and achieve higher spectacle independence than those patients using other types of prescription. This study also presented AcriLISA 366D and ReStor SA60D3 as the newest hybrid MIOLs and declares that their designs added modifications in asphericity and lower addition powers, which seem to improve visual performance in the inter-mediate distance range.

2.1.2.2 Simultaneous Vision Multifocal Contact Lenses

MCLs' users represent between the 15 and the 20% of the total number of contact lenses users since 2005 [44, 45, 46].

Historically and just as in the case of MIOLs, simultaneous vision MCLs can be divided in diffractive and refractive designs. However, only refractive designs are explained in this thesis, since none diffractive MCL is available at this moment, neither in soft nor GP CLs.

Refractive Multifocal Contact Lenses

The refractive designs have different zones with different radius of curvature. In contrast with refractive MIOLs, all the refractive MCLs are rotational symmetric. These lenses can be divided in two different groups: Concentric and Aspheric.

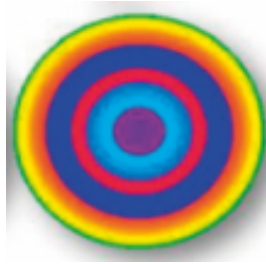


Figure 2.1.10: ACUVUE®OASYS®for Presbyopia Design (Source: [47])

Concentric designs consist on a number of concentric well-separated zones per each distance of vision. Currently, this kind of lenses alternate one distance of vision zone to another one. In previous designs there were no alternation but they have a high dependency of the pupil's diameter [15]. This fact did that the next spherical refractive designs had an alternation between near and distance vision (Figure 2.1.10).

Current examples of concentric designs are ACUVUE®OASYS®for Presbyopia (Johnson and Johnson Vision Care) or Multivue (Lenticon S.A.) as soft MCLs, and Menifocal Z Progressive (Menicon S.L.) or Polyfocal (Lenticon S.A.) as GP MCLs.

The aspheric designs have no alternation, but they have a very smooth transition among vision distances (Figure 2.1.11). This fact creates a progressive increase or decrease of the power, depending on if the central optical zone is for distance or for near vision. The asphericity can be in only one of the surfaces of the lens or in both. The gradient of power progression depends on the eccentricity factor or factors of each lens. The simple designs have only one aspheric curve, but the complex ones have different aspheric curves per each zone of the lens. Aspheric MCLs are the most popular kind in the last years [12].

Aspheric MCLs that can be found in the market are: Air Optix®AQUA Multifocal (Alcon®Vision Care), Biofinity Multifocal (CooperVision) or Saphir Multifocal (Mark'Ennovy) as soft MCLs and Menicon Z Progressive Comfort (Menicon S.L.) or SoCLear MF (Lenticon S.A.) as GP MCLs.

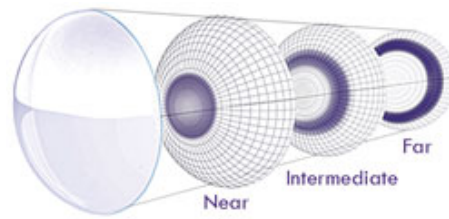


Figure 2.1.11: Air Optix®AQUA Multifocal (Alcon®Vision Care) design (Source: [48])

2.2 Characterization of Simultaneous Multifocal Vision Systems

MCLs and MIOLs have complex optical designs that require a complete and detailed characterization. In order to achieve this, it's necessary to evaluate the optical and the visual quality of them. Optical quality can be evaluated *in vitro* or *in vivo* conditions. In contrast, the visual quality can only be assessed by subjective tests. Consequently, this characterization is only performed *in vivo*, since the results depends on the perception of the subject that is adapted or implanted with MCLs or MIOLs.

Both kind of evaluation are described and detailed in this section.

2.2.1 Assessment of visual quality

As it is said before, visual quality is a subjective evaluation that depends on the perception of the subject adapted or implanted with a MCL or a MIOL. This means that visual quality takes into account the interpretation of the brain of the image that is projected on the retina.

At the beginning, the visual quality could be only evaluate once the adaptation or the implantation was done. This fact is not a problem in the adaptation of a MCL, since is not a permanent correction and if the subject is not satisfied, it is possible to adapt another one that achieves better results. However, it is not recommended to remove an implanted MIOL, since could produce several added difficulties. Due to this situation, different clinical instruments have appeared during the last decade to perform a visual characterization before the implantation. Therefore, this subsection presents the different tests and instruments that are used to evaluate the visual quality before and after the adaptations or implantation of a MCL or a MIOL.

2.2.1.1 Evaluation of the visual quality after an implantation of a MIOL or an adaptation of a MCL

Conventional optometry is based on the characterization of visual quality. In order to do that, there are a huge number of tests that can evaluate, visual acuity (VA), contrast sensitivity (CS), stereoacuity, color vision, etc. However, only VA, CS and stereoacuity are going to be explained in this section since are the most used to evaluate visual quality.

Visual Acuity

Visual acuity (VA) is the ability of the human visual system to distinguish spatial details in a test with the maximum contrast and a high level of illumination [49]. VA is typically measured with

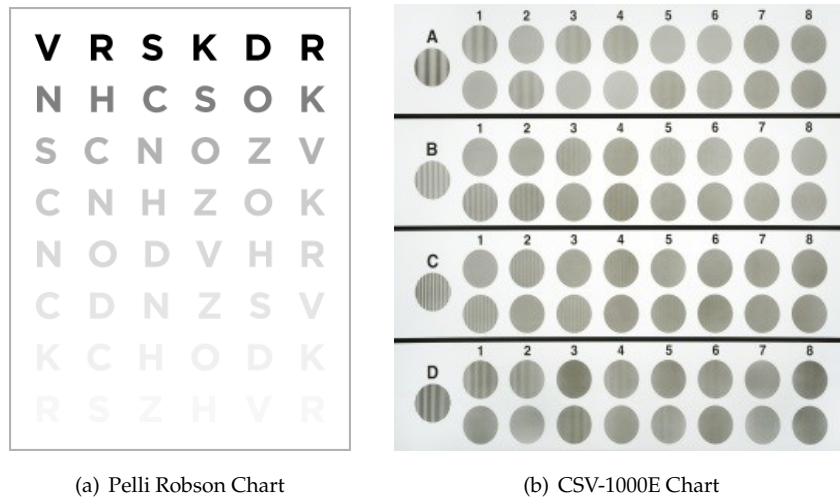


Figure 2.2.2: Example of two different tests to measure CS (Sources: [55, 56]).

and compare the effects of four MCLs with three monofocal ones under dim conditions, including the effects of induced glare. The main conclusion was that monofocal CLs had better results than MCLs, even under dim conditions [57].

In 2003 Montés-Micó *et al.* published a study where a refractive MIOL and a monofocal one were compared in terms of CS at distance and near vision after 1, 3, 6, 12, and 18 months after the implantation. Results proved that contrast sensitivity at distance vision of implanted eyes with the refractive MIOL was only comparable to that obtained with implanted eyes with monofocal IOL between 3 and 6 months after the implantation. At near distance, CS was always lower than the distance CS and than near-corrected monofocal IOL [58].

Stereoacuity

Stereoacuity is the evaluation of the ability of the visual system to detect depth differences between objects in binocular vision conditions. It is the minimum disparity that visual system is able to distinguish. Several standardized tests are available to measure it, as are TNO, Timus' test, Random Dot Test, or Lang's Test (Figure 2.2.3).

Due to the fact that simultaneous vision system can damage the stereoacuity of the patient, there are a lot of studies about MIOLs or MCLs that also obtained it. For example, Richdale *et al.* that presented similar results of near stereoacuity between patients adapted with MCLs and patients adapted with monofocal CLs in monovision technique (dominant eye was adapted with distance refraction and the contralateral one with near refraction) [63]. Although, Sivardeen *et al.* found better stereoacuity with patients adapted with MCLs than patients with monovision adaptation [64].

In terms of MIOLs, Hayashi *et al.* compared the effect of the implantation of the same MIOL at both eyes with different values of addition and the effect in eyes implanted with the same value of addition. The addition difference was 1.00D and the conclusion was that the stereoacuity was not compromised [65].



Figure 2.2.3: Images of stereoacuity tests and its complements to perform them (Sources: [59, 60, 61, 62]).

2.2.1.2 Evaluation of the visual quality before an implantation of a MIOL

In this part of the section are only explained the different instruments that have been developed in the last decade to be able to evaluate the visual quality of a MIOL before its implantation in the eye's patient. This means that the technological advances have allowed to create several instruments that simulates simultaneous vision, the wavefront of a MIOL or directly the virtual implantation of an specific MIOL. While the simulation is performed, the visual quality is evaluated presenting the tests explained in section 2.2.1.1.

There are different methods to achieve the characterization of the visual quality before the implantation of any MIOL.

Simultaneous Vision Simulator

On the first hand, it is possible to find some simulators that are able to reproduce the optical design of MIOLs or to reproduce the optical principle of the simultaneous vision.

In 2010, Dorrnsoro *et al.* patented a new instrument for simulating simultaneous vision corrections [66] which was then validated by De Gracia *et al.* in 2013 [16]. This instrument consists of two independent Badal optometers that send simultaneously two overlapping images on the retina of the observer (Figure 2.2.4). One image has focused distance objects and the other has focused near objects.

Three years later, in 2016, Dorrnsoro *et al.* published a new paper presenting an upgrade of the simulator [67]. As can be observed in figure 2.2.5, the main difference with the previous one

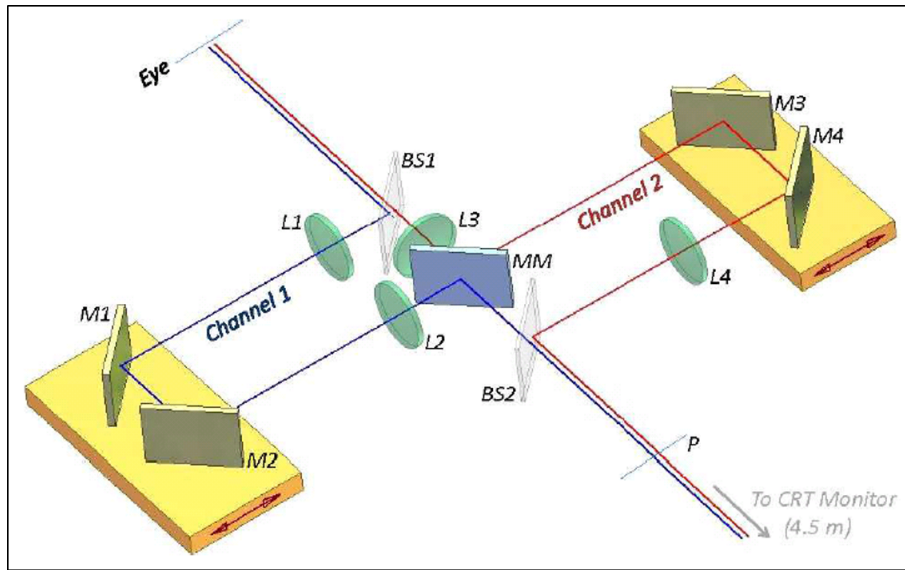


Figure 2.2.4: Schematic diagram of the simultaneous vision system. (Source: [16])

is the replacement of the Badal's systems for an electro-optical lens (EOL) working in temporal multiplexing [68]. This EOL allow to compact considerably the instrument and to have more mechanical stability, since it only needs to receive different level of electrical current to change its focal length and, consequently, its dioptric power. This publication demonstrated that this new simulator it is also effective to simulate multifocal corrections.

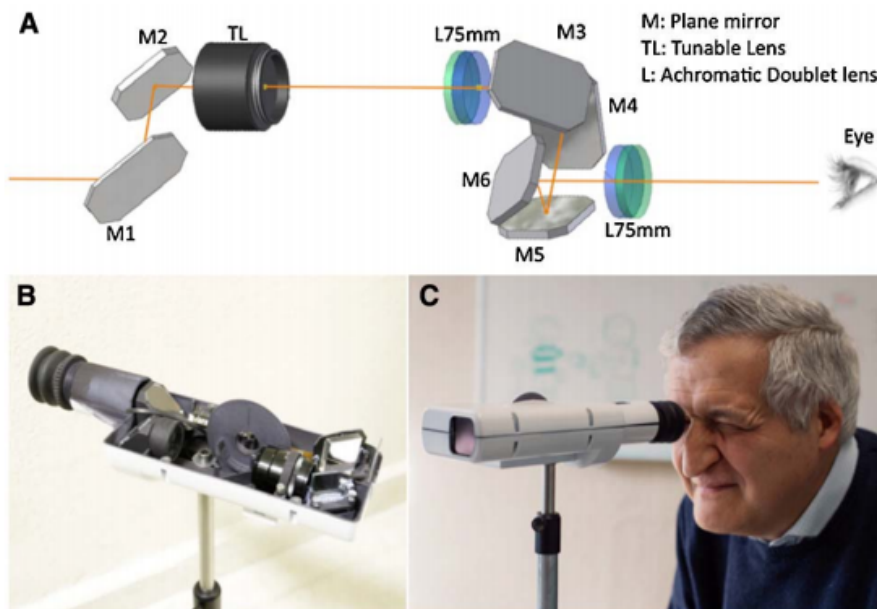
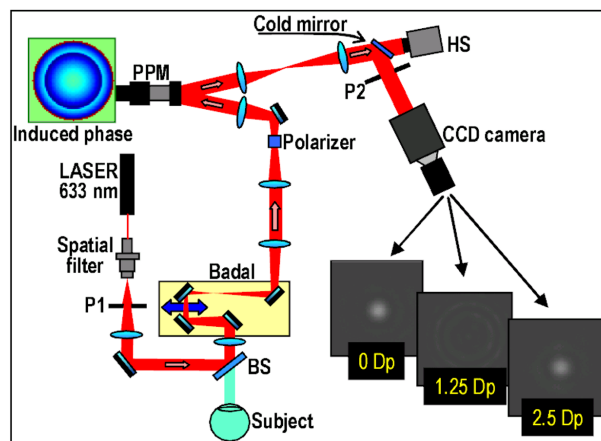


Figure 2.2.5: Schematic diagram of the upgraded simultaneous vision system. (Source: [67])

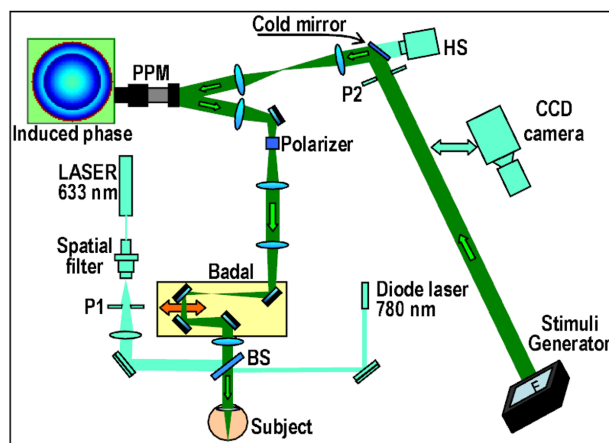
A new start-up company called 2Eyes Vision S.L. was created to produced and commercialize this new instrument [69].

Adaptive Optics Simulator

Another way to simulate multifocal corrections is using a vision instrument based on adaptive optics. Adaptive optics was first applied in astronomy, since it allows the improvement of the emitted optical signal taking into account the information of the environment in which is surrounded [70]. Although, adaptive optics is able to modify the optical system in anyway, either to improve or to make it worse. Consequently, this discipline was employed in vision applications, mostly to obtain high resolution images of the ocular tissues [71] and to study visual function changing the aberration levels of the image that is focused on the retina plane [72].



(a) Objective measurement channel



(b) Subjective measurement channel

Figure 2.2.6: Scheme of the optical design of AOVS where PPM is a liquid crystal programmable phase modulator and HS is a Hartmann-Shack wavefront corrector. First image (a) represents the optical path of an objective measurement. In contrast, image (b) shows the subjective measurement path. (Source: [17]).

In 2001 Fernández *et al.* demonstrated that was possible to develop a prototype for real-time closed-loop correction of aberration in the living eye by use of a wave-front corrector and a micromachined membrane deformable mirror [74]. This apparatus prototype was presented one year later as a visual simulator, named AOVS, to test in advance the effect of aberrations produced by ophthalmic devices or refractive surgery [75]. After several improvements of the system

2.2. CHARACTERIZATION OF SIMULTANEOUS MULTIFOCAL VISION SYSTEMS



Figure 2.2.7: Image of the current version of VAO (Source: [73])

(Figure 2.2.6), Manzanera *et al.* published a study in which the availability of the simulator to test and design ophthalmic elements was proved. In order to do that, different wavefront patterns simulating IOLs designs were presented and evaluated objectively and subjectively for two different subjects [17]. Some years after, AOVs has become the Visual Adaptive Optics simulator called VAO (Figure 2.2.7) [76] which is produced and commercialized by the Spanish start-up VOPTICA S.L. (Murcia, Spain).

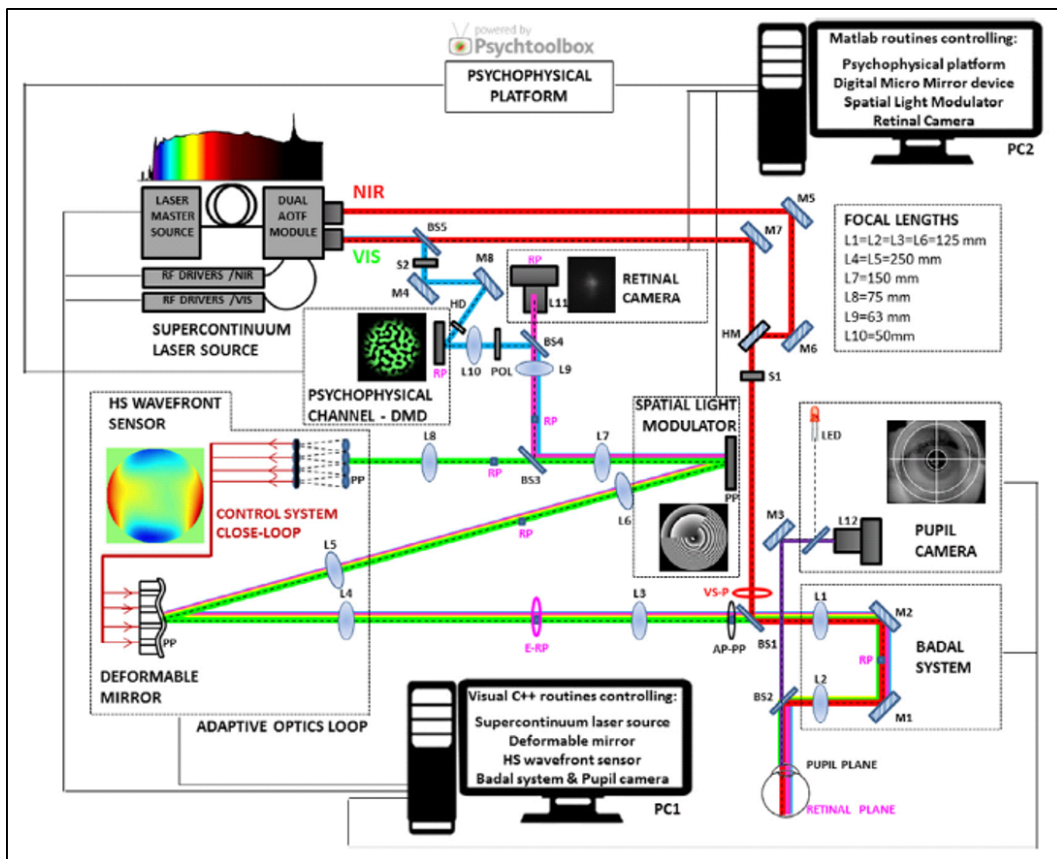


Figure 2.2.8: Schematic diagram of the VioBioLab AO II system with the different channels in its final configuration (Source: [18]).

Concurrently, Viñas *et al.* assembled another adaptive optics prototype to simulate multifocal patterns and test them (Figure 2.2.8) [18].

The published study showed the comparison of the optical and psychophysical results between three radial and three angular multifocal patterns presented to six young subjects. The authors concluded that patterns with only 2 vision zones had better results than 3 or 4 different vision zones as much in radial as in angular designs. They also affirmed that angular designs outperformed radial designs when only 3 and 4 vision zones patterns are evaluated.

The main conclusion of all the studies is the suitability of an Adaptive Optics systems to design new multifocal lenses, evaluate commercial ones or even, to select which is better for each user.

VirtIOL Vision Simulator

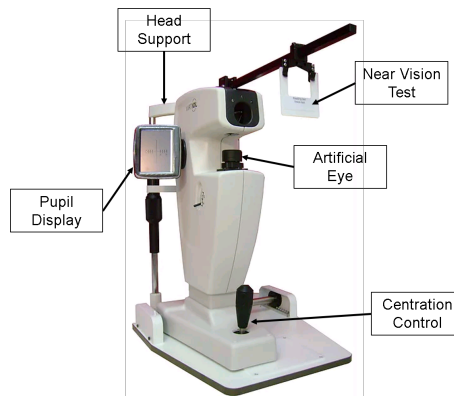


Figure 2.2.9: Image of the instrument (Source: [77]).

A different way to evaluate visual quality of multifocal lenses before their implantation is using the commercial instrument VirtIOL (10Lens S.L.U., Terrassa, Spain). VirtIOL vision simulator is an open-field instrument based on projecting a multi- or monofocal IOL onto the patients' pupil plane. The evaluated IOL is inserted in the artificial eye of the instrument (Figure 2.2.9) becoming the conjugate of the patient's pupil plane by the optical design of VirtIOL. Thanks to this optical system the eye is observing any visual quality test as it was implanted with the IOL inserted in the model eye of the system. Some studies about multifocality using VirtIOL had been presented in different international conferences [78, 19, 79].

2.2.2 Assessment of optical quality

Optical quality defines the quality of the image that is reproduced by any optical system. In this thesis, optical quality of the image projected onto retina's plane of a human or an artificial eye implanted with a MIOL or adapted with a MCL was objectively evaluated.

When first MIOLs were launched, optical quality was only possible to be measured in *in vitro* conditions, that is, using an artificial eye that can be implanted with a MIOL or adapted with a MCL and that can have an image sensor as a retina. Over the years and thanks to the technological advances, now it's possible to measure the optical quality *in vivo*. Therefore, there are different kinds of systems to obtain optical quality and they are explained right after.

2.2.2.1 Simple-pass systems

On account of the fact that a surgical implantation of a MIOL is mostly irreversible, the *International Organization for Standardization* (ISO) developed the regulation 11979-2 [80] which explains optical properties and test methods to characterize IOLs. It specifies the accepted range of wavelengths, the specifications of the model eye and how to perform the measurement. In summary, it presents the simple-pass technique as the method to measure the optical quality of any IOL.

Simple-pass technique is based on projecting a point light source through a model eye implanted with any IOL and capture the resultant image. Then, it will be analyzed and characterized to obtain optical quality of the system.

In a simple-pass system, the captured image is the *Point Spread Function* (PSF) of the system. PSF is the response of an imaging system to a point source. In other terms, PSF is the intensity distribution I_{SP} of the captured image (Equation 2.2.1).

$$I_{SP} = PSF(x', y') \quad (2.2.1)$$

PSF itself provide information about the optical quality, but it is common to work in frequency or Fourier domain to evaluate optical quality. Actually, *Modulation Transfer Function* (MTF) is the most used function to evaluate it. Due to the fact that MTF is the module of the *Optical Transform Function* (OTF), this has to be first calculated. Thus, a *Fourier* Transform of the PSF have to be done:

$$\mathcal{F}[PSF(x', y')] = OTF_{(u,v)} = MTF_{(u,v)} e^{iPTF_{(u,v)}} \quad (2.2.2)$$

As it is indicated in equation 2.2.2, OTF is formed by its module, the MTF, and its phase, the *Phase Transfer Function* (PTF). Consequently, the module of the OTF, which is also the module of the *Fourier* transform of the PSF, has to be calculate to obtain the MTF of the image:

$$\mathcal{F}|I_{PS}| = \mathcal{F}|PSF(x', y')| \quad (2.2.3)$$

$$\mathcal{F}|I_{PS}| = |MTF_{(u,v)} e^{iPTF_{(u,v)}}| \quad (2.2.4)$$

$$|\mathcal{F}|I_{PS}|| = MTF_{(u,v)} \quad (2.2.5)$$

MTF is widely used to characterize any optical system, also for the multifocal ones. MTF specifies the ability of the system to detect and distinguish different spatial frequencies. In other words, MTF represents the loss of contrast produces by the optics of the eye on a sinusoidal grating as a function of its spatial frequency [81]. There are some parameters that can be calculated from MTF, as are: cut-off and the Strehl ratio (SR).

On the first hand, cut-off of the MTF is the maximum spatial frequency that the eye is able to differentiate. The lower the cut-off, the lower the optical quality. On the other hand, SR can be defined as the ratio between the volumes under the MTF curve of the measured optical system and that of the aberration-free system, when it is calculated in the frequency domain [82, 83]. The closer to 1 the coefficient, the better the optical quality.

Due to the whole optical characterization that a simple-pass system is able to provide, a number of research groups decided to assemble a costume simple-pass system. Terwee *et al.* [84] published the comparison of spherical and aspheric diffractive and refractive MIOLs by a customized simple-pass system. Two different methods were performed to obtain the results: the projection of a green light point source, and the projection of the US Air force target [85] through the model eye implanted with the different MIOLs (Figure 2.2.10).

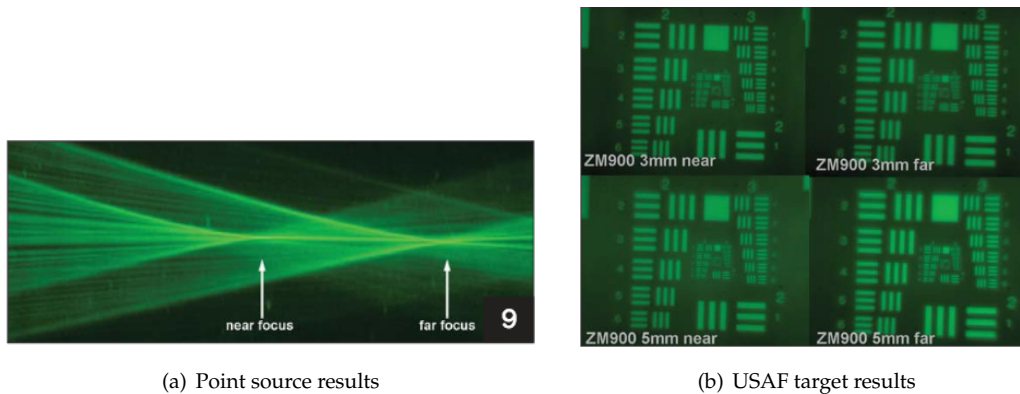


Figure 2.2.10: Results of the two methods of measurement of the diffractive Tecnis ZM900 MIOL (Source: [84]).

After the comparison of the MTFs of both methods, the study conclude that the visualization technique by USAF target gave a further understanding of the working principles and quality of the retina images produced by any monofocal or multifocal IOL. In 2011, Inoue *et al.* [86] also performed the visualization technique using the USAF target near to evaluate different MIOLs and compare with a monofocal IOL.

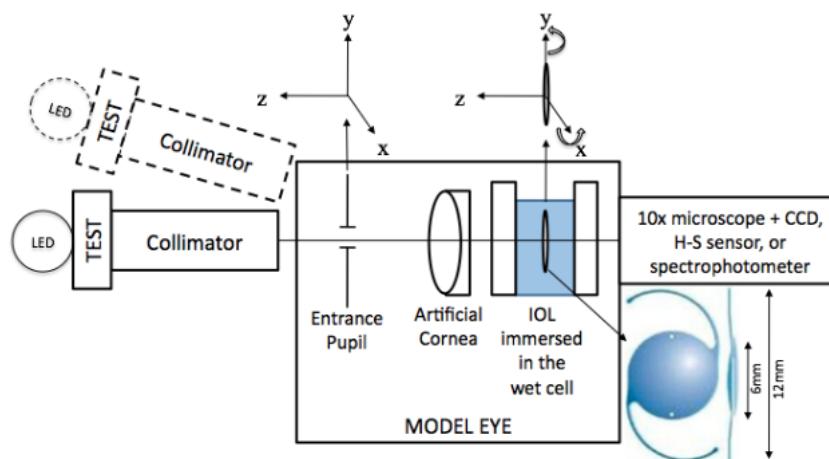


Figure 2.2.11: Design of the optical bench set-up (Source: [87]).

Alba-bueno *et al.* [87] assembled a similar simple-pass system to Terwee *et al.* [84], but with the advantage of having four different LEDs (blue, green, red, white) and an x, y, z axis movement of the IOL and the entrance pupil of the system that gives the possibility of evaluate the effects of decenter and tilt of any IOL (Figure 2.2.11). After preliminary measurements with monofocal IOLs,

it was proved that the system was able to characterize any IOL by different metrics, such as PSF, MTF, Strehl ratio or contrast measurements. After several months, they published the evaluation of the energy balance in apodized diffractive MIOs by using this simple-pass system [88].

While some research groups built up customized pass-simple systems, there were others that used commercial systems to characterize MIOs.

One of the commercial simple-pass system that was quite used was OPAL Vector System (Image Science Ltd., UK). OPAL Vector System is a simple-pass system based on a laser of $\lambda = 546nm$ as a point light source, an artificial eye to insert the IOL, a microscope lens and a CCD camera (Figure 2.2.12). It is no longer available in the market, but several published studies can be found in the bibliography.

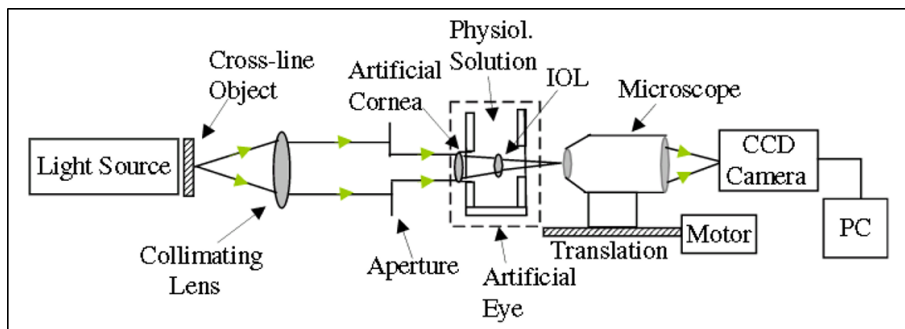


Figure 2.2.12: OPAL Vector System Scheme (Source: [89]).

Kawamorita *et al.* in 2005 used OPAL Vector System to compare the MTFs of one refractive MIOL and a monofocal IOL [90]. Later, in 2008, they compared the MTFs of two refractive MIOLs. The main conclusion was that Rezoom MIOL gave a better image quality than Array MIOL [91]. In the same period of time, Artigas *et al.* [89] presented the evaluation of the image quality and the effect of the pupil size of two hybrid MIOLs, one refractive MIOL and one monofocal IOL. It was proved that hybrid MIOLs gave a better near vision for all analyzed pupil sizes and that monofocal IOL provide the best distance vision.

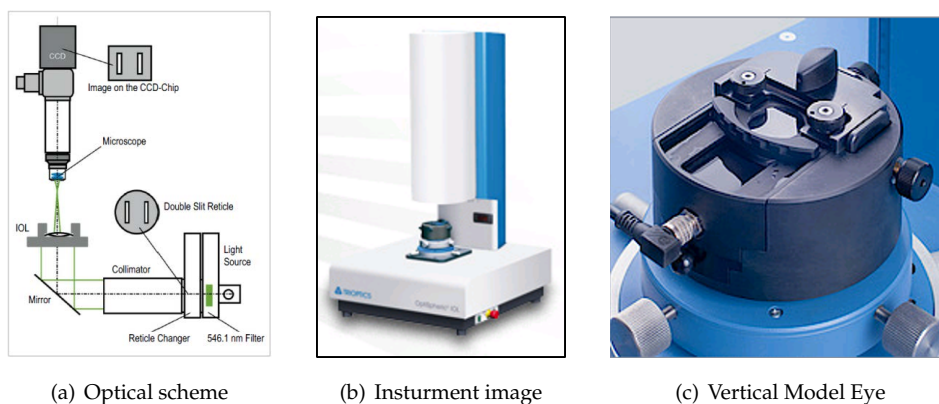


Figure 2.2.13: Images of OptiSpheric®IOL (TRIOPTICS, Gmbh., Germany) (Source: [92]).

Some time later, Soda *et al.* [93] published the effects of decentration on optical performance of two diffractive and two refractive MIOLs by using a commercial system named OptiSpheric®IOL (TRIOPTICS, Gmbh., Germany). The study concluded that the performance was different for each

design of MIOL and that clinically significant effects were not to be expected up to a decentration of 0.75mm .

OptiSpheric®IOL is a simple-pass system with a vertical optical design that allows the characterization of any kind of IOL (Figure 2.2.13). The instrument has its own software that provide PSF, MTF, resolution efficiency, back focal distance and curvature radius of the lens, doing simple and fast the characterization of any IOL.

2.2.2.2 Double-pass systems

Double-pass (DP) systems are based on the double-pass technique which consists on project the image of a point source on the retina and capture the retinal reflection of this image. Actually, when Flamant developed this technique in the 50's, the chosen light source was a fringe of light [94]. But DP technique got off the ground when Santamaría *et al.* replaced the fringe light source for a point light source and captured the image with a video camera [95]. A long the years, different improvements have been implemented in DP systems, as for example, the replacement of the video camera for a CCD [96] or a CMOS [97] camera. Another example is the use of an automated optometer based on a Badal system [81, 98] or an electro-optical lens [99] instead of a manual optometer. Regardless of this improvements, it is accepted that the main components of a DP system are a point light source, an optometer and a camera to register the DP image.

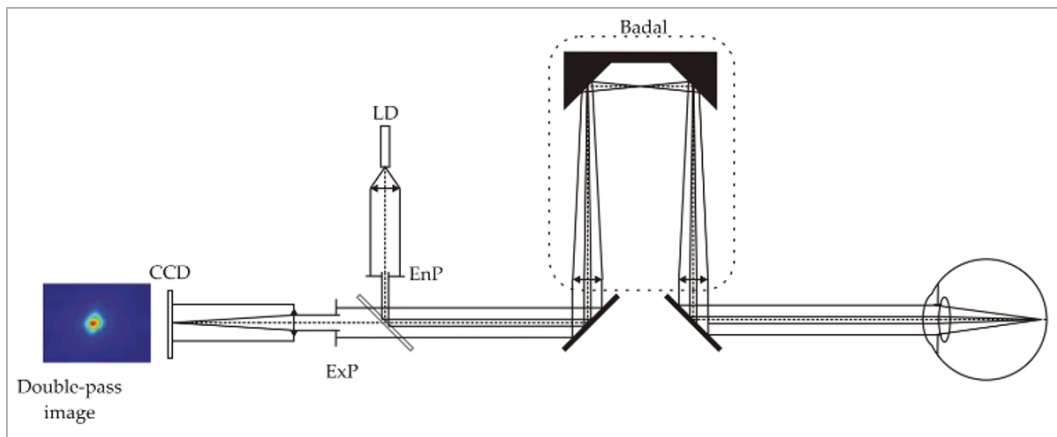


Figure 2.2.14: Scheme of a basic double-pass system (Source: [100]).

Figure 2.2.14 shows that the first pass starts with the collimated point light source passing through the entrance pupil (EnP) and then, through the optometer, that in this example consists in a Badal system. To finish the first pass, the point source is focused onto the retina of the eye. In the second pass this focused image passes across the eye, the Badal system and the exit pupil (ExP). Finally, the DP image is focused with a lens and captured by a camera (CCD).

DP systems works normally with asymmetric pupils, what means that entrance and exit pupil have different diameters. Artal *et al.* proved that if they have the same diameter, the information about asymmetric aberrations is lost [96]. It is for this reason that the major part of the DP systems use a little and permanent entrance pupil diameter, typically 2mm , and a variable exit pupil diameter, normally between 3 and 6mm . The fact of having a little entrance pupil makes possible to consider the MTF of the first pass as limited by diffraction and allows to calculate the MTF of

the second one, as is detailed below.

The intensity distribution obtained with double-pass system (I_{DP}) may be represented mathematically as the convolution of the PSF of the first pass (PSF_1) with the second one (PSF_2):

$$I_{DP} = PSF_1(-x'_1, -y'_1) \otimes PSF_2(x'_1, y'_1) \quad (2.2.6)$$

Taking into account that the Fourier transform of the PSF is equal to the OTF (Equation 2.2.2), the Fourier transform of the I_{DP} will be equal to the product of the OTF of the first pass with the OTF of the second one:

$$\mathcal{F}|I_{DP}| = \mathcal{F}|PSF_1(-x'_1, -y'_1)| \times \mathcal{F}|PSF_2(x'_1, y'_1)| \quad (2.2.7)$$

$$\mathcal{F}|I_{DP}| = MTF_{1(u,v)} e^{iPTF_{1(u,v)}} \times MTF_{2(u,v)} e^{-iPTF_{2(u,v)}} \quad (2.2.8)$$

$$\mathcal{F}|I_{DP}| = MTF_{1(u,v)} \times MTF_{2(u,v)} \times e^{i[PTF_{1(u,v)} - PTF_{2(u,v)}]} \quad (2.2.9)$$

Thus, the module of the OTF is the product of the MTF of the first pass and the second one:

$$|\mathcal{F}|I_{DP}|| = MTF_{1(u,v)} \times MTF_{2(u,v)} \quad (2.2.10)$$

Then, the MTF of the second pass can be obtained dividing the module of the Fourier transform of I_{DP} with the MTF of the first pass ($MTF_{1(u,v)}$):

$$MTF_{2(u,v)} = \frac{|\mathcal{F}|I_{DP}||}{MTF_{1(u,v)}} \quad (2.2.11)$$

Regarding the entrance pupil diameter, the $MTF_{1(u,v)}$ can be considered equivalent to the limited diffraction MTF (MTF_{LD}) if the pupil entrance diameter is equal or less than 2mm. This allows a simplification of the calculations.

One of the strengths of the DP systems is that DP technique consider the scattering of the light that is produced because of the loss of transparency of the ocular media. There is a direct correlation between the loss of transparency of any ocular media and the optical quality. The greater the loss of transparency, the worse the optical quality. Another strength is the possibility of characterized the optical quality *in vivo*. Consequently, in 2006 Díaz-Doutón *et al.* compared a commercial instrument based on the DP technique (OQAS) and a Hartmann-Shack (HS) aberrometer. The results showed that the optical quality of the eyes affected by scattering had worse results in the DP measurements than the aberrometer ones. That proved that DP system consider the effect of the scatter in the optical quality [81]. A new parameter called OSI (Optical Scatter Index) was determined to quantify the intraocular scatter light. OSI is computed as the ratio of the amount of light within an annular area of 12 and 20 min arc and that recorded within 1 min arc of the central peak of the DP image [101].

OQAS (Optical Quality Analysis System) was the first system that was based on the DP technique. It was developed in the CD6 with the collaboration of the LOUM (Laboratorio de Óptica de la Universidad de Murcia). A spin-off company from CD6, Visiometrics S.L., was created to produce and commercialize this system. At the present time, Visiometrics is part of

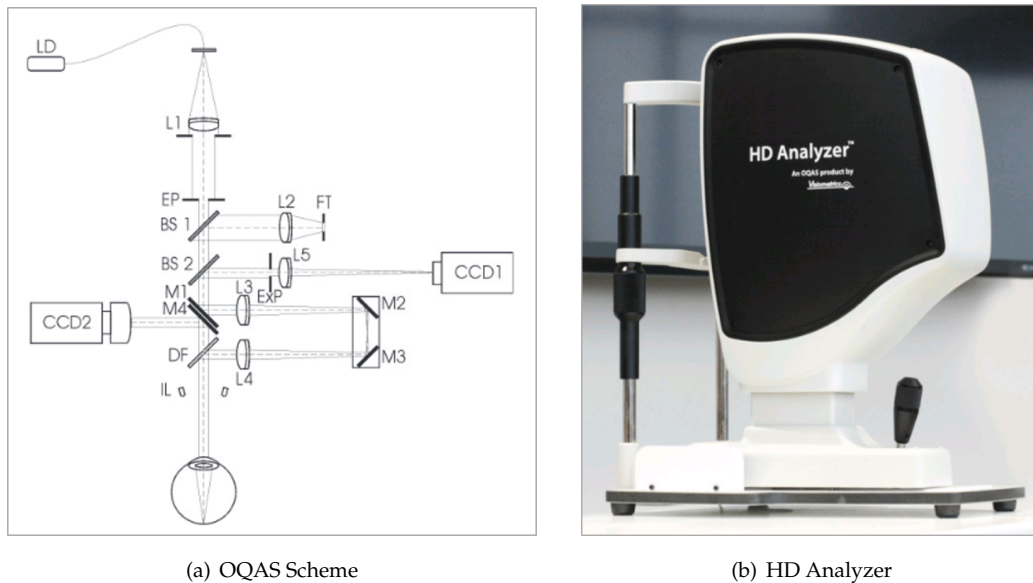


Figure 2.2.15: DP commercial instrument (Source: [81, 102]).

Halma plc (Amersham, UK). The third generation of OQAS is now in the market and it is re-named as HD Analyzer.

Due to the potential of this instrument, several studies with MCLs and MIOLs had published.

In 2002, Gispets *et al.* compared the optical quality of two concentric bifocal CLs. Both lenses were distance center design and performed a better optical quality for distance than for near vision. It was also detected the pupil dependency that those lenses had [103]. One year later, Pujol *et al.* evaluated the optical quality at distance, intermediate and near vision in subjects with and without MCLs. Two different pupil diameters were performed (3 and 5mm). It was concluded that the optical quality was better when subjects were without the MCL and that 3mm pupil obtained better results [104].

In terms of MIOLs, Alió *et al.* proved that the included MIOLs provided intermediate and near vision to the implanted subjects. In addition, the optical quality in intermediate vision was better with the refractive MIOL and the optical quality in near vision was better with the diffractive one [105]. In 2014, Lee *et al.* [106] investigated the correlations between optical quality parameters obtained from OQAS and ocular aberrations obtained from a ray-tracing aberrometer in eyes implanted with MIOLs. The study concluded that Strehl ratio were affected by RMS total aberration. However, Hwang *et al.* [21] were not able to characterize the optical quality of a diffractive MIOL and of a monofocal IOL using OQAS. In contrast with Alió and Lee *et al.*, it was concluded that was impossible to show the multifocal function of the diffractive MIOL compared to the monofocal IOL by OQAS (Figure 2.2.16).

The difficulty to characterize the optical quality of a MIOL along the through-focus can be produced by the dependency of the first and the second pass. A conventional DP system has only one optometer, this might create a defocus in the image of the first pass when intermediate and near vision optical quality is being evaluated. This means that the DP system should has first and second pass independents of each other to be able to perform a good optical characterization of an eye adapted or implanted with a MCL or a MIOL. In order to achieved this independence, a

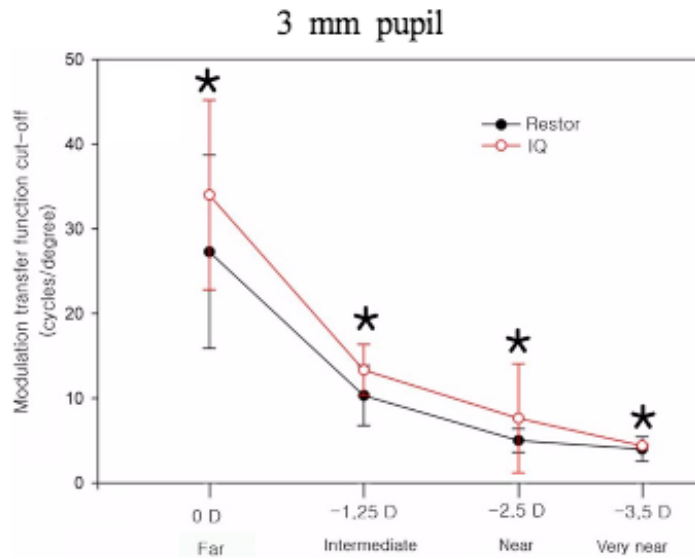


Figure 2.2.16: MTF cut-off results along the through-focus with a diffractive MIOL (Restor (black filled points)) and a monofocal IOL (IQ (red empty points)) (Asterisks indicates statistic significant differences between MIOLs)(Source: [21]).

second optometer has to be added in the second pass. In this way, it would be possible to have always the image of the first pass focused and perform the through-focus with the optometer of the second pass. A first prototype with two Badal systems was developed by Zuluaga *et al.* [107], but a deep study of this modification and its potential was necessary.

2.2.2.3 Aberrometers

Aberrometers are another systems that are able to characterize the optical quality of an eye *in vivo*. It is possible because they also used the retinal reflection to obtain and analyze the wavefront of the eye. As was commented in section 2.2.2.2, aberrometers can provide an accurate information of aberrations that DP can not. Due to this fact, there are several publications where experimental set-ups implementing both techniques are presented [108, 109, 97].

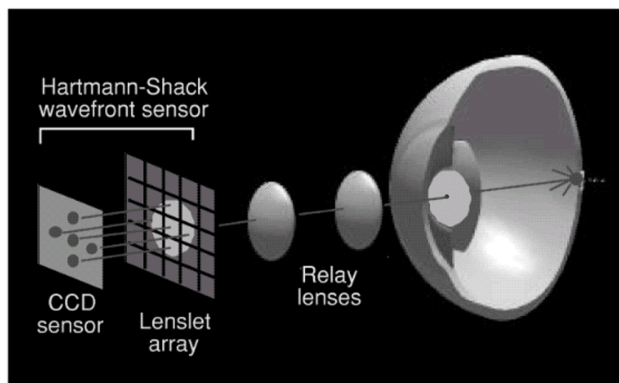


Figure 2.2.17: Simulation of the principles of HS technique (Source: [110]).

There are different techniques applied in aberrometers, but one of the most extended is the Hartmann-Shack (HS) technique. The purpose of this technique is to measure the shape of the wavefront of light that is reflected out of the eye from a point source on the retina [110]. In order to obtain the wavefront the retinal reflection of the point source pass through an array of micro-lenses. Each micro-lens projects an image on the CCD or a CMOS sensor registering the position of the points formed by each micro-lens (Figure 2.2.17). These positions are then compared with the positions that a free aberration optical system or eye would have. The position differences (Δx and Δy) between the two point-maps are calculated obtaining the wavefront of the measured eye.

Large number of publications have evaluated the optical quality of the human eye by experimental set-ups [111, 112] or commercial instruments [76] based on HS technique (Figure 2.2.18).

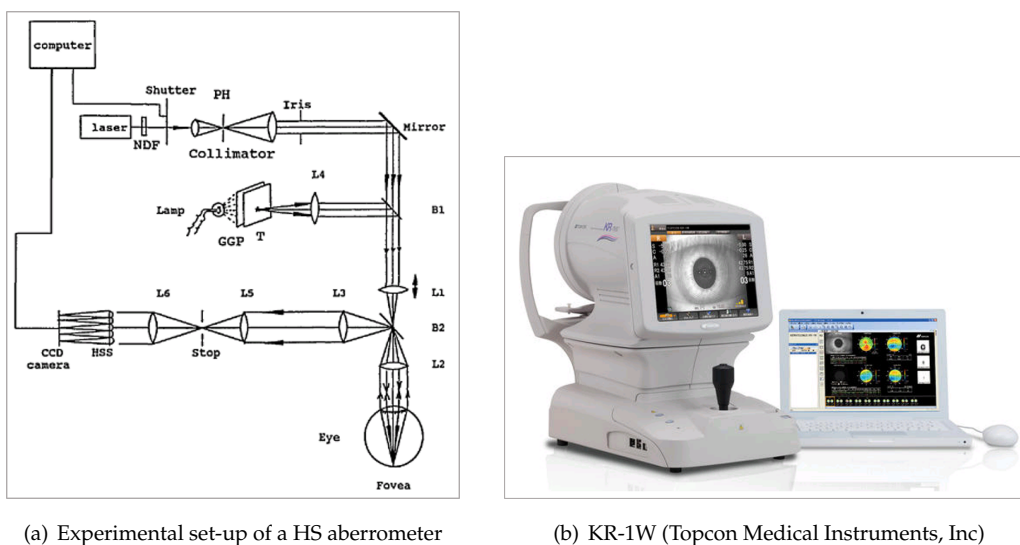


Figure 2.2.18: Examples of one experimental (a) and one commercialized HS aberrometer (b) (Source: [111, 113]).

These type of aberrometers have also used to perform optical quality of adapted or implanted eyes with MCLs or MIOLs.

Regarding MCLs, Patel *et al.* measured aberrations by a HS aberrometer and obtained Zernike coefficients. It was demonstrated that some specific Zernike coefficients could be useful objective markers of success or failure adaptation for MCLs included in the study [114].

In terms of MIOLs, Alió *et al.* compared optical and visual performance of one refractive MIOL and one accommodative IOL. A commercial HS aberrometer and a DP system were employed to perform optical quality. The main conclusion was that both lenses provided good distance vision. Nevertheless, refractive MIOL gave better near vision rehabilitation [115]. Ortiz *et al.* evaluated one monofocal IOL, one refractive and one hybrid MIOL in terms of aberrations for two different pupil diameters (3 and 5mm). Results proved that MIOLs had greater aberrations than the monofocal IOL. Also confirmed that hybrid MIOL had lower aberrations and less pupil dependency than the refractive MIOL [116]. On the contrary, Charman *et al.* concluded that aberrometry may not provide reliable information on the wavefront aberration associated with either the distance or near power of diffractive MIOLs [20].

Another type of aberrometers are the ones based on ray tracing technique [118]. This technique differs from HS one by the use of a thin laser (around 0.3mm) to scan the area of the pupil on

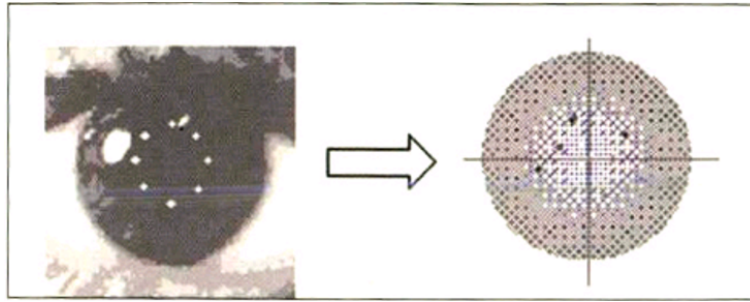


Figure 2.2.19: Scanning over pupil aperture. Example of a set of entrance points (Source: [117]).

the retina. This means that the laser is focused onto the retina from a set of different entrance points (Figure 2.2.19). Consequently, a set of projections will be registered by a camera [117]. The same way that in HS technique, the projections are compared with the ideal projections that a free aberration eye would have. Differences between them give the level of each aberration .

A preliminary study which consisted on the comparison of the objective and subjective visual performance of three different MCLs was published by Vasudevan *et al.* in 2014. The objective visual performance was evaluated by iTrace (Tracey Technologies) which is an aberrometer based on ray tracing technique. No statistically significant difference were found between included MCLs either in subjective or in objective measurements [119].

3. Suitability to perform objective measurements in users of multifocal contact lenses (MCLs)

This chapter includes the clinical study that was performed to evaluate the suitability of an infrared open-field autorefractor to obtain an accurate over-refraction evaluation for far viewing distances after fitting MCL in non-cycloplegic adult eyes.

In 2011, an international survey of contact lens prescribed for presbyopia was conducted by Morgan *et al.* in 38 different countries [44]. Results established that the average percentage of presbyopes that were adapted with a multifocal contact lens (MCL) from 2005 to 2009 was twenty-nine per cent.

Among other things, a contact lens adaptation implies a proper adjustment of the power of the lens by performing an over-refraction [120]. Over-refraction is the measurement of the residual refractive error of the eye when the patient is wearing the contact lens. In clinical practice an autorefractor is commonly used as a screening method of over-refraction for contact lenses users [121, 122]. Its suitability in monofocal contact lens over-refraction was demonstrated in 1997 by Strang *et al.*[123]. Due to the complex designs of MCLs, some inaccuracies in over-refraction measurements obtained with the autorefractor could occur, similar to the inaccuracies found when performing aberrometric measurements in other multifocal systems such as MIOLs [20]. However, not all authors report problems when measuring aberrations in MCLs [124] and objective accommodative responses have been successfully measured using an autorefractor [119]. Moreover, autorefraction has also been used after cataract surgery in patients with MIOLs [125, 126].

3.1 Methods

3.1.1 Subjects

Sixteen healthy young and middle-aged adults (11 men and 5 women) from a research centre environment participated in the study. The exclusion criteria for the study were any disease or medication that caused vision problems or contraindicated the use of contact lenses. The age ranged from 26 to 48 years old with a mean age \pm standard deviation (SD) of 31.38 ± 7.34 years. The study followed the tenets of the Declaration of Helsinki and all patients signed the informed consent after they were explained the nature, procedures and aims of the study.

3.1.2 Multifocal contact lenses

We used three commercially available soft MCL: Air Optix Multifocal, Acuvue Oasys for presbyopia and Proclear Multifocal. Air Optix®Multifocal (Ciba Vision), used in nine eyes of the study, has a near-center aspheric refractive design [119] composed of Lotrafilcon B with a $Dk = 110$ and a water contents of 33%. Its diameter is 14.2mm and the base curve 8.6mm . Acuvue®Oasys™ for presbyopia (Johnson & Johnson), used in six eyes, has also a near-center aspheric refractive design [127] composed of Senafilcon A with a $Dk = 147$ and a water contents of 58%. In this case, the diameter was 14.3mm and the base curve 8.4mm . Proclear®Multifocal (Cooper Vision), used in six eyes of the study, has a near-center aspheric refractive design [128] composed of Omafilcon A with PC with a $Dk = 27$ and a water contents of 60%. It has a diameter of 14.4mm and a base curve of 8.7mm .

3.1.3 Autorefractor

The Grand Seiko AutoRef/Keratometer WAM-5500 (Grand Seiko Co. Ltd., Hiroshima, Japan) employed in this study is a binocular open-field autorefractor and keratometer. The basic principle of refractive power measurement consists of capturing the image of a ring target of infrared light after reflection on the retina. The size of the pattern formed at the eye-ground varies in relation to the refractive power. This pattern is then detected by a CCD sensor and analyzed by image processing to calculate the refractive data. The instrument can measure refraction in the range of $\pm 22D$ sphere and $\pm 10D$ cylinder in increments of 0.01, 0.12 or 0.25D for power, and 1degree for cylinder axis. The vertex distance can be adjusted (to 0, 10, 12, 13.5 or 15mm); the minimum pupil size for measurement is 2.3mm [129].

In this study the selected vertex distance was 12mm . The measurements were performed in illuminance conditions low enough to obtain pupil diameters above 2.3mm ($\text{MeanPupilDiameter} = 6.27\text{mm}$ [from 5.6 to 6.8mm]). The Grand Seiko AutoRef/Keratometer WAM-5500 (Grand Seiko Co. Ltd., Hiroshima, Japan) had been previously validated for all these functions [130].

3.1.4 Measurement protocol

The measurements were obtained in two different sessions per person; only one eye was fitted with a MCL per session. The first session started with a medical history, followed by a complete optometric exam without MCL, which included keratometry, distance subjective refraction (Jackson crossed cylinder, maximum plus for best visual acuity) and objective refraction (Grand Seiko AutoRef/Keratometer WAM-5500). The visual acuity (VA) was evaluated with a Bailey & Lovie Chart 5 with the participant at a distance of 6m (20ft) [131]; observation through a slit-lamp ruled out any exclusion criteria conditions. Three subjective and objective refraction measurements were performed consecutively.

Once the initial exam was completed, one eye was selected and fitted with a MCL. The dioptric power of the contact lens was chosen randomly, without taking into account the subjective refraction of the patient. This procedure had been used in similar studies that fitted all lenses to ensure good movement and centration on the eye without controlling the power of the lens, thus enabling the evaluation of the autorefractor in a wide range of spherical powers [123]. As a result, in most cases the power of the MCL did not agree with the refraction distance of the patient.

After fitting the MCL, the patient spent one hour with it to achieve a correct adaptation, checked with the observation of the centration by means of a slit-lamp. Next, three consecutive repetitions of objective over-refraction with the autorefractor and three subjective distance over-refractions were performed to obtain the spherical and astigmatic components of the residual refraction.

In the second session the same procedure was used to fit the MCL on the eye not measured in the previous session.

All measurements were performed by the same optometrist.

3.1.5 Data analysis

Subjective and objective over-refraction results were indicated in negative cylindrical form and the spherical equivalent (SE; equation 3.1.1) and astigmatic refraction were determined. Power Vector analysis [132] was used for astigmatic data: J_0 (Equation 3.1.2) and J_{45} (Equation 3.1.3).

$$SE = sphere + \frac{cylinder}{2} \quad (3.1.1)$$

$$J_0 = -\frac{cylinder}{2} \cos(2axis) \quad (3.1.2)$$

$$J_{45} = -\frac{cylinder}{2} \sin(2axis) \quad (3.1.3)$$

Statistical analysis was performed with SPSS for Windows (SPSS Statistics 19, IBM, Chicago, IL). The Kolmogorov-Smirnov test was used to verify the normal distribution of the spherical equivalent (SE), J_0 and J_{45} for objective and subjective over-refraction with and without MCL. The pair of eyes was included as a factor to control for the intereye correlation. In those cases where correlation between eyes was confirmed, one of them was excluded from the study.

Agreement between the objective and subjective over-refraction was evaluated for each measured component with the mean differences \pm SD and the 95% confidence limits, as suggested by Bland and Altman [133]. Pearson's correlation coefficient was also calculated to compare both techniques. To evaluate if there was any tendency in the differences to systematically vary over the range of measurements, the Pearson correlation coefficient and its significance were also used in the Bland and Altman plots. Finally, a paired sample t test was carried out to analyze if there were significant differences between measurement methods for each parameter obtained in the study. A p value ≤ 0.05 was considered significant.

3.2 Results

Finally, twenty-one eyes were included in the study. The mean best corrected visual acuity without MCL was $-0.13 \pm 0.10 \log MAR$ (range: -0.28 to $+0.02 \log MAR$) and with MCL was $-0.07 \pm 0.08 \log MAR$ (range: -0.22 to $+0.18 \log MAR$). The results with and without MCL were analyzed to determine if the WAM-5500 is a valid screening method for over-refraction in MCL wearers. A Kolmogorov-Smirnov analysis indicated that all parameters had a normal distribution ($p > 0.05$).

Table 3.2.1 shows the refractions' data and table 3.2.2 the mean of the differences \pm SD between subjective and objective measurements with and without MCL, the Pearson's correlation coefficients and their significance, and the paired sample t test significance.

3.2. RESULTS

Table 3.2.1: Mean subjective and objective refractive errors with and without MCL in terms of SE , J_0 and J_{45} . The mean difference \pm SD (D) and range (D) are shown. (Values are in dioptres (D)).

| Refraction data | | | | |
|-----------------|--|---|--|---|
| | Without MCL | | With MCL | |
| | Mean subjective refraction \pm SD (Range) | Mean objective refraction \pm SD (Range) | Mean subjective refraction \pm SD (Range) | Mean objective refraction \pm SD (Range) |
| SE | -1.22 ± 2.44 (-8.08, 2.84) | -1.28 ± 2.36 (-8.11, 3, 16) | -1.26 ± 1.76 (-6.50, 0.67) | -1.13 ± 1.78 (-5.51, 0.77) |
| J_0 | -0.09 ± 0.40 (-0.54, 1.21) | 0.02 ± 0.37 (-0.35, 1.31) | 0.00 ± 0.38 (-0.60, 1.25) | 0.03 ± 0.47 (-0.78, 1.52) |
| J_{45} | -0.03 ± 0.12 (-0.23, 0.30) | -0.02 ± 0.20 (-0.39, 0.39) | 0.02 ± 0.24 (-0.65, 0.54) | 0.03 ± 0.24 (-0.60, 0.36) |

In terms of SE , the mean difference between subjective and objective measurements with MCL was nearly a quarter of diopter, whereas without MCL the differences were close to zero (Table 3.2.2).

Figure 3.2.1(a) plots the correlation of SE with MCL between objective and subjective over-refraction, with a high, significant Pearson's correlation coefficient; as well as without MCL measurements (Table 3.2.1). The Bland and Altman plot of the SE with MCL is shown in figure 3.2.1(b). Pearson's correlation coefficient and its significance for the Bland and Altman plot were 0.04 and 0.87, respectively. Finally, no significant differences were obtained between measurements with and without MCL by means of a paired sample t test (Table 3.2.2). When performing the analysis by groups based on the contact lens used no significant differences were found. In terms of SE , we obtained $p = 0.07$ for the Air Optix®Multifocal lenses, $p = 0.69$ for the Acuvue®Oasys™ for presbyopia and $p = 0.84$ for the Proclear®Multifocal lenses.

Table 3.2.2: Comparison between objective and subjective refraction with and without MCL. The mean difference \pm SD (D), Pearson's correlation coefficients and their significance and the paired sample t test significance are shown.

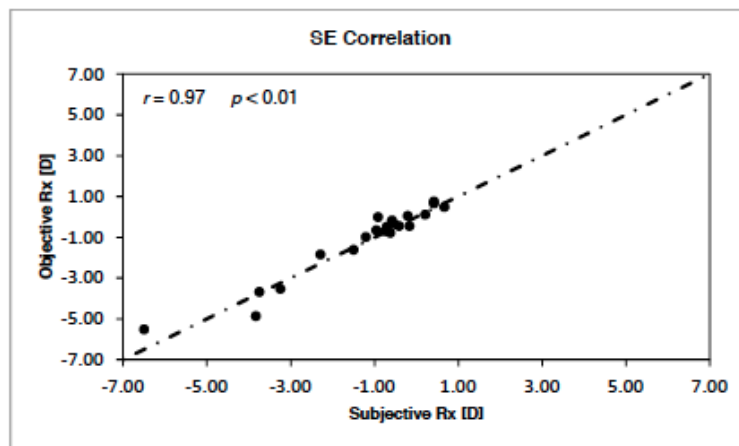
| Statistics data | | | | | | |
|-----------------|--|-----------------|---|----------------|-----------------------------------|----------|
| | Mean difference \pm SD (D) (objective-subjective) | | Pearson's correlation coefficient $r(p)$ | | Paired sample t test (p) | |
| | Without MCL | With MCL | Without MCL | With MCL | Without MCL | With MCL |
| SE | -0.06 ± 0.42 | 0.13 ± 0.42 | $0.98(< 0.01)$ | $0.97(< 0.01)$ | 0.55 | 0.18 |
| J_0 | 0.12 ± 0.13 | 0.03 ± 0.32 | $0.94(< 0.01)$ | $0.73(< 0.01)$ | 0.00^a | 0.71 |
| J_{45} | 0.02 ± 0.15 | 0.00 ± 0.17 | $0.65(< 0.01)$ | $0.75(< 0.01)$ | 0.66 | 0.92 |

(a)Significant differences

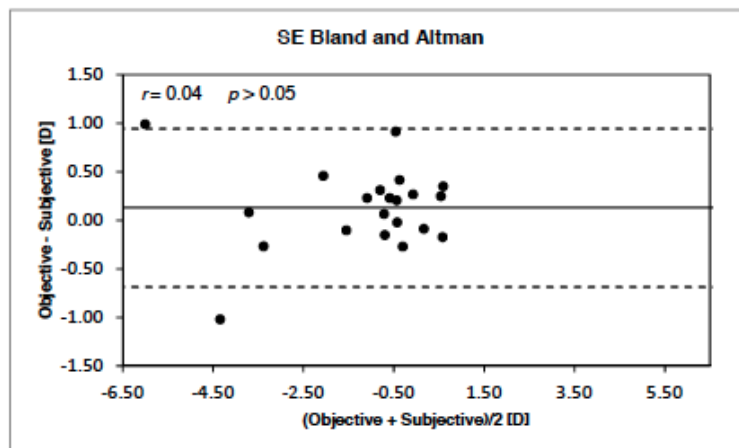
With regard to the astigmatic vectors J_0 and J_{45} , the mean differences for both vectors with and without MCL measurements were close to 0. The correlation of J_0 and J_{45} when measuring with MCL is shown in figure 3.2.2(a). Although lower than in the SE , the Pearson's correlation coefficients are still high and significant. Comparing these results with the results without MCL,

3.2. RESULTS

the Pearson's coefficients are almost the same for J_0 and J_{45} (Table 3.2.2). The Bland and Altman plot for J_0 and J_{45} with MCL is shown in figure 3.2.2(b). The Pearson correlation coefficient for the Bland and Altman differences was 0.28 and -0.02 , respectively, and it did not reach statistical significance in any of the cases (0.22 and 0.93). Finally, no significant differences were found in the paired sample t test carried out with J_0 and J_{45} over-refraction data when wearing MCL (Table 3.2.2). In contrast, the comparison of results without MCL found significant differences for J_0 . The statistical analysis performed with the different MCL used showed no significant differences for J_0 or J_{45} ($p = 0.64$ and 0.88 for the Air Optix®Multifocal, 0.77 and 0.38 for the Acuvue®Oasys™ for Presbyopia and 0.89 and 0.69 for the Proclear®Multifocal).



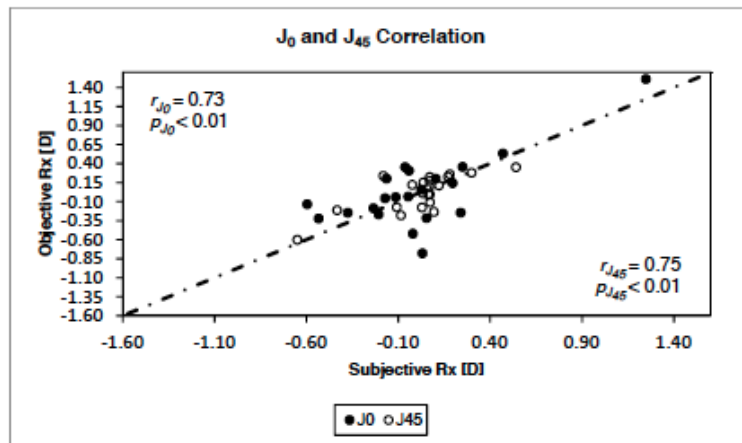
(a)



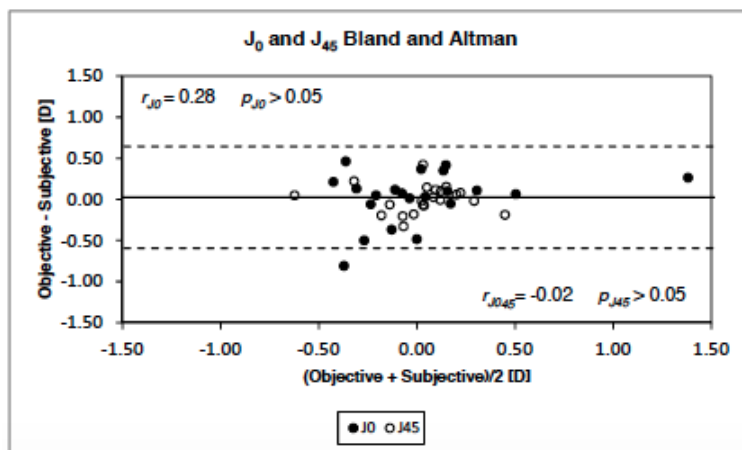
(b)

Figure 3.2.1: Correlation plot of the SE results between objective and subjective over-refraction with MCL (a); Bland and Altman plot of the SE with the mean difference and the confidence limits (CL) comparing the objective and the subjective over-refraction (b).

3.3. CONCLUSIONS



(a)



(b)

Figure 3.2.2: Correlation plot of J_0 and J_{45} results between objective and subjective over-refraction with MCL (a); Bland and Altman plot of J_0 and J_{45} with the mean difference and the confidence limits (CL) comparing the objective and subjective over-refractions (b).

3.3 Conclusions

With regard to the spherical equivalent measured without MCL, only a small mean difference between autorefractor and subjective measurements was found, as well as an excellent correlation and no statistically significant differences, which is in good agreement with the results of previous studies without CL [129]. The results obtained in the measurements without MCL corroborated the good performance of the protocol. When the measurements were performed with MCL, an excellent correlation between autorefractor values and subjective refraction was found. The results of the mean difference and the SD and their behaviour were represented by means of a Bland and Altman plot. When the data for the different MCL were analyzed, no differences among MCL were found. The mean difference had a value of $0.13 \pm 0.42D$ although it was not significant. Other authors [125] measuring refraction in MIOL (diffractive multifocal Tecnis®ZM900, Abbott Medical Optics, Inc.) found equivalent mean differences ($-0.12D$) between autorefractor and subjective values. Additionally, the standard deviations were also similar in both cases (Bissen-

3.3. CONCLUSIONS

Miyajima 0.38D; this study 0.42D) and comparable to those obtained in measurements without contact lenses (Sheppard 0.38D; this study 0.42D) [129]. Consequently, the accuracy and precision of the autorefractor measurements in MCL over-refraction is comparable to MIOL over-refraction. On the other hand, Muñoz et al. [126] found mean differences of $-1.00 \pm 0.61D$ and statistically significant differences when measuring a refractive MIOL, a result that differs from our measurements and from Bissen-Miyajima's data. Muñoz et al. argued that these differences were caused by the geometry of the IOL they used (refractive multifocal ReZoom®, Abbott Medical Optics, Inc.), which can interfere with the infrared beam of the autorefractor.

Our data support that the spherical over-refraction measured with the WAM-5500 autorefractor when wearing MCL is practically identical to the subjective over-refraction. Indeed, it was lower than the minimum dioptric change applied in clinical practice (0.25D). Moreover, these differences were not significant and the precision of the measurement was similar to that obtained in monofocal measurements. We were able thus conclude that the autorefractor provides a good estimate of the spherical refraction in patients wearing MCL.

With regard to astigmatic vectors when evaluating without MCL, the mean difference, Pearson's correlation coefficient, the Bland and Altman plot and the t-test results showed the good agreement between autorefractor and subjective measurements, except for the t-test results in J_0 , where significant differences were found. In their study of the clinical evaluation of the Grand Seiko WAM-5500, Sheppard et al. [129] also found significant differences in J_0 with similar values in the mean difference (0.04D). Although statistically significant differences are found, they are below 0.25D and therefore of no clinical significance. Indeed, results in astigmatic subjects also demonstrate the good performance of the protocol. In the results with MCL, the mean differences for the astigmatic vectors were close to zero, there was a good Pearson's correlation coefficient and the Bland and Altman plot showed the good agreement between measurements for both J_0 and J_{45} vectors. Finally, in astigmatic vectors the differences found were not statistically significant for all MCL considered together and when the different MCL were analyzed. The results with MCL are in good agreement with the results obtained by other authors [125, 126] that used autorefraction in patients with MIOL and who found mean differences close to zero and good Pearson's correlation coefficients. Moreover, when comparing the performance of the autorefractor with and without MCL, the results can be considered similar. Consequently, we concluded that the performance of the WAM-5500 autorefractor with MCL is as valid as without MCL. Furthermore, the autorefractor gave a good estimation of the astigmatic refraction of MCL wearers.

In summary, we concluded that the Grand Seiko WAM-5500 is a valid screening method of over-refraction in the clinical fitting of MCL.

This study was presented in ARVO meeting 2013 [134] and published in the journal Contact lens & Anterior eye in 2015 [135].



Figure 4.0.2: Image of VirtIOL while the patient is observing a vision test through the inserted MIOL.

sibilities in the MIOLs market. Therefore, a study based on the validation of this instrument was done. Furthermore, two different studies were performed using VirtIOL during the development of the new MIOL Precizon Presbyopia (OPHTECH BV).

4.1 Preliminary clinical study to assess visual quality of MIOLs before its surgical implantation

The purpose of this study was to evaluate the suitability of the VirtIOL to predict the visual performance obtained with a MIOL prior to surgery.

4.1.1 Methods

4.1.1.1 Patients

Ten eyes of ten healthy presbyopic adults were included in this study (6 women and 4 men). The range of age was from 52 to 81 *years* old with a mean \pm Standard Deviation (SD) of 67.91 ± 10.26 *years*. The mean \pm SD decimal best distance corrected visual acuity (BDCVA) was 0.92 ± 0.11 and best distance corrected near visual acuity (BDCNVA) was 0.93 ± 0.10 . All the exclusion criteria were a BDCVA and a BDCNVA less than 0.7, problems of transparency in ocular mediums except incipient cataracts and any disease or medication that caused vision problems.

The study followed the tenets of the Declaration of Helsinki and all patients signed the informed consent after they were explained the nature procedures and aims of the study.

4.1.1.2 Multifocal Intraocular Lens (MIOL)

Only one MIOL was included in this study to perform the measurements by means of VirtIOL.

The MIOL included in this study was the Lentis®Lentis®MPlus (Oculentis®). This lens is based on a 6mm optic zone with an aspheric distance-vision zone combined with a surface-embedded near-vision zone [136]. It achieved the Conformité Européenne (CE) marking in March 2009.

4.1.1.3 Measurement protocol

The measurements were performed in two different sessions:

- **1st Session:** MPlus was inserted in the artificial eye of VirtIOL. The eye of the patient which was not yet implanted (the eye with its natural crystalline lens) was centered in the instrument. Thus, visual quality was determined for far and near vision with the presbyopic eye observing the test through the MPlus inserted in the VirtIOL.
- **2nd Session:** it consisted in obtaining the evaluated parameters (explained below) three weeks after the implantation of the MPlus without VirtIOL.

The evaluated parameters were decimal Visual Acuity (VA), Contrast Sensitivity (CS) and visual perception. Snellen chart and CSV-1000E (explained in section 2.2.1.1.) were employed to asses VA and CS respectively. In terms of visual perception, the patient did subjective comparison of the vision of a letter and a point light source between virtual multifocal implant and post-implantation vision. The range of the comparison was from 0 to 5, being 0 different and 5 completely the same. All the patients were corrected for distance vision.

VA differences were presented in decimal scale for best distance corrected VA (BDCVA) and best distance corrected near VA (BDCNVA) vision. In terms of contrast sensitivity, the differences were expressed in the logarithmic scale per each analyzed frequency.

The room was under low luminance conditions and the patients had a pupil of around 4–5mm for distance vision. All the measurements were performed by the same optometrist.

4.1.2 Results

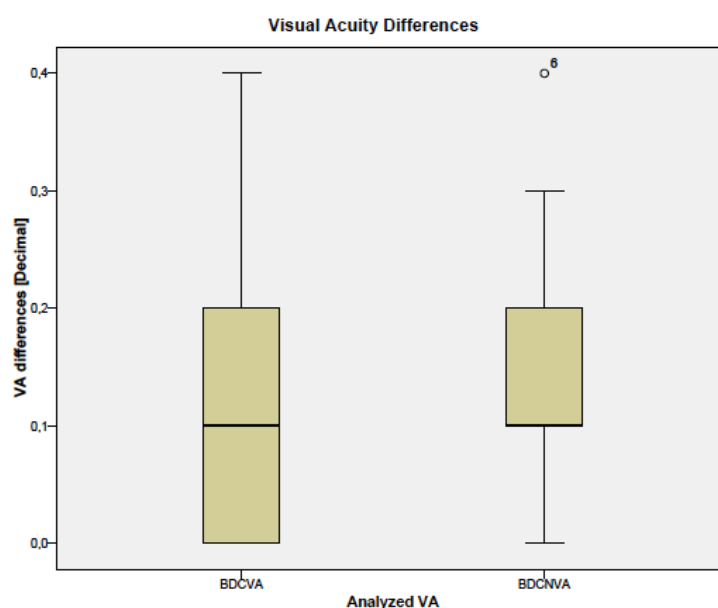


Figure 4.1.1: Visual acuity differences between first and second session for the BDCVA (Best Distance Corrected Visual Acuity) and BDCNVA (Best Distance Corrected Near Visual Acuity).

4.1. PRELIMINARY CLINICAL STUDY TO ASSESS VISUAL QUALITY OF MIOLS BEFORE ITS SURGICAL IMPLANTATION

The mean absolute difference in BDCVA and BDCNVA between simulated multifocal implantation and three weeks post-implantation were 0.10 ± 0.13 and 0.16 ± 0.12 respectively (Figure 4.1.1).

In terms of CS, the mean absolute differences between simulated multifocal implantation and real implantation were: 0.29 ± 0.38 for *3cycles/degree* frequency, 0.74 ± 0.68 for *8cycles/degree* frequency, 0.73 ± 0.59 for *12cycles/degree* frequency, and 0.52 ± 0.32 for *18cycles/degree* frequency (Figure 4.1.2).

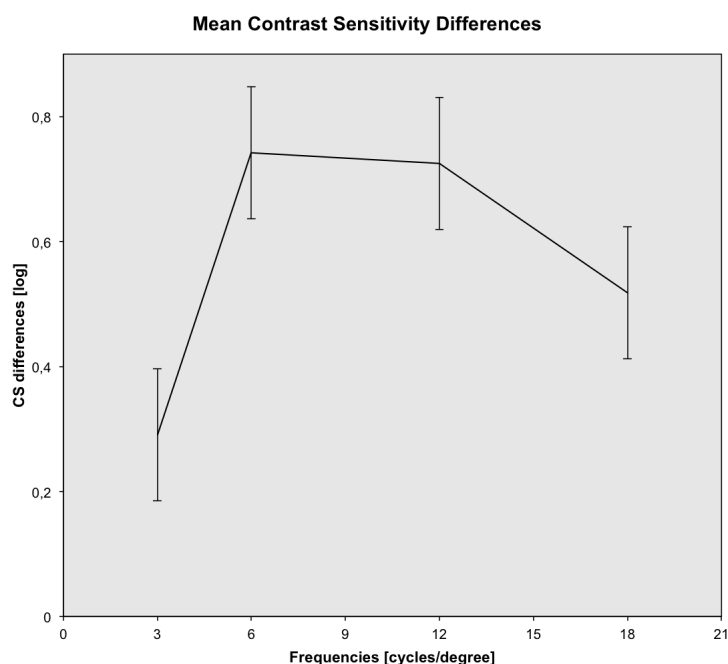


Figure 4.1.2: Mean contrast sensitivity differences curve between first and second session for BDCVA (Best Distance Corrected Visual Acuity).

Furthermore, the results (mean \pm SD) of the subjective comparison were $3.20 \pm 0.79points$ and $2.50 \pm 0.71points$ for the letter and the point light source, respectively.

4.1.3 Conclusions

The new instrument VirtIOL was a useful tool to predict the visual performance of a patient before surgery.

Differences found between simulated and real implant are associated with little opacification of the crystalline lens. It was required that the patient had a clear eye at the simulation time as it happens in Refractive Clear Lens Exchange. This was confirmed with one patient, who showed very similar results between simulated implantation and real implantation, due to the normal transparency of his eye.

This study was presented in ARVO meeting 2015 [79].

4.2 Visual quality performance of different MIOLs by means of a simulated implantation

This study was part of the development process of the new MIOL Precizon Presbyopia (OPHTECH BV). The main goal of it was to simulate the performance by means of the VirtIOL vision simulator in a new MIOL design and compare it with the performance of a commercial one. Moreover, the study was also used to improve the final design.

4.2.1 Intraocular lenses

Four IOLs were measured in the present study. Three MIOLs were tested: a new MIOL design (NDIOL, OPHTEC prototype, $P = +20.00D$ Add = 2,75D) with the central zone corresponding to far refraction (NDIOL-FC), the same but with the central zone corresponding to the near refraction (NDIOL-NC) and a commercial one (Lentis®MPlus, Oculentis®, $P = +20.00D$ Add = +3.00D). Finally, a monofocal IOL (Artisan Aphakia, OPHTECH BV, $P = +20.00D$) was also tested and used as reference.

4.2.2 Measurement protocol

A through-focus with different contrast levels, evaluation of decentration and rotation effect and performance under small pupils for high ($L = 250cd/m^2$), intermediate ($L = 150cd/m^2$) and low ($L = 15cd/m^2$) background luminance was performed per each lens in each condition.

The through-focus was performed from far (0D) to near vision ($-3D$) in 0.5D steps, evaluating at each step the VA and subjective perception in natural pupil conditions. The VA for far and near vision was evaluated with contrast of 100%, 25% and 10% (ETDRS Charts).

The subjective perception was assessed whereby a questionnaire in which the patient has to gradate the intensity of the double vision and the halos from 0 (there was no perception of double vision or halos) to 3 (double vision or halos were clearly presents) for each lens.

The effect of decentration was evaluated measuring the VA and subjective perception when a positioning error of $\pm 0.5mm$ is induced in x and y axis. The decentration is controlled through the reticle of the display of the VirtIOL (Figure 4.0.2).

The effect of orientation was evaluated measuring the VA and subjective perception at three IOL rotations (0, 120 and 240degrees).

Finally, performance under small pupils was evaluated by means of a through-focus with different contrast levels at fixed 3mm pupil.

All the measurements were performed by the same operator and the same well trained observer in order to maintain the same criterion. The observer was a male of 54 years old with a refraction of +1.25D (Add = +2.00D) in the measured eye. Measurements were repeated three times showing similar results.

4.2.3 Results

The through-focus results referring the VA for all the evaluated lenses for a high background luminance are shown in figure 4.2.1. In far vision conditions the best VA was obtained, as

4.2. VISUAL QUALITY PERFORMANCE OF DIFFERENT MIOLS BY MEANS OF A SIMULATED IMPLANTATION

expected with the Artisan IOL ($-0.20 \pm 0.00 \log\text{MAR}$). MIOL lenses showed similar values, with little or no differences, specifically VA for the MPlus was $-0.10 \pm 0.00 \log\text{MAR}$, for the NDIOL-CF $-0.10 \pm 0.00 \log\text{MAR}$ and for the NDIOL-CN $-0.07 \pm 0.05 \log\text{MAR}$. In near vision, the best VA was obtained with the NDIOL-CN ($-0.07 \pm 0.05 \log\text{MAR}$) followed by MPlus ($-0.05 \pm 0.07 \log\text{MAR}$), the NDIOL-CF ($-0.03 \pm 0.05 \log\text{MAR}$) and, as expected, by the Artisan IOL ($0.50 \pm 0.00 \log\text{MAR}$). When measuring under intermediate background luminance, the through-focus curves changed slightly, the MPlus showed a more marked bifocal behavior than the NDIOL. This behavior consisted on an accommodative curve with well identified peaks for far and near vision and decreased intermediate vision. For low luminance conditions NDIOL lens had a nearly flat curve all over the stimulus range, while the MPlus IOL showed two peaks for far and near vision.

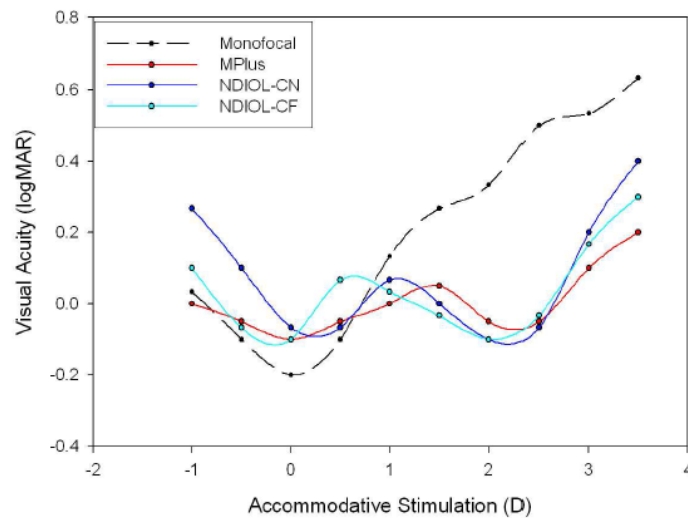


Figure 4.2.1: Visual acuity results for the through-focus for all lenses with natural pupils in high luminance conditions and 100% of contrast.

In terms of subjective perception, the MPlus and NDIOL lenses showed similar results, with low scattering in all the steps of the scanning and increasing double vision in the steps where the VA decreases.

Table 4.2.1: Far Visual Acuity (FVA) and Near Visual Acuity (NVA) in LogMAR units for each contrast level (100%, 25% and 10%) in high luminance conditions.

| MIOL | 100% Contrast | | 25% Contrast | | 10% Contrast | |
|----------|------------------|------------------|------------------|-----------------|-----------------|-----------------|
| | FVA \pm SD | NVA \pm SD | FVA \pm SD | NVA \pm SD | FVA \pm SD | NVA \pm SD |
| Artisan | -0.20 ± 0.00 | 0.50 ± 0.00 | -0.17 ± 0.00 | 0.53 ± 0.00 | 0.04 ± 0.00 | 0.73 ± 0.00 |
| NDIOL-CF | -0.10 ± 0.05 | -0.03 ± 0.05 | 0.03 ± 0.05 | 0.10 ± 0.05 | 0.10 ± 0.05 | 0.17 ± 0.05 |
| NDIOL-CN | -0.07 ± 0.05 | -0.07 ± 0.05 | 0.06 ± 0.05 | 0.06 ± 0.05 | 0.13 ± 0.05 | 0.13 ± 0.05 |
| MPlus | -0.10 ± 0.00 | -0.05 ± 0.07 | 0.03 ± 0.05 | 0.03 ± 0.05 | 0.10 ± 0.05 | 0.15 ± 0.05 |

The VA with lower contrast measurements showed the Artisan IOL losing $0.03 \pm 0.00 \log\text{MAR}$ units at 25% contrast, while the MPlus and NDIOL decreased $0.13 \pm 0.05 \log\text{MAR}$ units at the same contrast. When reducing the contrast up to 10%, all the three lenses showed a similar decrease in the VA of around 2 lines (Table 4.2.1).

Finally, when measuring with small pupils, the overall performance in terms of through-focus with different contrast levels was similar to the obtained under natural conditions. In the MPlus IOL there was a decrease of $0.05 \pm 0.05 \log MAR$ units at the peak VA with $3mm$ pupils, while in the NDIOL there was an increase to $0.08 \pm 0.05 \log MAR$ units.

4.2.4 Conclusions

In terms of VA with lower contrast levels, there were small differences between lenses. As expected, the Artisan IOL showed the best performance under low contrast conditions, with the multifocal designs having slightly higher VA decreased in those conditions.

There was no or little impact of the positioning errors on the visual performance of the IOLs. The only case where there was a change of VA was in the MPlus upper decentration for far vision, where there was an increase of one line of VA as the lens was acting as a monofocal lens due to the decentration.

Due to rotational symmetry of the NDIOL and the Artisan IOL, there was no effect on the visual performance when measuring at the different rotation positions of the lenses. On the other hand, the MPlus, which has a non-rotational symmetrical design, showed angle dependent visual performance.

When measuring with small pupils, the MPlus IOL increased the VA in half line, which is a small difference and could be attributed to be acting as a monofocal lens when operating with such small pupils. On the other hand, the NDIOL lens, suffered a decrease of $0.085 \log MAR$ units when using small pupils of $3mm$.

In summary, VirtIOL vision simulator allowed assessing visual performance of IOL before surgery. In this study this instrument had used to evaluate the performance of the MPlus IOL and to assess the development of a new multifocal IOL prototype, NDIOL. The VirtIOL was able to simulate any IOL design, even the more complex as the MIOLs. The results obtained with the MPlus were in good agreement with the results previously published by other authors [137] when measuring through-focus in patients implanted with MPlus IOL. The through-focus measurements of the VA showed that the MPlus had more marked bifocal lens behavior than NDIOL lenses. Both lenses showed good subjective perception in terms of double vision and halos, and in the preliminary steps of the NDIOL development those measurements helped in a design improvement of the lens.

This study was presented in the 7th European coinciding with the 1st World Meeting in Visual and Physiological Optics (Wroclaw 2014) [78].

4.3 Visual performance comparison between new prototype of a multifocal intraocular lens and a commercial one.

This study was the last one included in the OPHTECH project to finally have all the needed information to add the last improvements in the new MIOL. The study was performed in collaboration with Hospital Universitari Mútua de Terrassa.

The main goal of the study was the improvement of a new MIOL during the development process assessed by the visual performance evaluation measured with VirtIOL (10Lens S.L.U.).

4.3.1 Intraocular lenses

Two different MIOLs and one monofocal IOL were included. A new MIOL design, M5 by OPHTEC, with a central zone corresponding to far refraction was studied. This is a spherical refractive symmetric MIOL with +2.75D of addition. The last version of the M5 IOL (M5CF-O) was used in this study. The commercial Lentis®MPlus (Oculentis®, Add = +3.00D) MIOL was also included. The MPlus is an aspheric asymmetric design with surface-embedded near section [138]. Finally, a monofocal IOL, Artisan Aphakia (OPHTECH BV) was used as a reference.

4.3.2 Patients

Twenty-five eyes of twenty-five healthy presbyopic patients (16 women and 9 men) were included in this study. The mean age \pm the SD of them were 62.96 ± 3.78 years and a range from 58 to 70 years. All of them had been bilaterally implanted with monofocal IOLs 6 months before the measurements. Due to this, problems of transparency or of accommodation are avoided. In terms of refractive error, the value of the sphere was between $-1.00D$ and $+1.00D$ and a value of astigmatic error between $0.00D$ and $-0.50D$. Furthermore, the visual acuity was 1.0 or upper in the decimal system.

Only one eye of each patient was measured. It was chosen randomly since both eyes were at the same conditions.

The study followed the tenets of the Declaration of Helsinki and all patients signed the informed consent after they were explained the nature procedures and aims of the study.

4.3.3 Measurement protocol

Visual Acuity (VA) and visual preception were evaluated per each included lens by means of a through-focus using VirtIOL. The through-focus was performed from $+1.00D$ relative to the far vision of the patient to $-3.00D$ in steps of $-0.50D$, that is equivalent to an accommodative stimulation from $-1.00D$ to $+3.00D$. Contrast Sensitivity (CS) was only evaluated for far (accomodative stimulation of $0.00D$) and near vision (accomodative stimulation of $2.75D$). Trial lenses were used for inducing the accommodative stimulus.

VA was evaluated using Snellen chart which presents 4 different letters per each line of vision. The visual perception was assessed in terms of dispersion, halos and double vision in each step of the through-focus. The patient punctuated his perception form 0 to 3 (0: minimum, 3: maximum). CSV-1000 test was employed to obtain CS data.

The room was under low luminance conditions and the patients had a pupil of around 4-5mm for far vision.

The three IOLs (M5CF-O, MPlus and Artisan) were randomly evaluated in order to avoid a possible learning effect.

4.3.4 Results

The through-focus curves of the three IOLs are shown in figure 4.3.1. The graph plots the visual acuity (in decimal units) against the accommodative stimulation (D).

4.3. VISUAL PERFORMANCE COMPARISON BETWEEN NEW PROTOTYPE OF A MULTIFOCAL INTRAOCULAR LENS AND A COMMERCIAL ONE.

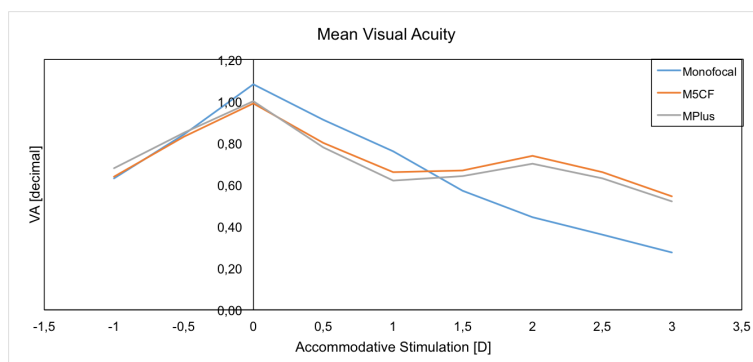


Figure 4.3.1: Mean defocus curves, representing the visual acuity (VA) in decimal units [decimal] against the accommodative stimulation in diopters [D].

The best visual acuity for far vision was achieved by means of the monofocal IOL (Artisan), as expected. There was a slight difference between the multifocal lenses, MPlus and M5CF-O. Regarding the near vision, both MIOLs had again similar values, while the monofocal one (Artisan) had a clearly lower near VA.

In terms of the shape of the curve, the Artisan IOL showed only one peak, as it is normal due to its design. On the contrary, the MIOLs showed a bifocal shape, with good far and near visual acuity and slightly worse at intermediate distances. Both MIOLs had very similar curves.

The results about visual perception in terms of halos, dispersion and double vision were also analyzed. In all perception parameters both MIOLs obtained similar values. Regarding halo perception, it is a little bit lower in the case of the M5CF-O. In terms of double vision and dispersion were practically the same. No detection of halos, dispersion or double vision was expressed by any included patient for the Artisan IOL.

In agreement with VA and visual perception results, both MIOLs obtained pretty similar results both in far and in near vision. Artisan IOL had a higher contrast sensitivity in far vision and a similar one in near vision in comparison with the MIOLs.

4.3.5 Conclusions

The behavior of the new multifocal IOL prototype, M5CF-O, was tested and compared with a monofocal (Artisan Aphakia) and a commercial one (MPlus) by means of the VirtIOL prior to surgery.

The main conclusion was that M5CF-O was as good as MPlus and that some changes should be applied in the optical design to be able to improve the intermediate vision.

5. Open-field double-pass system with asymmetric focus (DPAF)

This chapter presents the new compact open-field double-pass system with asymmetric focus (DPAF) that it has developed throughout this thesis.

As it was mentioned before, the main difference between this system and other commercial or customized double-pass systems is the fact that this has asymmetric focus. This means that the focus of the first and the second pass are totally independent. This property makes possible to send a focused source point image on the retina of the patient while a through-focus along the power range of the MCL or MIOL is performed with the second pass. So as to achieve this condition a customized opto-mechanical design and management software have been developed.

5.1 Opto-mechanical design and assembled prototype

Some important factors had considered to decide the optical design. One of them was the use of electro-optical lenses (EOLs) as an optometers. This way was possible to optimize as much as possible the dimensions of the instrument. Sanabria *et al.* demonstrated the suitability of these kind of lenses to be used as an optometer [99]. Another factor was the decision of assembling an open-field instrument to avoid instrument myopia [139]. Finally, it was also decided to use a high sensitivity camera to be able to notice any difference among all the images of the through-focus. Once all these considerations were clear, different configurations were simulated to choose the one represented in figure 5.1.1.

The optical design shows that the first pass starts with a collimated laser of 780nm wavelength (C7805M – SMF, Monocrom S.L.) that passing through an entrance pupil (EP) of 2mm and the EOL 1 (Optotune EL-10-30 IR (Optotune Switzerland AG)), is then reflected by mirror 1 (M1) to the hot mirror (HM) going through a beamsplitter (BS) and a 60mm focal length achromatic doublet (L1). The HM reflects again the light to cross the dichroic filter (DC) and arrive to the eye, which focuses the laser point source on the retina. At this point, the first pass ends and the second pass starts with the reflection of the point source on the retina. After going through the optics of the eye, the DC, the HM and the L1 again, BS reflects the retinal reflection to the EOL 2 (Optotune EL-10-30 IR (Optotune Switzerland AG)). The EOL 2 collimates the light and direct it by mirror 2 (M2) to an afocal system, constituted by two 100mm focal length achromatic doublets (L2 and L3). Then the collimated light is reflected by mirror 3 (M3) and arrive at the camera lens passing first through the 4mm exit pupil (ExP). The camera lens focuses the retinal reflection on the CMOS (Complementary Metal Oxide Semiconductor) sensor of the camera (DP camera)(ORCA-flash 4.0 V2 CMOS camera C11440-22CU (Hamamatsu Photonics K.K.)), finishing the measurement with the registration of the DP image. Following manufacturer's suggestions, both EOLs were horizontally positioned to prevent coma aberration (Appendix 2).

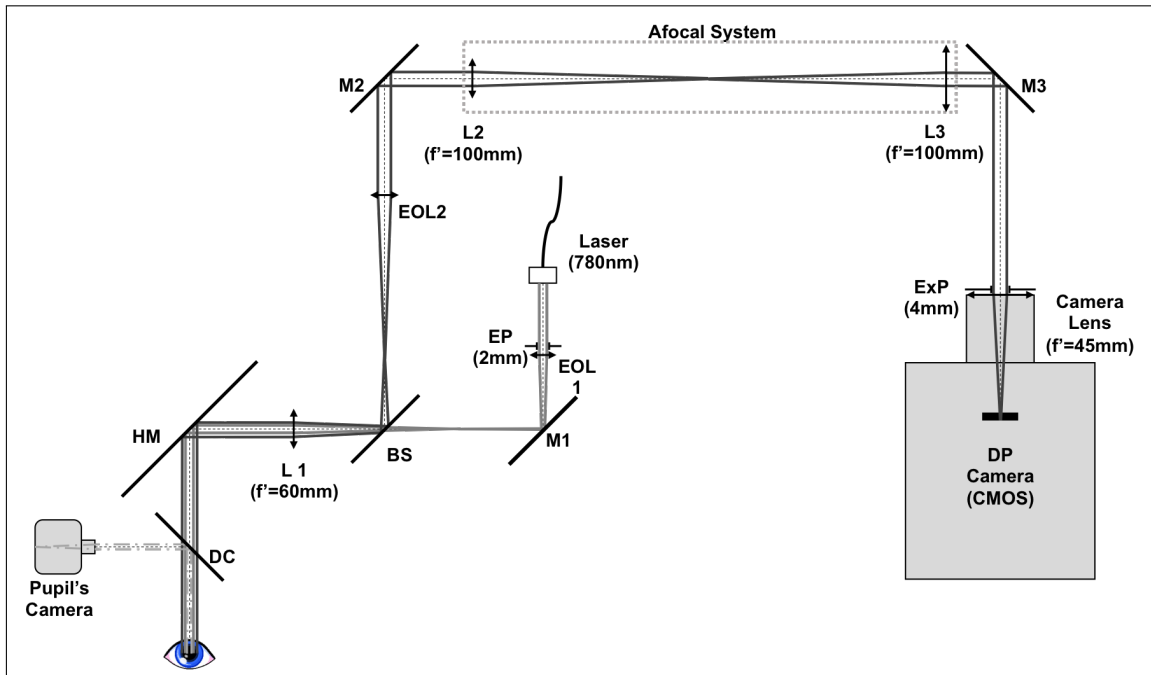


Figure 5.1.1: Optical System Design composed for laser, EP (entrance pupil), EOL1 (electro-optical lens 1), M1 (mirror 1), BS (beam splitter), L1 (lens 1), HM (hot mirror), DC (dichroic filter), Pupil's Camera, EOL2 (electro-optical lens 2), M2 (mirror 2), Afocal System (L2 (lens 2) and L3 (lens 3)), M3 (mirror 3), ExP (exit pupil), Camera Lens and DP Camera (double-pass camera).

A vibrating motor was added in the mounting of the HM to act as a scanning mirror [140] and avoid speckle problems.

A pupil's control system have been also added in the design to control the centration of the eye and to be sure that the eye's pupil plane is conjugated with entrance and exit pupil of the instrument. The pupil's control system is composed for IR LEDs ($\lambda = 950nm$), the DC mentioned before, and a camera (pupil's camera). The camera has to be focused where the eye's pupil plane has to be placed to be conjugated with entrance and exit pupil of the system.

The diameters of the EP and the ExP are different to not loose the phase information of the OTF (explained in chapter 2). In 1995, Artal *et al.* demonstrated that if a DP system works with symmetric pupil's diameters this loss takes place. As a consequence, the coma aberration is disregarded and the optical quality of the measured optical system is overestimated [96].

A customized semi-closed mechanical system was created to assembled the prototype of this new and compact DPAF (Figure 5.1.2). The global dimensions of the system are $60 \times 40 \times 40cm$ (length x width x height). A head support was also added in front of the IR LEDs to be able to fix the position of the patient's eye that has to be evaluated *in-vivo*.

In addition, there are some elements of the instrument that need to be managed electronically. For this reason, are also part of the system one customized electronic box and a personal computer (PC). The laser, the IR LEDs, the vibration motor, and both EOLs are connected to the customized electronic box. Pupil's camera, DP camera and the electronic box are directly connected to the PC. A couple of softwares were employed to control the system and manage the DP data. A detailed explanation is found in the following section.

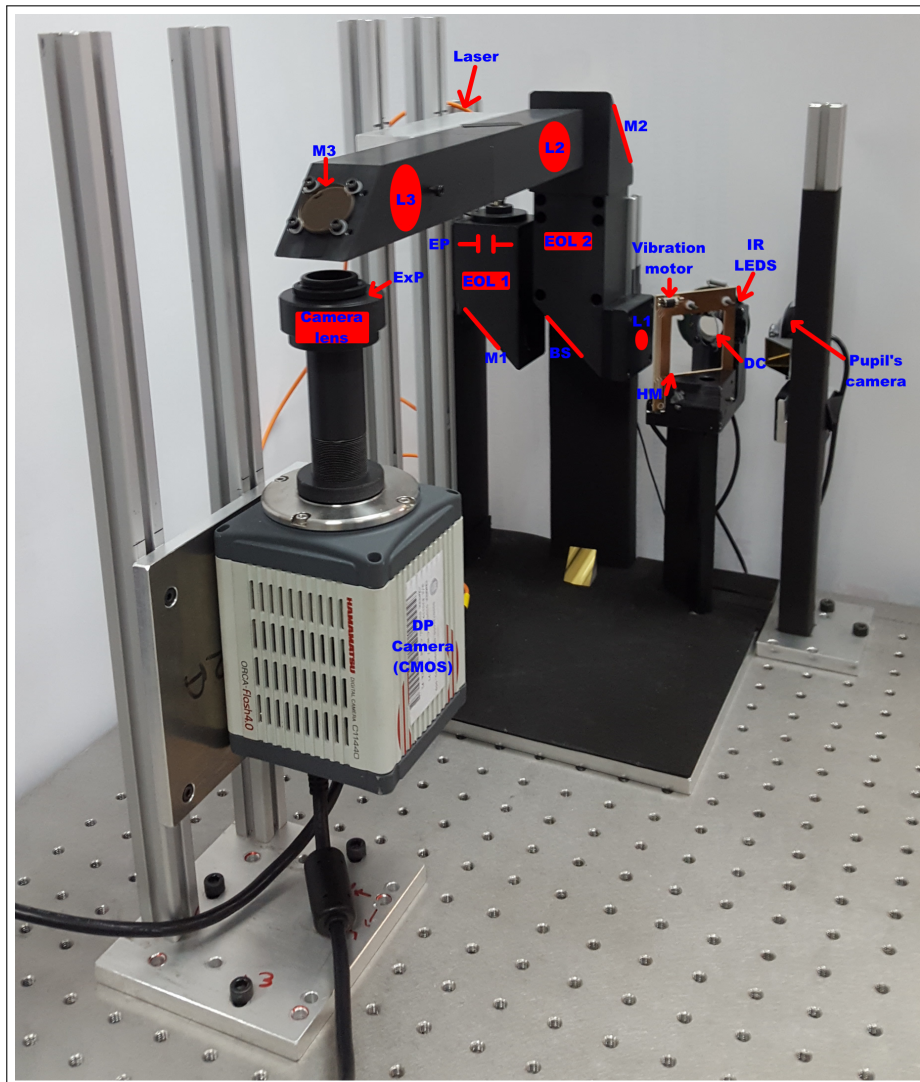


Figure 5.1.2: Image of the DPAF prototype assembled in our laboratory.

5.2 Control and analysis software

A software based on two different interfaces was employed for the DPAF: the first one, to control all the hardware of the system (laser, IR LEDs, vibration motor, EOLs, and both cameras), and the second one, to analyze the data that is needed to evaluate the optical quality of the measured human or model eye adapted with a MCL or implanted with a MIOL.

The software was developed by using Matlab (Mathworks, 2016).

5.2.1 Control interface

Control interface can be divided in three different parts (figure 5.2.1): management of the hardware (green square), measurement options (purple square), and data acquisition (orange square).

The management part has first the real-time image of the DP and the pupil's camera. Just below the initialization box is found and it used to switch on or off: the electronic box (*Port*), both cameras, vibrator, and IR LEDs. It is possible to control the intensity of the IR LEDs (from

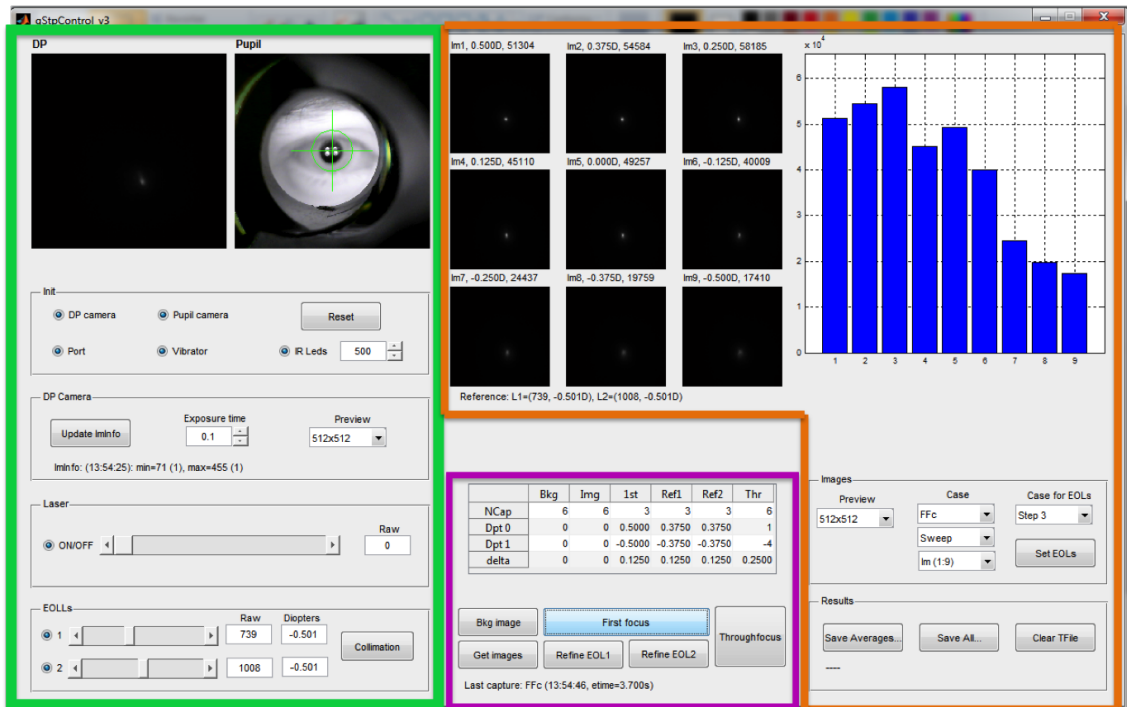


Figure 5.2.1: Image of the graphical interface of the control part.

0 to $1000a.u.$). DP camera has a specific box where the highest grey level of the real-time image can be gotten at any moment (*Img info: + Update ImInfo*), the exposure time can be chosen (from 0.01 to 10.00ms), and the size of the real-time DP image can be changed (2048×2048 , 1024×1024 , 512×512 , or 256×256). Finally, a control box for the laser and another for both EOLs are also included in this part. In the case of laser can be activated or deactivated and its intensity can be controlled (from 0 to $2000a.u.$). The EOLs can be switched on or off and the level of current (from 0 to $2000a.u.$) and/or the dioptric power of them can be manually changed (from -8.00 to $+7.00D$). They have also a collimation button to automatically change their dioptric power to $0D$.

The purple square contains the different possibilities to measure. As it is easy to distinguish, there are six kinds of measurements:

- Background Image (*Bkg images*): to get background images at an specific dioptric power of the EOLs.
- Images (*Get images*): to register DP images at an specific dioptric power of the EOLs.
- First focus (*First focus*): to capture all the images of the symmetric DP analysis in any diopter range. In this measurement both EOLs have the same dioptric power along the scan.
- Refine 1st pass (*Refine EOL 1*): to make a scan of a little range of diopters only changing the dioptric power of EOL 1.
- Refine 2nd pass (*Refine EOL 2*): *idem* than *Refine EOL 1* but only changing the dioptric power of EOL 2.
- Through-focus (*Throughfocus*): to register every DP image along all the power range of the implanted MIOL or adapted MCL of the analyzed eye. This is the main measurement of

our prototype. In this case the EOL 1 reminds in the dioptric power that compensates the refraction of the measured eye and the EOL 2 change its dioptric power to analyze all the power range of the multifocal lens.

Is it possible to choose the number of captions ($NCap$), the range of dioptric power that needs to be scanned ($Dpt\ 0$ and $Dpt\ 1$) (from $-8.00D$ to $+7.00D$) and the power steps of the analysis which can be from $0.125D$ to $2.00D(\delta)$. Taking as example the through-focus column of the characteristics table (Thr), the information should be understood that 6 images are going to be captured and averaged at each step. The analyzed power range is going to be from $+1D$ to $-4D$ of the initial power position of the EOL 2 in steps of $0.25D$. This can be change in any moment for any kind of measurement explained above.

There's a third part which function is to check and saved the acquired DP images. Any averaged image for each step of the scanning can be observed in the group of the nine little squares. In addition, the maximum grey level of each image is shown on the top of each square. In the left big square there is a bar graphic of the maximum grey level of each image, making easier the choice of the best or group of best DP image/s. Thanks to the images box (*Images*), the size of the shown images can be chosen by *Preview* option (2048×2048 , 1024×1024 , 512×512 , or 256×256), the specific correlatives nine averaged images of the scanning that are shown can be changed by *Case* option ($1 - 9$, $10 - 18$, $19 - 27, \dots$), and the power of both EOLs can be changed to the specific power of any acquired image by using the option *Case for* and clicking *Set EOLs* button. Finally, two different options to save the DP images are possible. One option is only save the averaged image for each step (*Save Averages...*) and the other is to save every caption and the averaged image for each analyzed step (*Save All...*).

5.2.2 Analysis interface

The analysis interface is necessary to process the DP images and to obtain the value of several parameters which determinate the optical quality of the measured eye along the power range of the MIOL or the MCL with which is implanted or adapted.

Figure 5.2.2 shows that the analysis graphical interface is divided in two main parts.

The first part indicated with the green square gives all the visual information about the analyzed DP image. In the included image are represented two different pseudo-colored DP images where each color indicates each grey level (*blue = low*), *red = high*). This way it is possible to do a visual interpretation of the energy distribution of any image. The image represented in the left square is indicated as *DPL* (Double-Pass Left) and the one in the right square is indicated as *DPR* (Double-Pass Right). The *Image* menu allows to choose the DP image or images that have to be analyzed and also the background image or images that should be subtracted from the DP one/s. If more than one image is selected, the averaged image is represented in the graphic dialog. The centered drop-down menu is used to choose the image or curve that the professional wants to observe (Figure 5.2.3). The *Point Spread Function* (PSF) and the *Modulation Transfer Function* (MTF) of any processed image can be represented once the analysis and calculations are done. The name of the selected files are next to this drop-down menu. The table that is just below of the *Image* menu allows to configure other parameters of the images that were not used in this thesis.

The second part includes the analysis box where it can be chosen which image have to be

5.2. CONTROL AND ANALYSIS SOFTWARE

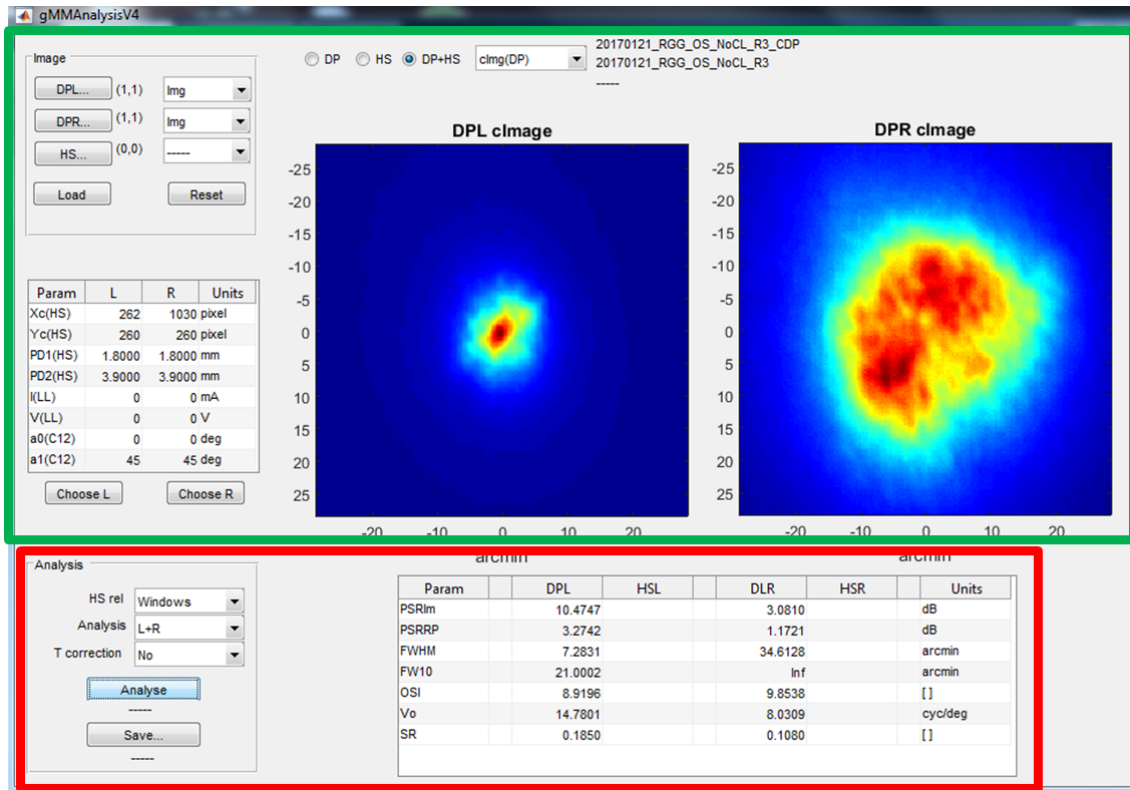


Figure 5.2.2: Image of the graphical interface of the analysis part.

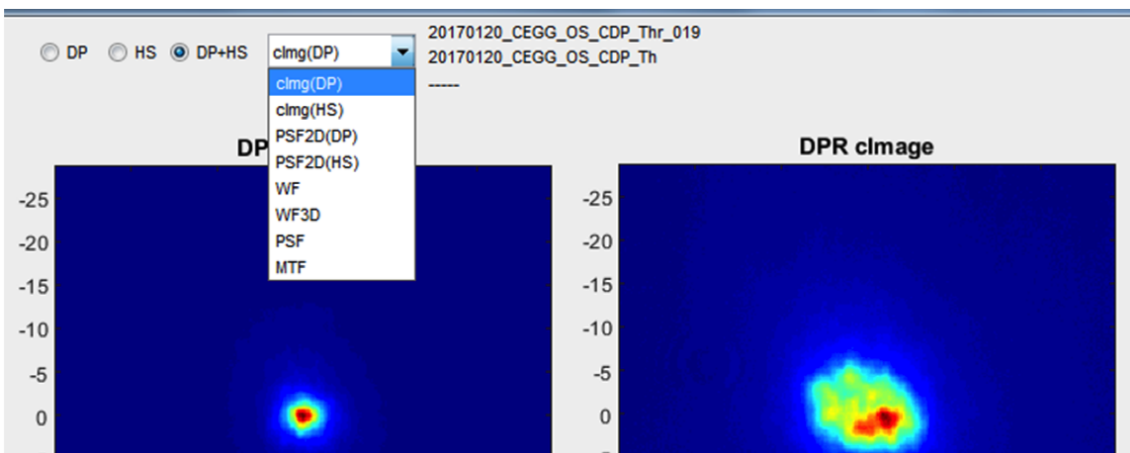


Figure 5.2.3: Image of the centered drop-down menu to choose the image or curve that can be shown in the graphical areas.

analyzed: the (*DPR Image*), the (*DPL Image*), or both at the same time. The rest of the options included in this menu were not either employed in this thesis. This second part also includes the DP parameters table. This table contains seven different parameters, but only three of them were considered in our work: the *FWHM* (Full Width Half Maximum) of the PSF, the cut-off of the MTF (*Vo*), and the Strehl ratio (*SR*).

All the graphical and numerical information obtained with this interface has made it possible to do a complete evaluation of the optical quality of the measured eyes implanted with a MIOL

or adapted with a MCL in each analyzed position of their power range.

5.3 System's validation

Different characterizations and validations of some elements and the whole system were done.

5.3.1 Characterization of electro-optical lenses (EOLs)

The DPAF prototype is compounded by several programmable elements as are the cameras, the laser, etc... But ones of the most important are the EOLs, since they are the base of the function of the system. EOLs are essential to achieve the assessment of the optical quality along the whole through-focus. Due to this reason, the first thing that it was done to evaluate the function of the system was the characterization of both EOLs (Figure 5.3.1). It consisted on placed the EOLs on a lensmeter and registered the dioptric power for each level of current. The current level was change in steps of $20a.u.$. Four different rounds were performed for each EOL: two of them were done from the maximum level of current to the minimum, and the other two in the inverse direction. Based on the power results, focal lengths were calculated obtaining that the focal length range \pm SD for EOL 1 is from $141.18 \pm 6.99mm$ to $46.60 \pm 0.16mm$, and from $164.38 \pm 5.22mm$ to $53.33 \pm 0.21mm$ for EOL 2.

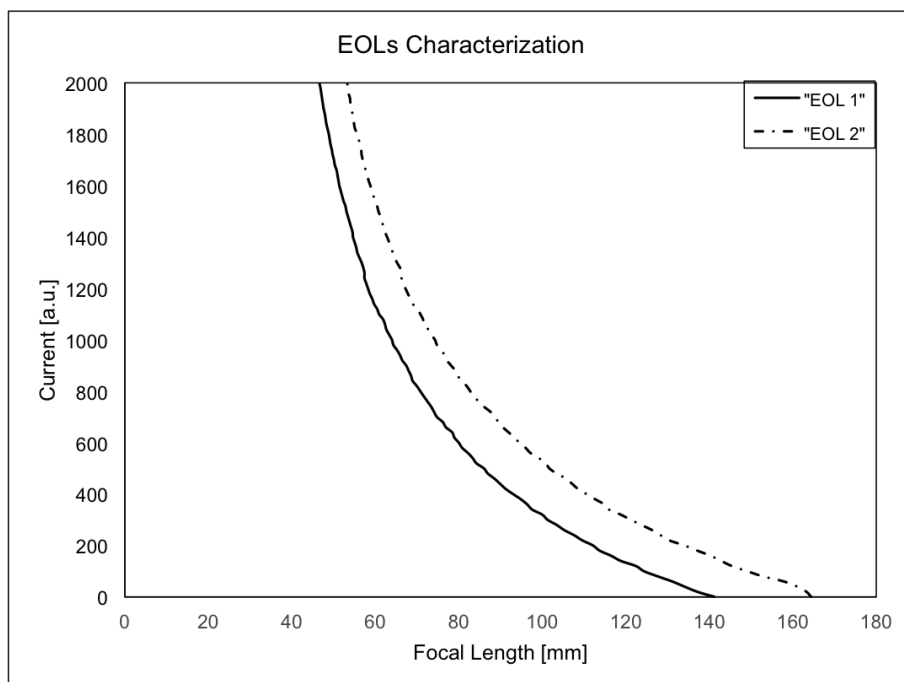


Figure 5.3.1: Characterization of the focal length of both EOLs based on the level of current.

These curves of the focal length dependent on the level of current allowed to estimate the current offset that it is necessary to apply to have the same dioptric power with both lenses, the amount of current that is necessary to change the power in any dioptric step (f.e: steps of a quarter or a half diopter), the amount of current that each EOL needs to measure an emmetropic eye (collimated configuration) and the power correction range of the system.

Once the DPAF was assembled, it was proved that the light was collimated at the end of the 1st and the 2nd pass in the collimated configuration. So as to check the collimation at the end of the 1st pass, a camera focused to infinity was placed in the Exit Pupil (ExP) plane of it and a focused point source image was captured. Then, a flat mirror was positioned at the Entrance Pupil (EP) plane of the 2nd pass, which is also the ExP plane of the 1st one, and the camera used before was placed in the ExP plane of the 2nd pass. A focused point source image was also registered. Finally, the DP camera of our prototype was added and it could be checked that it was also well focused to infinity.

Another aspect that was verified was the power correction range of the system. This time the pupil's plane of the model eye, described in chapter 4, was situated at the ExP's plane of the 1st pass. A monofocal IOL was inserted in the model eye to act as a crystalline lens and a black cardboard was placed after the last BK – 7 window to act as a retina. Trial spherical lenses with positive and negative powers were placed in front of it to change the refraction of the eye and correct it with the optometers of the set-up. A symmetric double-pass analysis of 2D in steps of 0.25D was performed per each used trial lens. Then, the 8 images were analyzed to check that the current level of both EOLs of the best image corresponded to the created ametropia of the model eye. The result was a power correction range from $-9.00D$ to $+10.00D$, as expected (Figure 5.3.2).

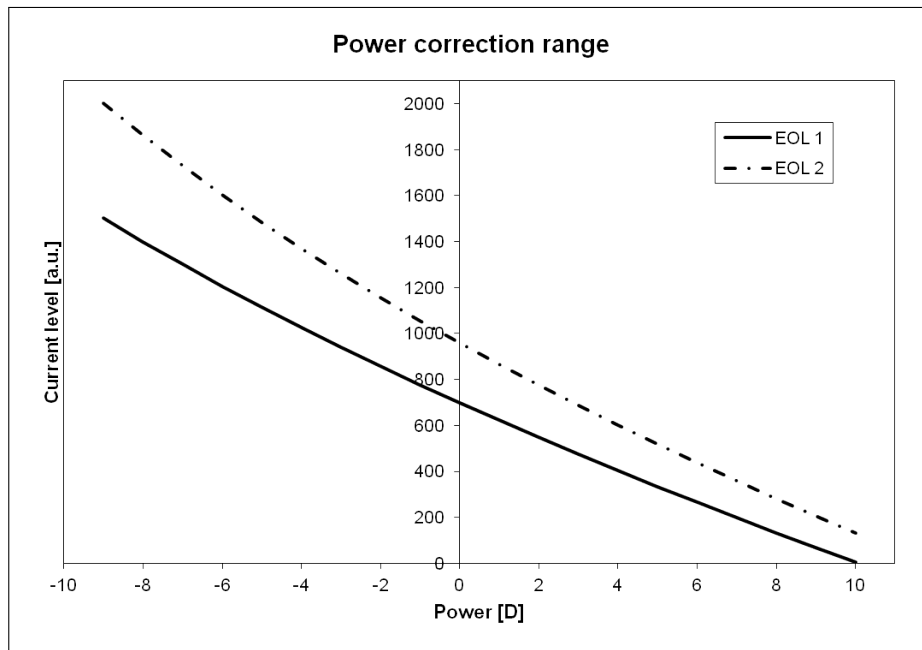


Figure 5.3.2: Power correction range based on the current level of each EOL.

5.3.2 Validation of the laser power

Due to the fact that this system has to do in vivo measurements, it was also necessary to measure the intensity of the laser to verify the intensity established in the regulation IEC 60825-1 [141]. It defines the maximum tolerable values of a laser exposure depending on the wavelength of the laser and the exposure time. The DPAF has a laser of 780nm wavelength and exposure times longer than 10s. Thus, the maximum tolerable exposure for this prototype power on the cornea is $14.45W/m^2$.

The maximum value of a the laser exposure on the cornea in the DPAF is $6.99W/m^2$. Although, the system was never used in this condition. The value was never higher than $1.98W/m^2$ in all the measurements. The power of the laser was measured by means of the power meter PM100D with the power sensor S120C (Thorlabs, Inc). All the measurements were performed in dark room conditions.

5.3.3 Optical validation of the DPAF

Once the specific elements characterization and validation was finished, the optical validation of the whole system was performed.

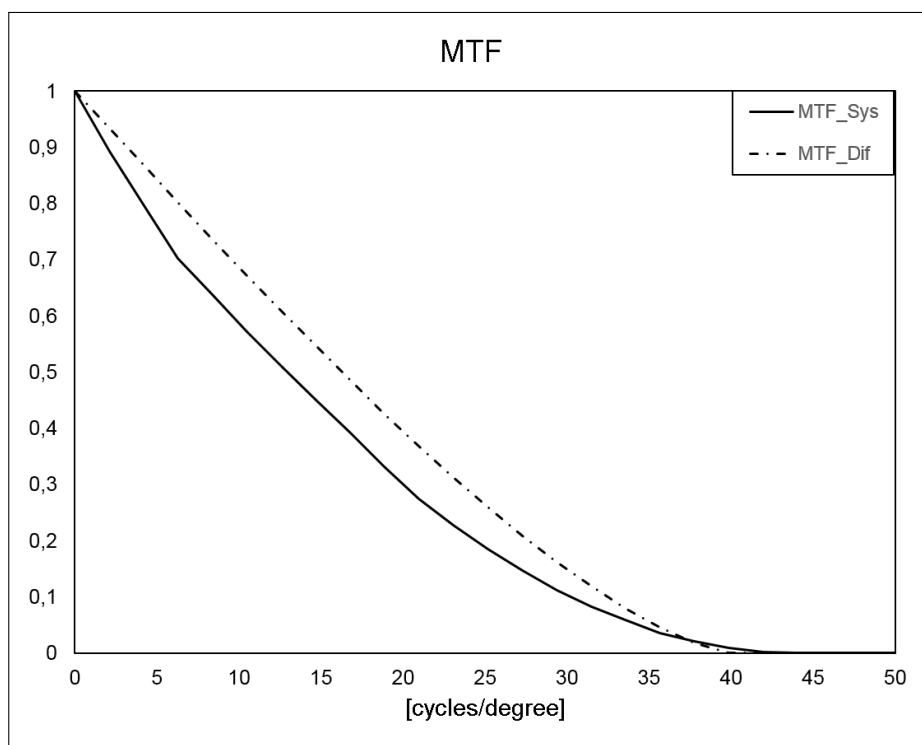


Figure 5.3.3: Graphic representation of the MTF of the system (solid line) and the MTF limited by diffraction (dashed line) that were used to do the optical validation.

As in the collimated configuration validation is explained, a plate mirror was placed in the ExP's plane of the 1st pass and three images of the laser point source going through the whole system were captured. The measurements were done with an EP's diameter of $2mm$. The average of those images were obtained and different Fourier calculations were done to get the MTF of the experimental set-up. This MTF was compared with the MTF limited only by diffraction and the Strehl ratio was calculated. As figure 5.3.3 shows, the obtained MTF of the system is a little bit lower than the limited by diffraction. However, the value of the Strehl ratio was 0.86, thus it is possible to consider the system as limited by diffraction [142, 143].

5.3.4 Validation of the through-focus measurements

The last step in the validation of the assembled system was the optical quality characterization of two different MIOLs implanted in a model eye.

5.3.4.1 Methods

Model Eye

The used model eye was the same customized model eye presented in chapter 4. The same way that in the validation of the power range (Subsection 5.3.1), a black cardboard was placed after the second $BK - 7$ window to act as a retina.

MIOLs

Two MIOLs were used to perform the in vitro measurements: One concentric diffractive MIOL (AcrySof®IQ ReSTOR®SN6AD1, Alcon Novartis Company) and, one non-concentric refractive MIOL (non-commercialised MIOL). The diffractive MIOL has a large number of concentric rings with little sharp edges that create different and independent focal points thanks to constructive interferences [144]. The diffractive lens used in this study has a dioptric power of $+21.00D$ with an addition of $+3.00D$. In contrast, the non-concentric refractive MIOL has an asymmetric distribution of different refractive zones that correspond to different distance vision. Each zone has a different value of curvature radius. The refractive MIOL has a power of $+20.00D$ with an addition of $+2.75D$. In contrast with the diffractive MIOLs which the whole optical zone contributes to all focal points, in the refractive MIOLs each refractive zone refracts the light to the associated focal point [84].

Measurement protocol

First of all, the MIOL was introduced and well-centred in the wet cell of the model eye. Then, a symmetric double-pass analysis was performed to find the far focus of the lens. This means, that the first and the second pass change their focal position symmetrically at the same time. After the far focus was found and consider it as $0.00D$ position, an asymmetric double-pass analysis was done. The asymmetric analysis consists in performing a through-focus 5 dioptres changing the focal position of the second pass, while the first pass was remaining fixed in the focal position found in the symmetrical analysis. EOL 2 change its power from $+0.75D$ to $-4.00D$ in steps of $0.25D$ to do the through-focus. As a consequence, the system is creating an accommodative stimulation from $-0.75D$ to $+4.00D$ in steps of $0.25D$. Six images per each step were gotten. This procedure was repeated three times. The intensity of the laser was adjusted for far focus results and remained constant along the whole through-focus.

Data analysis

The double-pass images gotten per each step of the through-focus were averaged and from these images the MTF of each step were obtained. Normally, the MTF is normalized to 1 at frequency 0, but in our analysis the normalization is done by an exponential adjustment. This needs to be done due to the peak that appears at frequency 0 in the modulus of the Fourier transform of retinal images [96].

The Full Width at Half Maximum (FWHM) values of each double-pass image and the MTF cut-off and the Strehl ratio values were calculated by the analysis software (Section 5.2.2).

5.3.4.2 Results

Four of the most representative double-pass images of the through-focus of each lens are shown in figures 5.3.4 and 5.3.5. The differences between the images that correspond to one of the focus and the out of focus images are very noticeable. It is also possible to distinguish differences between the refractive and the diffractive MIOL.

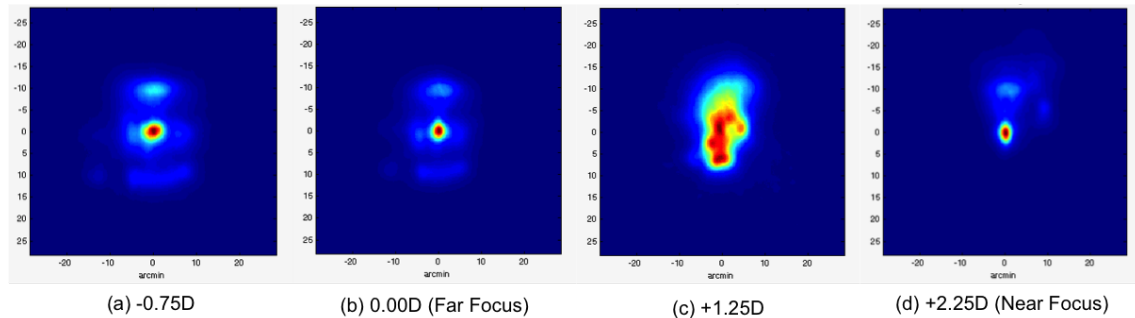


Figure 5.3.4: Double-pass images of a non-concentric refractive MIOL (Power = +20.00D / Addition = +2.75D). The power indicated in the images is the value of the accommodative stimuli per each one.

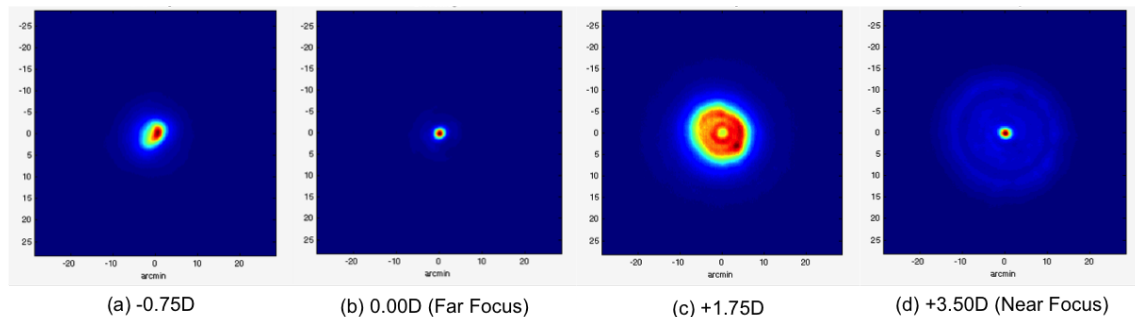
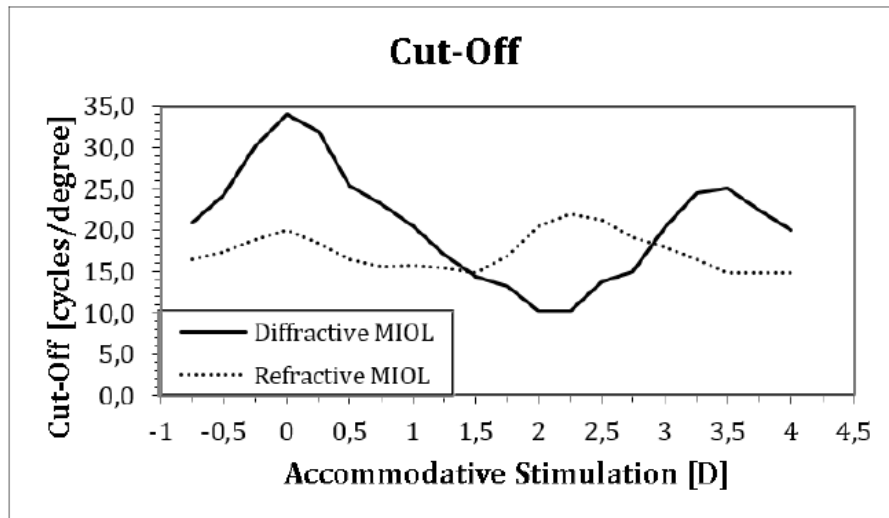


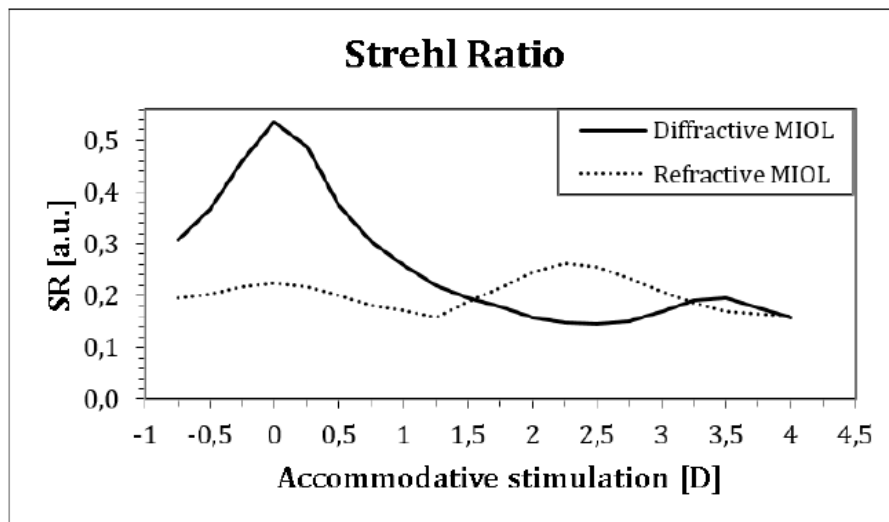
Figure 5.3.5: Double-pass images of the concentric diffractive MIOL (AcrySof®IQ ReSTOR®SN6AD1) (Power = +21.00D / Addition = +3.00D). The power indicated in the images is the value of the accommodative stimuli per each one.

Taking into account the described analysis of the data (section 5.3.4.1), the results of the FWHM, MTF cut-off and Strehl ratio are also shown in figure 5.3.6.

The curves of the MTF cut-off and the Strehl ratio indicate that the optical quality of the far focus is significantly better than the near focus in the case of the diffractive MIOL. The values of the MTF cut-off and the Strehl ratio are $34.05 \pm 0.18 \text{cycles/degree}$ and 0.53 ± 0.01 for the far focus and $25.015 \pm 0.27 \text{cycles/degree}$ and 0.19 ± 0.00 for the near focus. In contrast with the diffractive MIOL, the curves of the MTF cut-off and the Strehl ratio of the refractive MIOL show that the near focus and the far focus have similar results. In this case, the values of the MTF cut-off are $20.06 \pm 0.14 \text{cycles/degree}$ and $21.91 \pm 0.18 \text{cycles/degree}$ for far and near focus, and the values of the Strehl ratio are 0.23 ± 0.00 and 0.26 ± 0.01 respectively.



(a)



(b)

Figure 5.3.6: (a) MTF cut-off values of the diffractive and the refractive MIOL along the through-focus; (b) Strehl ratio values of the diffractive and the refractive MIOL along the through-focus.

5.3.4.3 Conclusions

A through-focus has been able to perform with a refractive MIOL and with a diffractive MIOL implanted in a customized wet model eye. In both cases, the imaging and the numerical results determine the far and the near focus.

Results show that the optical quality of the far focus of the diffractive MIOL used in this study is quite better than the far focus of the refractive MIOL. However, the optical quality of the near focus of the refractive MIOL is similar to the near focus of the diffractive MIOL. Moreover, it is also perceptible that the optical quality of the far and the near focus of the refractive MIOL are similar, yet in the diffractive MIOL are different.

Taking into account all these facts, the main conclusion is that the DPAF was able to perform a through-focus measurement along the power range of two different MIOLs.

5.3. SYSTEM'S VALIDATION

This validation was published in "*Óptica Pura y Aplicada*" last April with the following title: *New compact open-field double-pass system with asymmetric focus* [145].

6. Objective evaluation of the optical quality of patients implanted with multifocal intraocular lenses by means of DPAF: Preliminary study

This chapter includes a preliminary study to assess the suitability of the new DPAF to determine the optical quality of eyes implanted with a Multifocal Intraocular Lens (MIOL) in *in-vivo* conditions.

6.1 Assessment of the optical quality of patients implanted with a multifocal intraocular lens

6.1.1 Patients

This time were included seven eyes of seven different patients (4 women and 3 men). The mean age \pm SD was 62.29 ± 6.34 years with a range from 55 to 72 years. All the patients were bilaterally implanted with MIOLs six months before the participation in this study, the earliest, and one year before, the latest. Thanks to these conditions, any adaptation or transparency problems were avoided.

Only the left eye of each patient was measured. The exclusion criteria for this study was the fact that the patient need any spectacle support to have a focus vision in any distance. The study followed the tenets of the Declaration of Helsinki and all the patients signed the informed consent after they were explained the nature, procedure and aims of the study.

6.1.2 Multifocal Intraocular Lens

The seven included patients were bilaterally implanted with the new MIOL Precizon Presbyopic (OPHTEC B.V., Groningen, Netherland). This lens is thoroughly described in section 2.1.2.1 of the second chapter of this thesis.

6.1.3 Measurement protocol

The measurement protocol used in this study was the following. First of all, through-focus of the VA of the left eye from -4 to $+1.5D$ in steps of $0.50D$ was done by negative lenses and a logMAR chart. Then, the measured eye was centered in the DPAF to assess the optical quality of it. At the beginning, a symmetric Double-Pass (DP) analysis along $2D$ in steps of $0.25D$ was done to correct the spheric refractive error. The spheric refractive error corresponded to the best double-pass

6.1. ASSESSMENT OF THE OPTICAL QUALITY OF PATIENTS IMPLANTED WITH A MULTIFOCAL INTRAOCULAR LENS

image found with the symmetric DP analysis. Once the best double-pass image was found, the initial position to perform the through-focus was defined and the configuration of the first pass of the system was fixed. Secondly, a whole through-focus from $-4D$ to $+1.5D$ in steps of $0.50D$ was performed by the second pass. Three repetitions were registered. Each captured image was the average of 6 captions in each step of the through-focus. Finally, the analysis of each image was done to assess the optical quality of each measured eye with the implanted MIOL.

All the measurements were performed with the natural pupil of the patient in a very low illumination conditions (the only light of the room was the monitor of the PC in the lowest possible brightness mode). This fact assure that the natural pupil of the patients were $\geq 4mm$ achieving that the pupil of the system was the one that limited the measurements. Non cyclopegic drugs were used.

The measurements were done by the same optometrist in only one session per each patient.

6.1.4 Results

The most representative results of this study are included in this subsection.

Figure 6.1.1 shows the DP images of a complete through-focus from $-4D$ to $+1.5D$ in steps of $0.50D$ registered by the DP camera of the DPAF system. When this through-focus is just visually observed, it looks like the DP images from $-1.00D$ to $+1.00D$ remain with a similar optical quality.

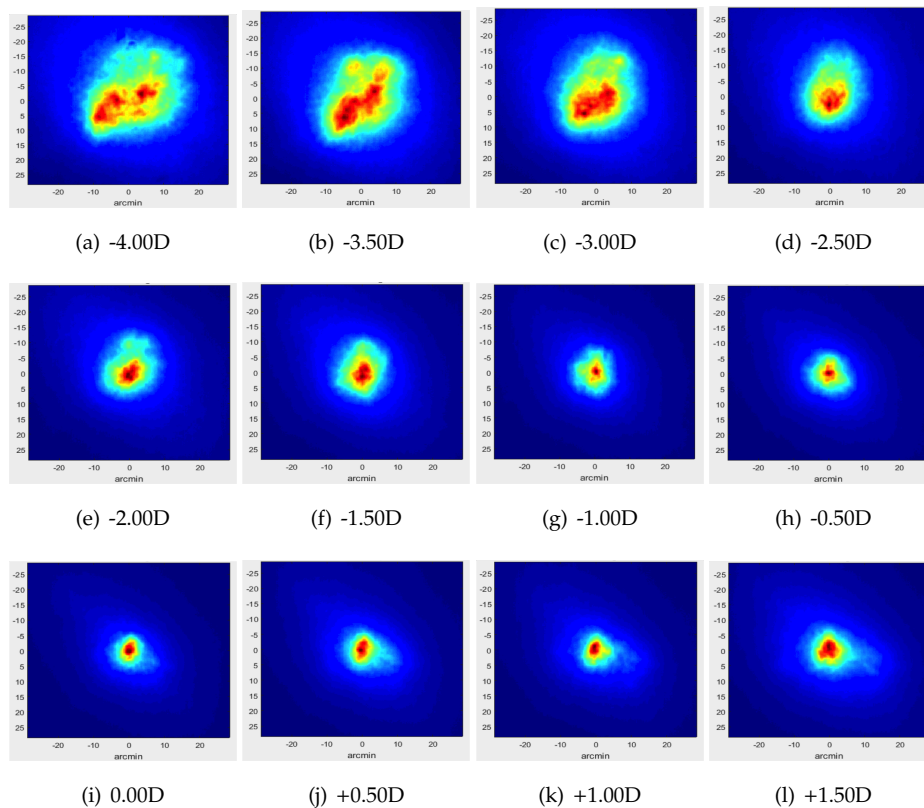


Figure 6.1.1: DP images of a through-focus from $-4D$ to $+1.5D$ in steps of $0.50D$.

Once all the DP images were obtained, an optical quality analysis was done per each step of the through-focus by means of the analysis software described in section 5.2.2 of the previous chapter.

6.1. ASSESSMENT OF THE OPTICAL QUALITY OF PATIENTS IMPLANTED WITH A MULTIFOCAL INTRAOCULAR LENS

On one hand, the mean Modulation Transfer Function (MTF) of each step of the through-focus was obtained. Figure 6.1.2 shows the MTFs from $-4D$ to $+1.5D$ in steps of $0.50D$. The theoretical MTF of a perfect optical system only limited by the diffraction that a pupil of $4mm$ would produce, is also represented in this graph in black (indicated as DIF in the legend). Such as the DP images suggested, the best MTFs were the ones between $-2D$ and $+1D$. Although, the MTF of $0D$ and the one of $-0.5D$ are lightly better than the others.

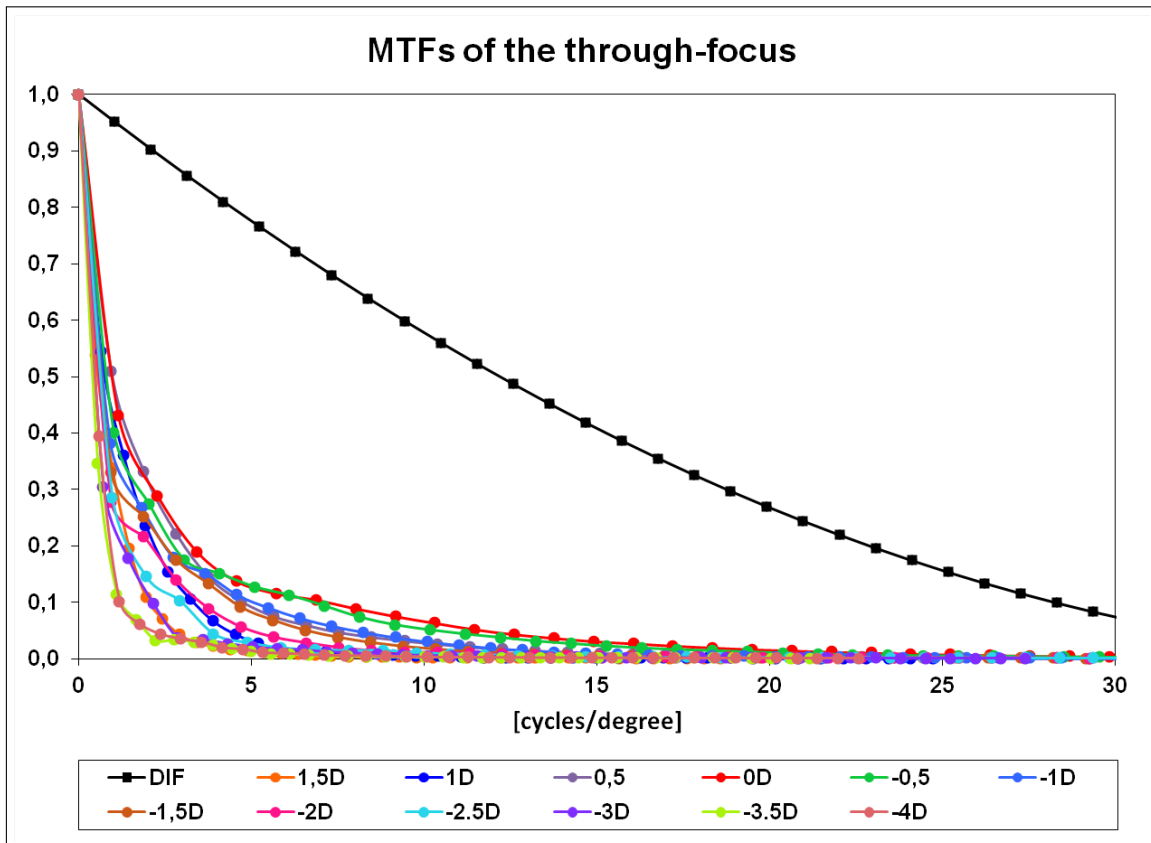


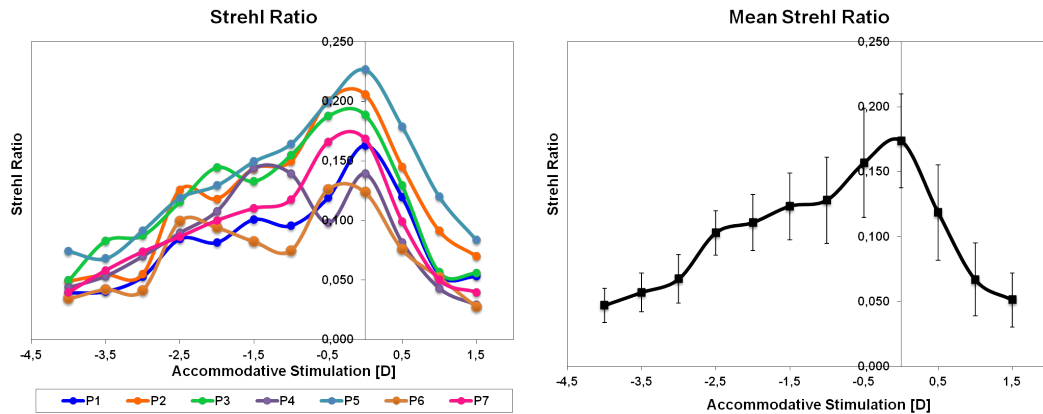
Figure 6.1.2: MTFs of each step of the mean through-focus from $-4D$ to $+1.5D$ in steps of $0.50D$. The black curve is the MTF only limited by diffraction (DIF).

On the other one, Strehl Ratio (SR) and Cut-Off frequency were the chosen parameters to be compared with Visual Acuity (VA) results. Two graphs per each parameter have been included below. Figures 6.1.3, 6.1.4 and 6.1.5 show the SR, the Cut-Off frequency and the VA values along the through-focus from $-4D$ to $+1.5D$ in steps of $0.50D$ for each patient in the graphs positioned on the left. The graphs located on the right represent the mean values with the Standard Deviation (SD) bars along the whole through-focus of each parameter.

When the results of each patient were compared with the others for any of the three included parameters, it was noticed that even with different values, the behavior of the curves were quite similar for all of the participants. However, there were some exceptions as were patient 4 (P4) and 7 (P7) in SR results (Figure 6.1.3 a), and P4 again in Cut-Off frequency results (Figure 6.1.4 a). The mean curves were after analyzed.

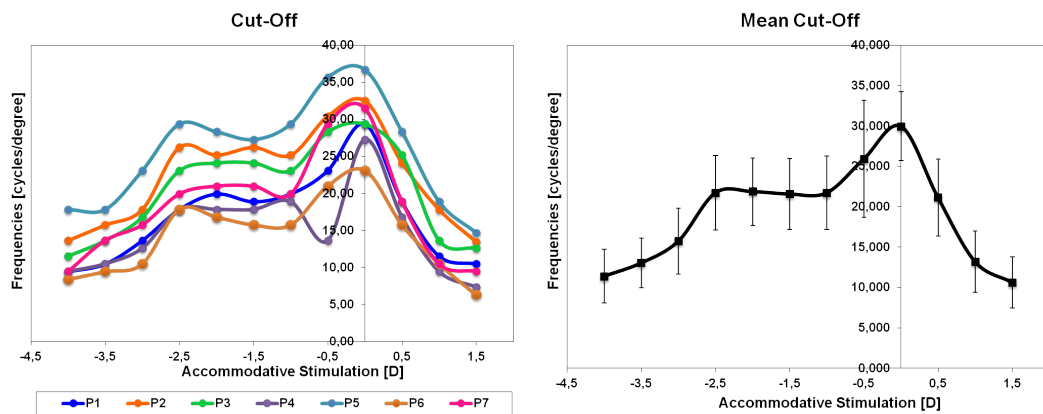
As it can be observed, the mean SR curve (Figure 6.1.3 b) presented a clear peak on $0.00D$ and then the curve fell abruptly until $-1.00D$. After that point the values kept decreasing, but in a

6.1. ASSESSMENT OF THE OPTICAL QUALITY OF PATIENTS IMPLANTED WITH A MULTIFOCAL INTRAOCULAR LENS



(a) SR values along the through-focus of each participant. (b) Mean SR values along the through-focus with SD bars included.

Figure 6.1.3: SR values for each patient on the left and mean SR values including SD on the right.



(a) Cut-Off frequency values along the through-focus of (b) Mean Cut-Off frequency values along the through-focus with SD bars included.

Figure 6.1.4: Cut-Off frequency values for each patient on the left and mean Cut-Off values including SD on the right.

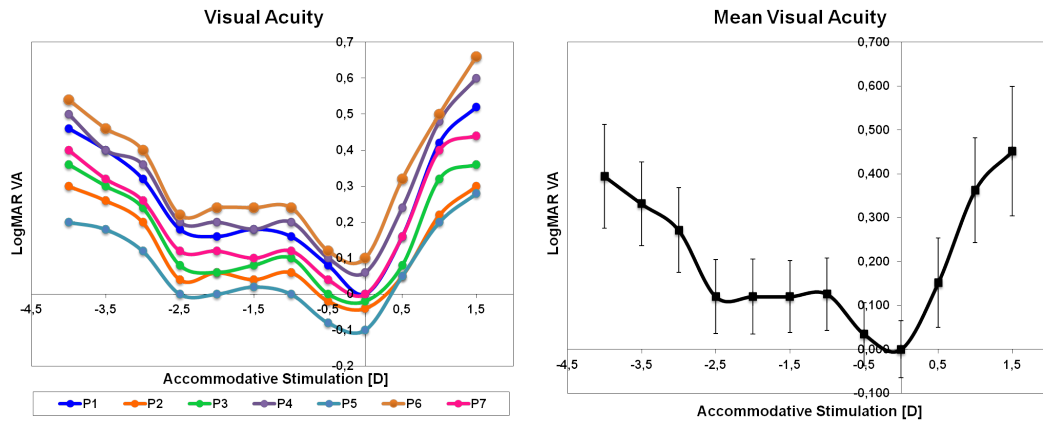
more slow way until $-2.50D$. Finally, the values decreased significantly from $-2.50D$ to $-4.00D$. From $+1.50D$ to $0.00D$ was found a great slope.

In the event of the Cut-Off frequency curve (Figure 6.1.4 b), presented a very similar behavior from $+1.50D$ to $-1.00D$ compare with mean SR curve. On the contrary, there was a very light increased of the Cut-Off values from $-1.00D$ to $-2.50D$. The last part of the curve, from $-2.50D$ to $-4.00D$, the curve dropped with values similar to the one obtained in $+1.50D$.

At the end, the subjective parameter VA was studied (Figure 6.1.5 b). A lot of similarities with the mean Cut-Off curve were found. Both curves were practically the same, but in an inverse position. This was in account of the fact that the lower value of logMAR VA, the better VA of the observer.

Figure 6.1.6 shows the normalized values of the three mean curves. In the case of VA, its inverse was previous calculated. This way was possible to see that, actually, from $+1.50D$ to $-1.50D$ the

6.1. ASSESSMENT OF THE OPTICAL QUALITY OF PATIENTS IMPLANTED WITH A MULTIFOCAL INTRAOCULAR LENS



(a) LogMAR VA values along the through-focus of each participant. (b) Mean logMAR VA values along the through-focus with SD bars included.

Figure 6.1.5: LogMAR VA values for each patient on the left and mean logMAR VA values including SD on the right.

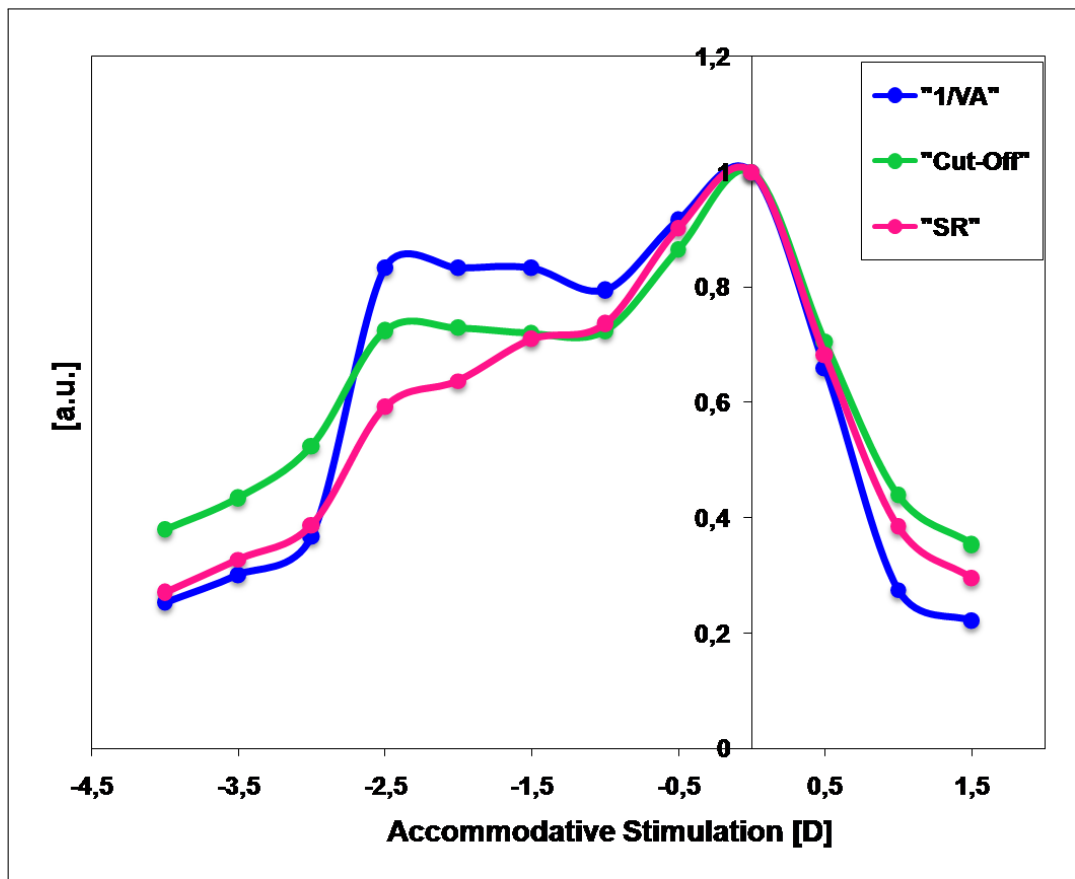


Figure 6.1.6: Normalized mean values for SR, Cut-Off and 1/VA are included. SR values are in pink, Cut-Off in green and 1/VA in blue.

curves were quite the same for the three parameters. From $-1.50D$ to $-2.50D$, the inverse of VA and Cut-Off had a little increased, while SR started to decreased. At the end, Cut-Off and

SR showed a similar significant decreased from $-2.50D$ to $-4.00D$, whereas the inverse of VA dropped.

6.1.5 Conclusions

This preliminary study with a little number of participants was designed and developed to be able to validate the suitability of the DPAF system *in vivo* conditions.

After analyzed all the objective and the subjective information, it could be concluded that results were very similar in terms of the visual behavior along the through-focus. When the values were taken into account, VA obtained the best result, as expected. This circumstance is, probably, the result of being a subjective parameter, that is to say, the value of this parameter is influenced by the visual neuronal process. Nevertheless, it was demonstrated that the objective through-focus obtained with the new DPAF system is comparable to the VA one which is consider the gold standard. As a consequence, it was able to be confirm that the main conclusion for this preliminary study was that the new DPAF system is suitable to use it *in vivo* conditions.

Actually, the objective through-focus obtained with the DPAF system can be proposed as an advantageous alternative to the subjective one, since the first one is significantly faster than the second. Meanwhile an optometrist spend around 30minutes to perform a VA through-focus of 4D, only 1minuteand12seconds were spent to do the objective through-focus with the DPAF system. Moreover, this measure time can be reduced optimizing the measurement software.

In terms of the included MIOL, it looks like the optical behavior of the new MIOL Precizon Presbyopic (OPHTEC B.V., Groningen, Netherland) consists on having a focused range around $2 - 2.50D$, being at the same time almost the same as the addition value of it, which, according to the manufacturer, is $2.75D$. It is true that this lens still have a differentiate optical quality peak for far distance, but it is also proved that from intermediate to near vision the optical and the visual quality remain quite constant. This kind of MIOLs, the ones of having a range around $2.00D$ or more, where the optical quality remains constant is the latest tendency in this field. The measurements performed in this study confirm that the new MIOL Precizon Presbyopic has a focused range from intermediate to near distance vision with a comfortable visual and optical quality. Although, the distance vision results are still better.

7. Conclusions and future work

The main goal of this thesis was the design and the assembly of a new open-field double-pass system with asymmetric focus to characterize optical quality *in vivo* in patients implanted or adapted with multifocal intraocular or contact lenses. This has been achieved. The system was also tested to prove its suitability to measure the optical quality of any eye implanted with a MIOL both *in vitro* and *in vivo* conditions.

The main conclusions of the different stages performed during this project are shown below:

1. Objective over-refraction wearing MCLs.

A study performing an objective over-refraction with patients wearing MCLs were done. No significance statistical differences were found between over-refraction using an open-field infra-red autorefractor and a subjective over-refraction. Thus, it was concluded that the used over-refractor was suitable to perform an over-refraction in patients wearing MCLs. This study revealed that the complex optical designs of the MCLs allowed the option of performing objective measurements to characterize them. Due to the similarities of the designs of the MCLs and the MIOLs, this study was considered as the first step to carry out this thesis.

2. Verification of the suitability of one commercial simulator.

Three different studies were carried out to prove the suitability of the commercial vision simulator VirtIOL (10Lens, S.L.) to assess the visual quality of an eye implanted with a MIOL before the implantation of it. The main conclusions of them were:

- (a) VirtIOL was suitable to simulate a virtual implantation of any MIOL that is found in the market.
- (b) It is required that the patient has a clear lens of the eye at the simulation time.
- (c) VirtIOL allowed to qualified any visual quality attribute that can be tested.

3. Design and assembly of the double-pass system with asymmetric focus.

A compact double-pass system with asymmetric focus, suitable to work in clinical environment was designed using ZEMAX (ZEMAX LLC). A compact prototype for use in clinics was developed designing mechanical assembly using the software CREO 3.0 (Pro/Engineer, PTC). The electro-optical lenses that contains the system were validated. The power of the laser, which goes into the eye, was limited below the security levels. The optical validation of the system was also performed resulting as it can be considered as a system only limited by diffraction. Finally, the methodology to obtain the curve of the through-focus was validated by measuring one diffractive and another refractive MIOL implanted in a model eye.

4. Programming of the softwares.

Two different softwares were developed by means of using Matlab (Mathworks, 2016). The first one, to control all the hardware of the system (laser, IR LEDs, vibration motor, EOLs,

and both cameras), and the second one, to analyze the data that is needed to evaluate the optical quality of the measured human or model eye adapted with a MCL or implanted with a MIOL.

5. Validation of the new prototype.

A study with patients implanted with multifocal intraocular lenses was carried out to validate the developed prototype. After all the work performed to develop this thesis, it was demonstrated that the new compact and open-field double-pass system with an asymmetric focus was suitable to characterize the optical quality of an eye implanted with a MIOL both *in vitro* and *in vivo* conditions.

Taking into account the final point of this thesis, we think that the future work should be the fact to prepare the system for being used in a clinical environment and perform a clinical study including patients implanted with different types of MIOLs. Some of the changes that should be are: close the system, put the system on a mobile base, and optimize the management software, among others.

A. Appendix 1: Design of the Double-Pass System with Asymmetric Focus (DPAF)

This appendix shows just a little summary of the design of the DPAF by using the optical design software ZEMAX.

In order to make easier the task of the design, it was decided to divide the system in two. Consequently, a system called first pass and another one named second pass were created and analyzed as independent ones. The goal with that division was to be able to obtain results as similar as possible with both and then, simulate the complete system combining them.

A.1 First Pass

As commented in chapter 5 of this manuscript and as it could be observed in figure A.1.1, the first pass was composed by: a laser ($\lambda = 780nm$) (1), a collimator lens (2), one electro-optical lens (EOL 1) (3), mirror 1 (4), a beam splitter 50%/50% (5), a vehicle lens ($f' = 60mm$) (6), a hot mirror (7), a dichroic filter (8) and an artificial eye (9).

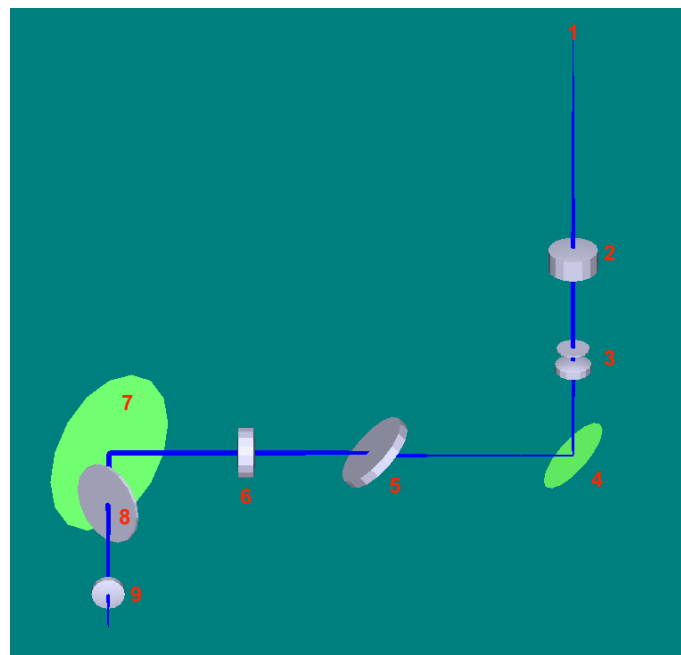
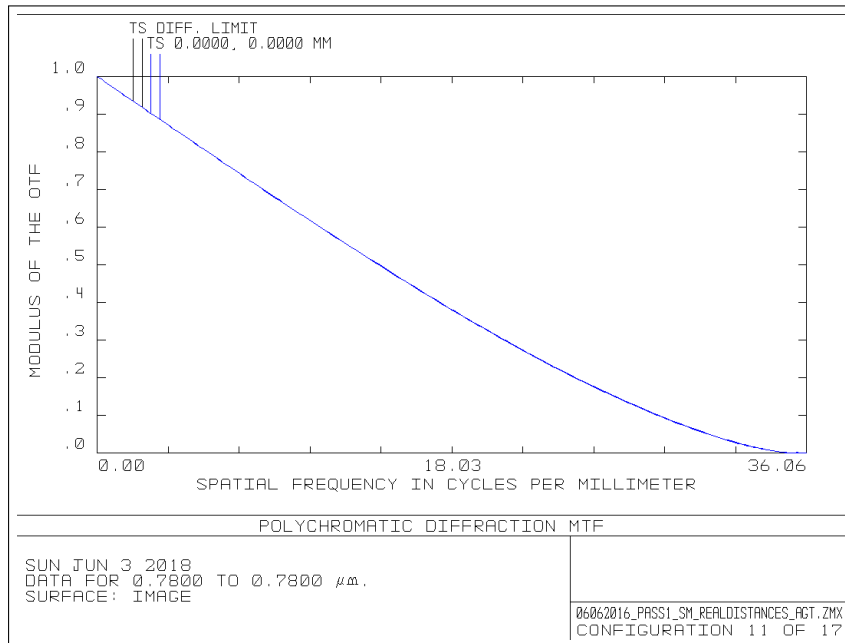


Figure A.1.1: Caption of the shaded model lay-out of the non-sequential mode: (1) laser, (2) collimator, (3) EOL 1, (4) M1, (5) BS, (6) VL, (7) HM, (8) DC and (9) Eye.

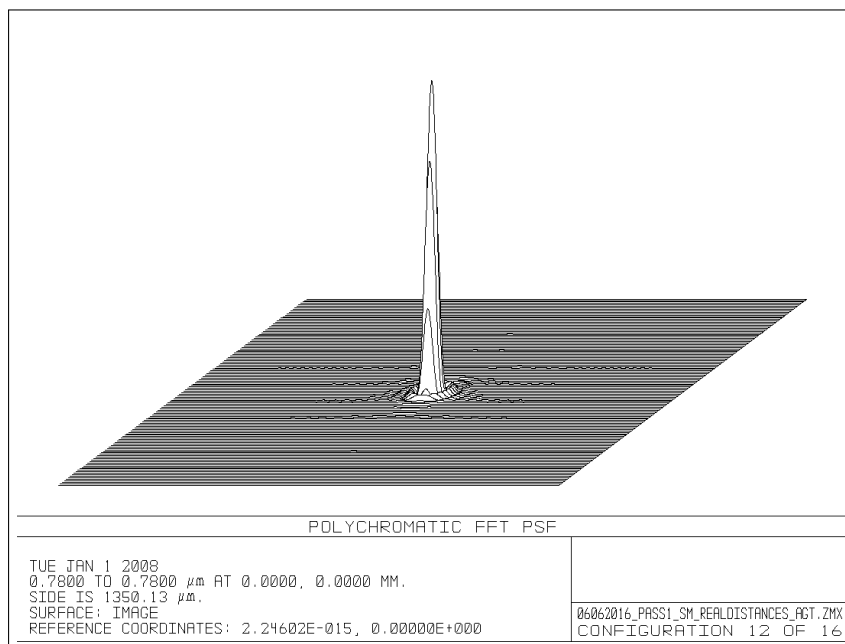
A.1. FIRST PASS

Three different files were created to analyze all the aspects of an optical system. First of all, a sequential mode file was performed to be able to obtain the spot diagram, the MTF or the PSF, among others. Secondly, a non-sequential mode file was developed to take into account the laser cone and the light dispersion. Finally, mixed-mode file was obtained to combine all the information.

Figure A.1.2 shows the MTF and the simulated retinal image of the first pass.



(a) MTF curve



(b) System's image

Figure A.1.2: Representation of the MTF of the simulated system and the one only limited by diffraction on the left (a). Simulation of the retinal image on the right (b)

A.2 Second Pass

The second pass starts at the end of the first one. Thus, the light source of the second pass was placed at the focal image plane of the whole first pass system. Then there's a common part composed by the artificial eye (1), the dichroic filter (2), the hot mirror (3), the vehicle lens (4) and the beam splitter (5). The beam splitter is only acting as a mirror in the simulation of the second pass. From that point, it were included the EOL 2 (6), the mirror 2 (7), the afocal system (8), the mirror 3 (9) and the lens of the DP camera (10). The afocal system consisted on two achromatic lenses with a focal length of 100mm .

Figure A.2.1 presents the lay-out of the simulated second pass, while figure A.2.2 shows the MTF and the PSF of it. In this case were also created the sequential mode, the non-sequential mode and the mixed mode files.

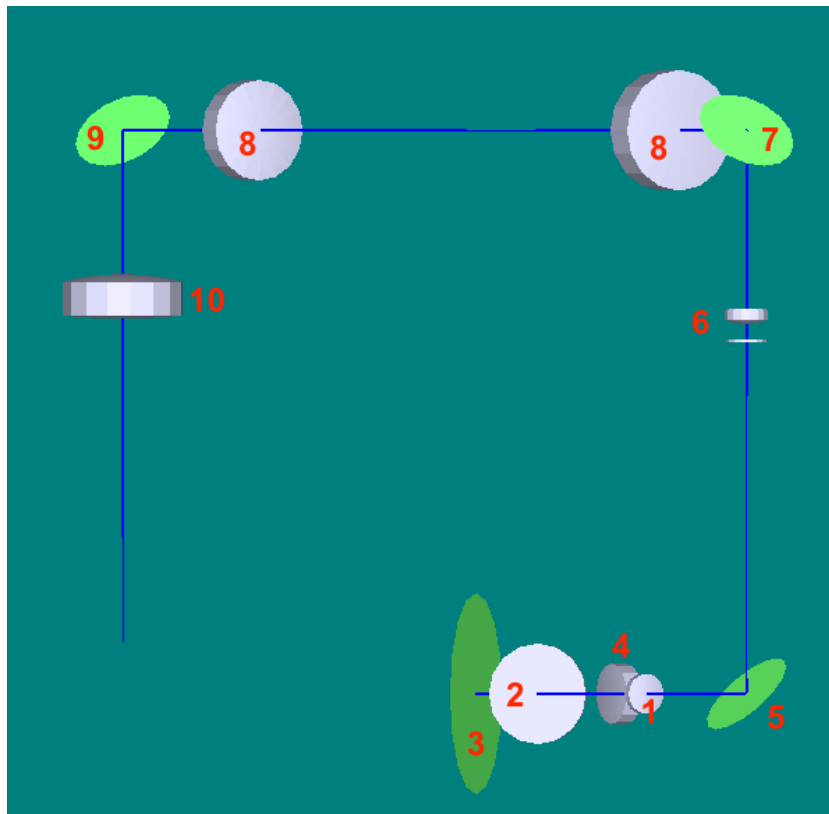
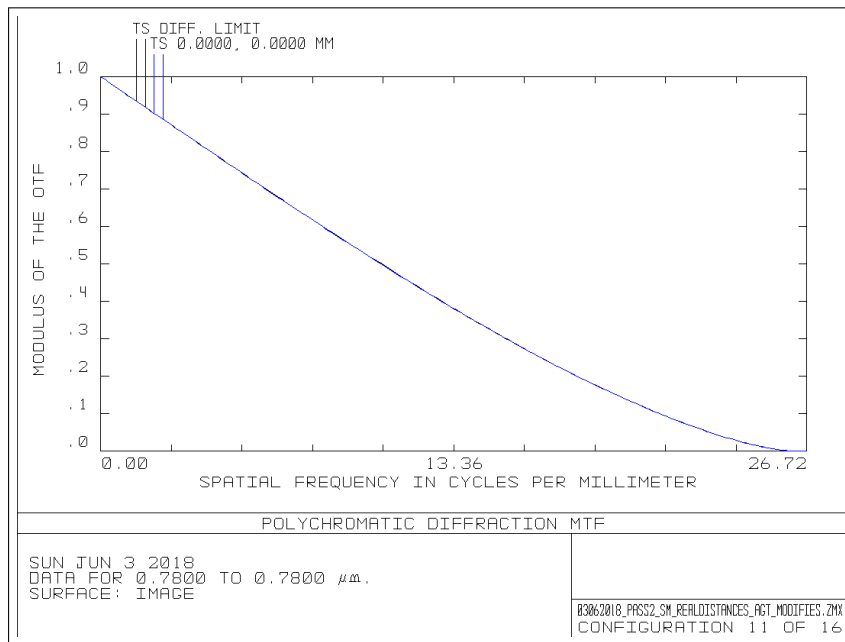


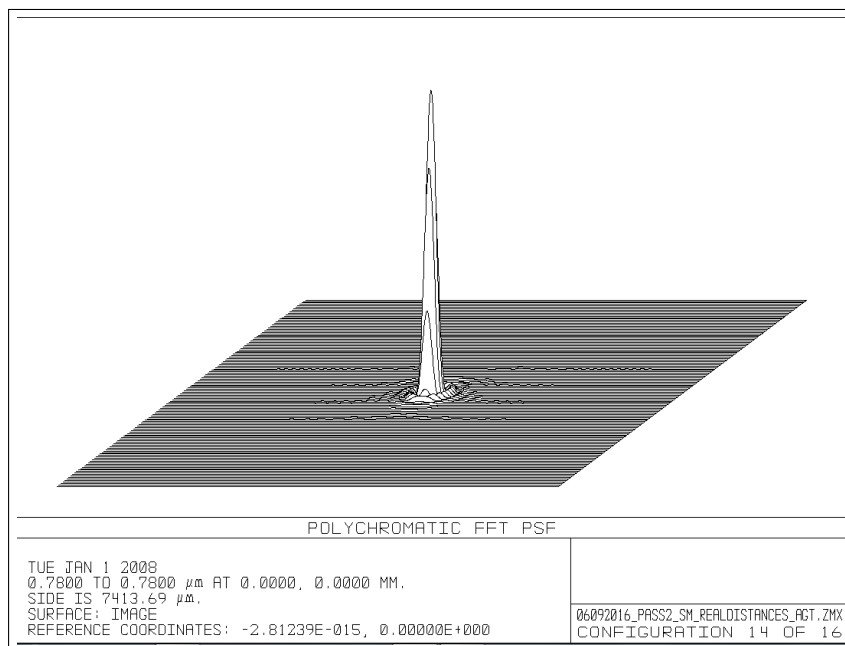
Figure A.2.1: Caption of the shaded model lay-out of the non-sequential mode: (1) eye, (2) DC, (3) HM (4) VL, (5) BS, (6) EOL 2, (7) M2, (8) Afocal System, (9) M3 and (10) Lens of the DP camera.

If MTF of the first pass is compared with the one of the second pass, it is easy to see that both fit perfectly with the one only limited by diffraction. Although, they don't have the same cut-off. This difference is justified by the fact that the second pass includes also the afocal system and the lens of the DP camera.

A.3. COMPLETE SYSTEM



(a) MTF curve



(b) PSF 3D

Figure A.2.2: Representation of the MTF of the simulated system and the one only limited by diffraction on the left (a). PSF curve in 3 dimensions on the right (b)

A.3 Complete system

After it was achieved the best first and second pass systems, a combination of both was developed to simulate the whole optical system that today is the DPAF included in this thesis (Figure A.3.1).

Two different light sources with the same λ and cone angle were included to differentiate first pass (green rays) from the second pass (blue rays).

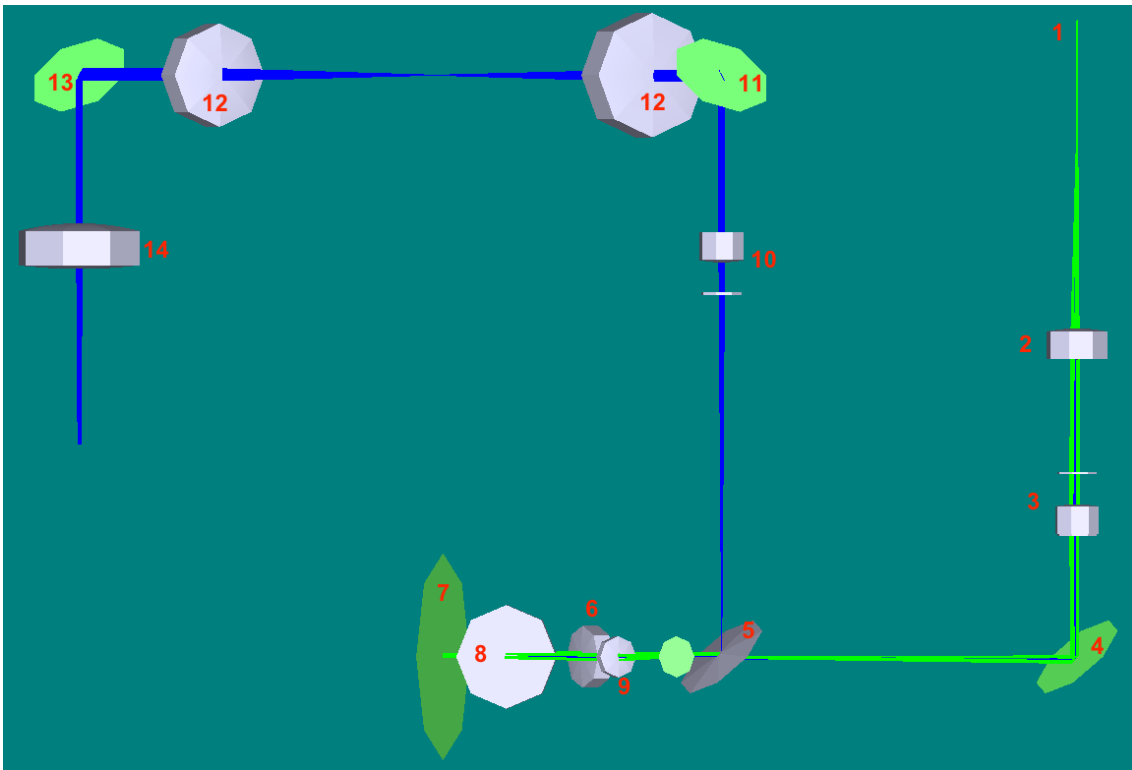


Figure A.3.1: Caption of the shaded model lay-out of the non-sequential mode of the whole system: (1) laser, (2) collimator, (3) EOL 1, (4) M1, (5) BS, (6) VL, (7) HM, (8) DC, (9) Eye, (10) EOL 2, (11) M2, (12) Afocal System, (13) M3 and (14) Lens of the DP camera.

It is also necessary to take into account that more than ten versions were created to finally arrive to the definitive ones, since the simulation task was done while the mechanical design and the validation of the EOLs or the DP camera or the laser were performed.

A. Appendix 2: Data sheets

Data sheets are presented in the following order:

1. Monocrom Laser ($\lambda = 780nm$)
2. Optotune Tunable lenses *EL – 10 – 30*
3. THORLABS Power Meter
4. Hamamatsu ORCA-flash 4.0 v2 (Double-pass Camera)



Division



LDM

Laser Diode Modules

Product

C7805M-SMF

Description

Fibre Coupled Laser Diode Module
LDM 780nm 5mW Single-Mode FO FC-PC with Power-regulation.

Main Features

- Single mode fibre coupled.
- Collimator ended available.
- Circular beam after SM fibre.
- Compact design.
- Power regulation.
- High quality optics and excellent beam performance.

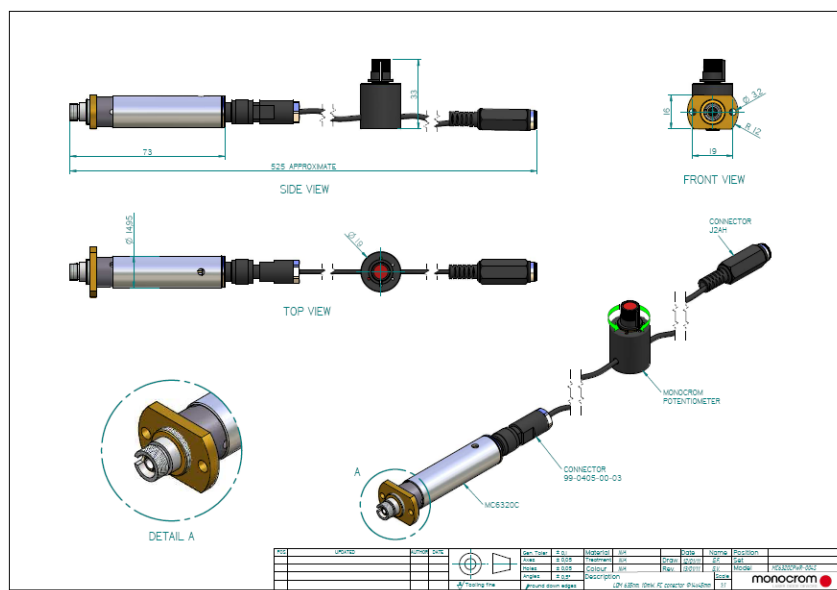
Some applications

- Automatics & Robotics.
- Metrology.
- Guidance.
- Bio-medics.
- Lighting & Imaging.
- Fibre check.

Picture



Outline



Power regulator along cable optional

MODULATABLE-FIBER COUPLED LASER DIODE MODULE



| GENERAL SPECIFICATIONS | |
|------------------------------------|--|
| Model: | C7805M-SMF |
| Wavelength [nm] | 785±10 |
| Po. Typ. [mW] | 5.0±0,4 |
| Op. current @ Po.max [mA] | < 100 mA |
| Op. temperature [°C] | 0 to 40 under no condensation conditions |
| Storage temperature [°C] | -40 to 85 |
| Output power stability (1) | < 1.5% |
| Reverse voltage protection circuit | Built in |
| Op. voltage for cw operation | 5±0,5% Vdc |
| Expected lifetime | >10.000 Hours |
| Wires | Standard 3 pin- connector or 200mm Flying leads. Feeding: Red/black wires. Modulation/Regulation: RG174 cable |
| Laser product class | 3B According with the radiant flux and EN-60825 classification, duly identified by labels. |
| Housing | C type : Diam.15 x 73mm length / Al and Brass / FO connectorized |

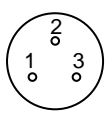

Conditions @ 25°C while not specified. See below typical characteristics curves of the LD mounted.

(1) From a stable input signal

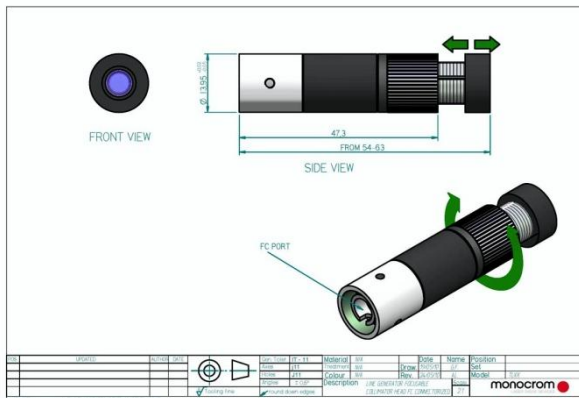
| FIBER PATCH-CORDS Types (to add at module p.n.) | -005S |
|--|---------|
| Polarization maintaining | No |
| Coupling efficiency (% of Po), typical | 30-50% |
| Connector repeatability, typical | 85% |
| Mode field diameter [µm] | 5.6 |
| Numerical aperture | 0,12 |
| Cladding [µm] | 125±2 |
| Jacket [µm] / Protec slip [mm] | 250 / 3 |
| Min. bend diameter [mm] | 25 |
| Connector type | FC-PC |
| Length, typical | 2 m |

| POWER REGULATION / MODULATION MODES | ANALOGUE | DIGITAL |
|---|-----------------------------|--|
| | Input signal, Vmod, typical | 0.5 to 4V (For Power from 0 to PoMax) |
| Typ. modulation range | | CW to 10 kHz |
| Rise & fall time [µs], typical | | < 10 µs |
| Input impedance | | >500 KΩ |
| Po without input signal (coaxial cable unplugged) | | 0 |

| ACCESSORIES: | |
|---|--|
| PSLDM5-PWR | |
| <p>F.A. Converter 220V AC to 4,8-5V_{DC} / 1,2 A Knob for power regulation Estabilised Europlug</p> |  |
| PWR | |
| <p>Power regulator along cable</p> |  |

| PSLDM5-BIND Power supply AC/DC converter | | |
|---|--|---|
| <p>Converter 220V AC to 4,5VDC / 1,2 A Stabilised Euro-plug Screw lock output connector</p> |  <p>Pin 1: +3V Pin 2: GND Pin 3: N.C.</p> |  |

| FOCUSABLE OPTICS HEADS | Focal Length | Max. CA Effective. Do[x] | N.A. max | Focusing Range, typ. [mm] | Dimensions Øxlength [mm] |
|------------------------|-------------------------------|--------------------------|----------|---------------------------|--------------------------|
| -TxA10 | 10mm @ 670nm | from 2 to 6 mm | 0,33 | 60±40 to infinite | 14x55 |
| -TxA15 | 15mm @ 670nm | 6 mm | 0,30 | 250±50 to infinite | 14x55 |
| TLxx | Full angle : 5,10,20,50 & 99° | | - | 60±40 to infinite | 14x60 |



Fast Electrically Tunable Lens EL-10-30



The curvature of the lens can be rapidly changed by applying a control voltage. The focal length is accordingly tuned to a desired value within milliseconds. Optotune currently offers three lens versions:

- EL-10-30-VIS-HR: High refractive index ($n_D=1.559$), visible anti-reflection coating (400-700nm)
- EL-10-30-VIS-LD: High Abbe number ($V=100$), visible anti-reflection coating (400-700nm)
- EL-10-30-NIR-LD: High Abbe number ($V=100$), near infrared anti-reflection coating (700-1100nm)

The following table outlines the specifications of our standard electrically tunable lens EL-10-30. Lens aperture, thickness and tuning range can be adapted on demand.

Mechanical specifications

| | | |
|-----------------------------|-------------|----|
| External diameter | 30 | mm |
| Clear aperture ¹ | 10 | mm |
| Thickness | 9.8 | mm |
| Weight | 22.6 | g |
| Lifecycles | >10'000'000 | |

Electrical specifications

| | | |
|------------------------------|--------|----|
| Control voltage | 0 to 5 | V |
| Response time (10%-90% step) | 10 | ms |
| Power consumption | 0 – 2 | W |

Optical specifications

| | EL-10-30-VIS-HR | EL-10-30-VIS-LD, EL-10-30-NIR-LD |
|---|-----------------|-------------------------------------|
| Focal tuning range @ 525nm ² | +20 to +60 mm | +45 to +120 mm |
| Dispersion | | |
| 486nm | 1.572 | 1.302 |
| 589nm | 1.559 | 1.300 |
| 656nm | 1.554 | 1.299 |
| 800nm | 1.546 | 1.298 |
| 1065nm | 1.541 | 1.297 |
| 1300nm | 1.537 | 1.296 |
| 1550nm | 1.535 | 1.296 |
| Abbe number V | 31 | 100 |
| Lens type | plano-convex | |
| Transmission spectrum | see Figure 5 | |
| Optical damage threshold @ 1064nm | 25 | kW/cm ² |
| Centration | <2 | arcminutes |
| Polarization | Preserving | |

Thermal specifications

| | | |
|-----------------------|-----------|----|
| Storage temperature | [-40,+85] | °C |
| Operating temperature | [-20,+65] | °C |

Test conditions

80 % of clear aperture, 20°C

¹ Recommended useful aperture is 80% of clear aperture

² Different focal tuning ranges available upon request

Figure 1 shows the dimensions of the EL-10-30 lens. As indicated, the focal length is measured from the housing.

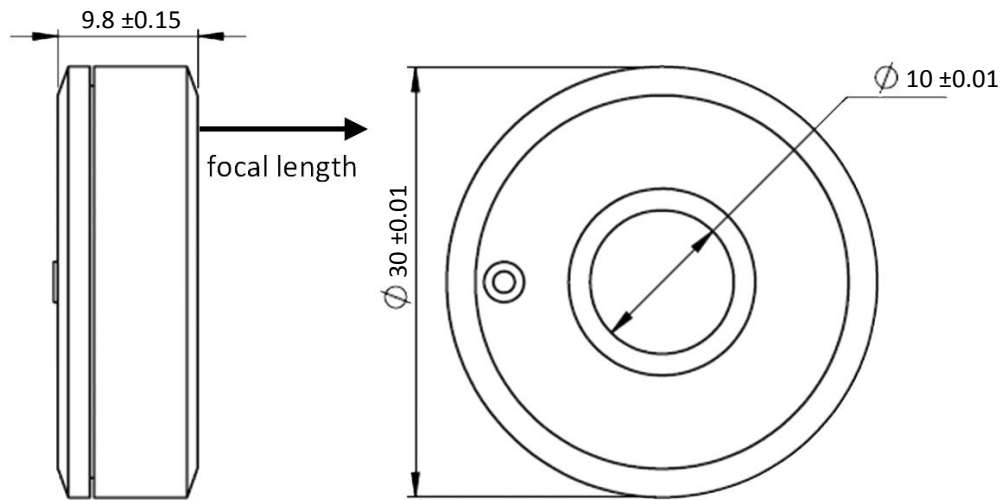


Figure 1: Mechanical drawing (unit: mm)

Figure 2 contains the information needed to model Optotune's electrical lens for simulations. A more detailed design guide and a ZEMAX plug-in can be downloaded from www.optotune.com.

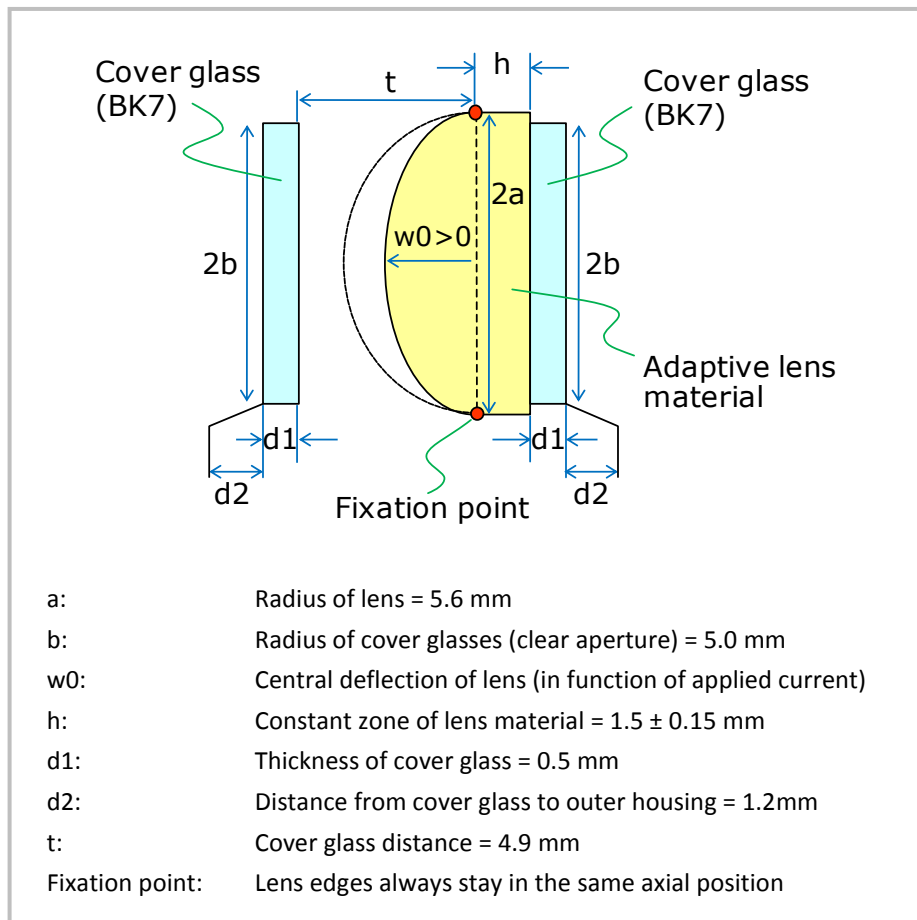


Figure 2: Optical layout with corresponding terminology (lens in the same orientation as in Figure 1).

Working principle

The EL-10-30 is a shape-changing lens. It basically consists of a container, which is filled with an optical fluid and sealed off with an elastic membrane. The deflection of the lens is proportional to the pressure in the fluid. The EL-10-30 has an electromagnetic actuator that is used to exert pressure on the container. Hence, the focal distance of the lens is proportional to the current flowing through the coil of the actuator.

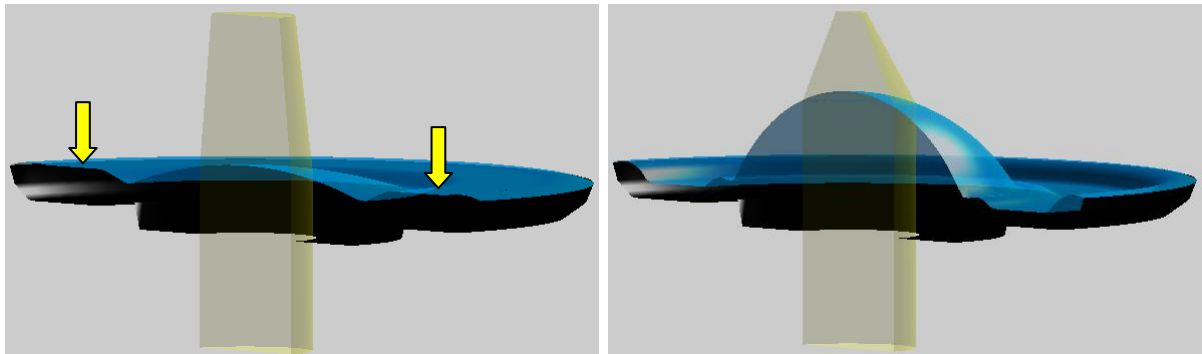


Figure 3: Working principle of the EL-10-30

Focal length versus current

Due to manufacturing tolerances, the relation of focal length to current varies from lens to lens. However, the specified range (e.g. 45 – 120mm for the EL-10-30-VIS-LD) is always contained. In open loop systems, a calibration of the lens with look-up tables is recommended.

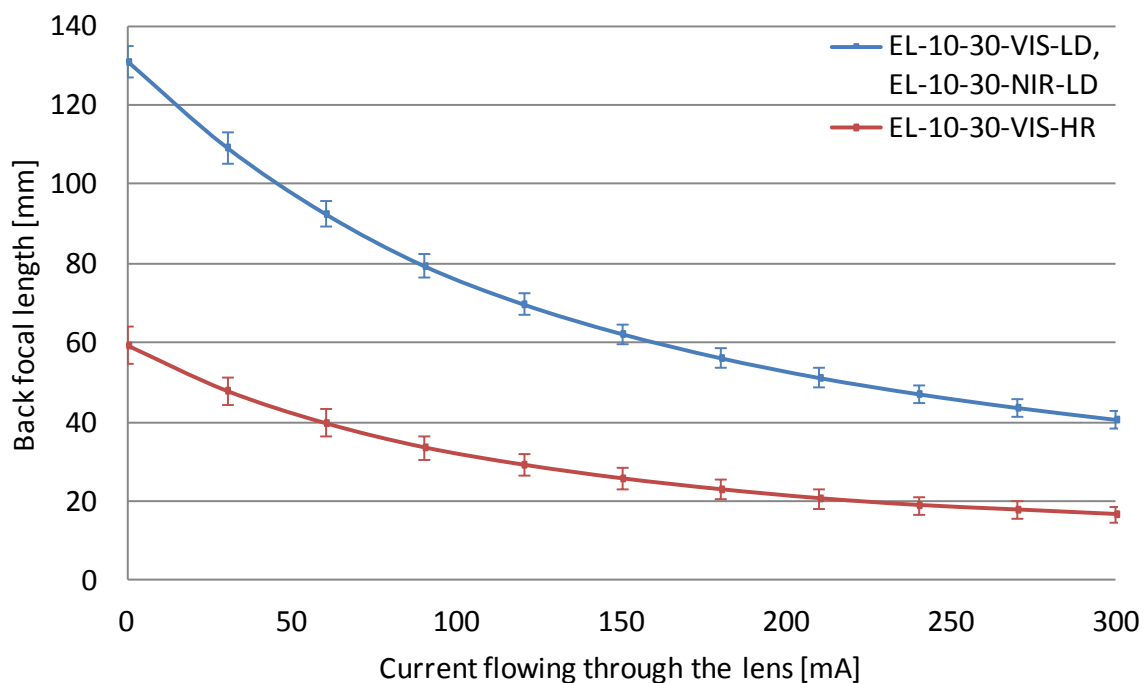


Figure 4: Typical relation of focal distance to current of the EL-10-30.
The error bars show the standard deviation from lens to lens

Transmission range

Both the optical fluid and the membrane material are highly transparent and hardly absorbing in the range of 250 – 2500nm. As the membrane needs to be elastic it cannot be coated using standard processes. Cover glasses can be coated as desired. The figures below show the transmission spectrum for our two standard broad-band coatings (visible and near infrared) as well as two custom narrow-band coatings:

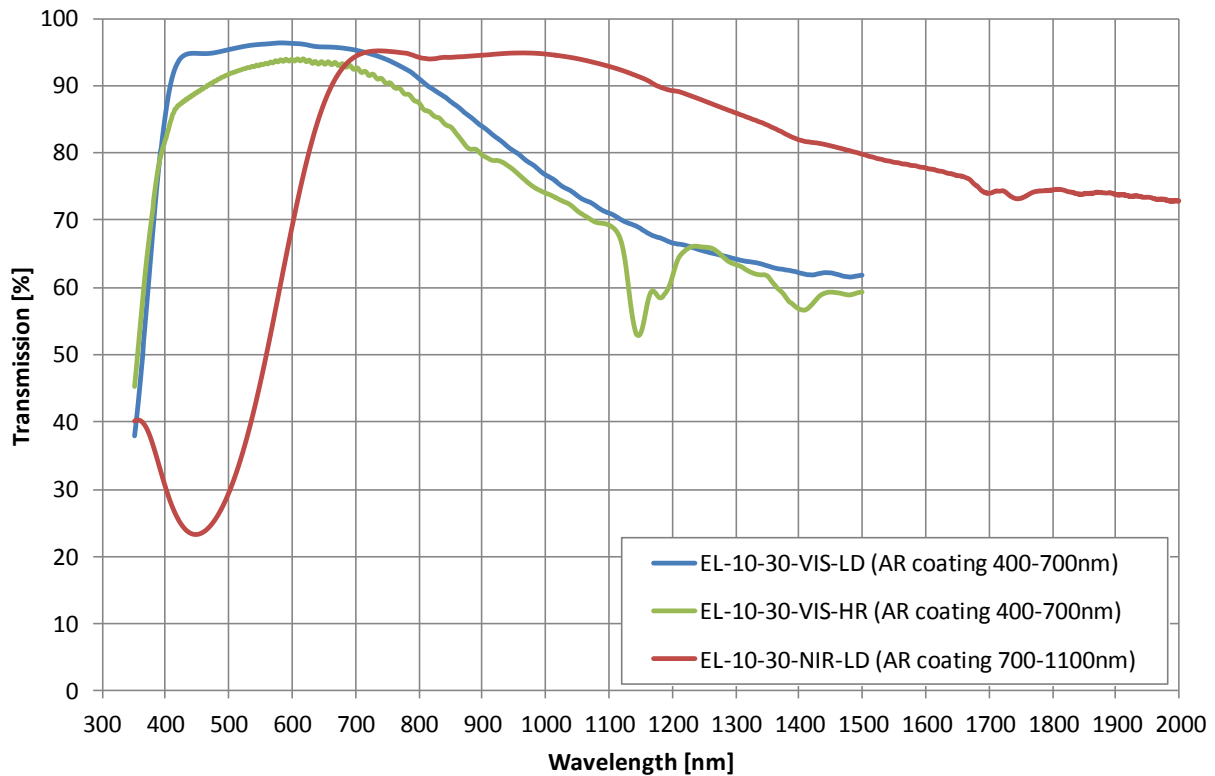


Figure 5: Transmission spectrum of the EL-10-30 for standard broad-band coatings

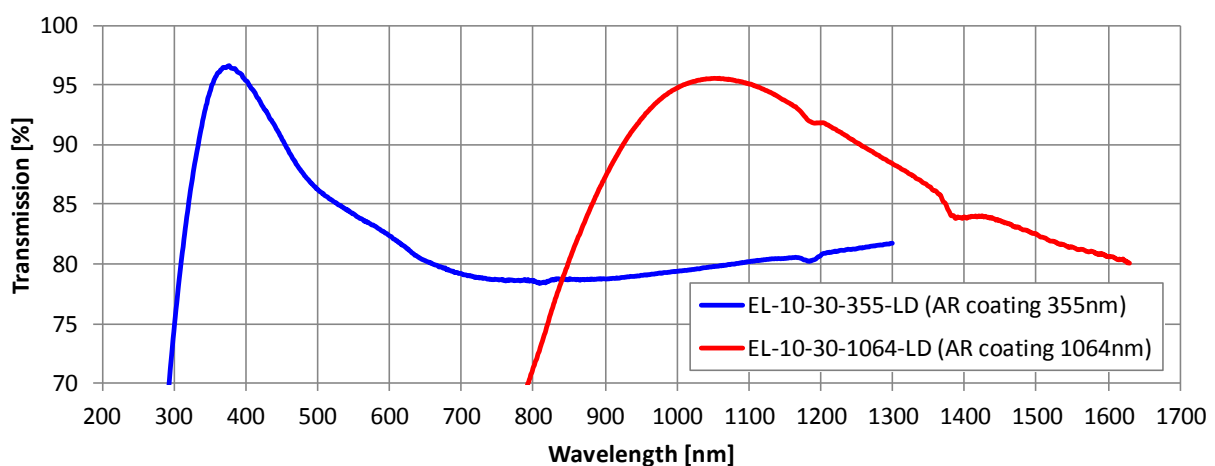


Figure 6: Transmission spectrum of the EL-10-30 for custom narrow-band coatings

The following graph represents the transmission of the lens material only³ (i.e. assuming perfect cover glasses).

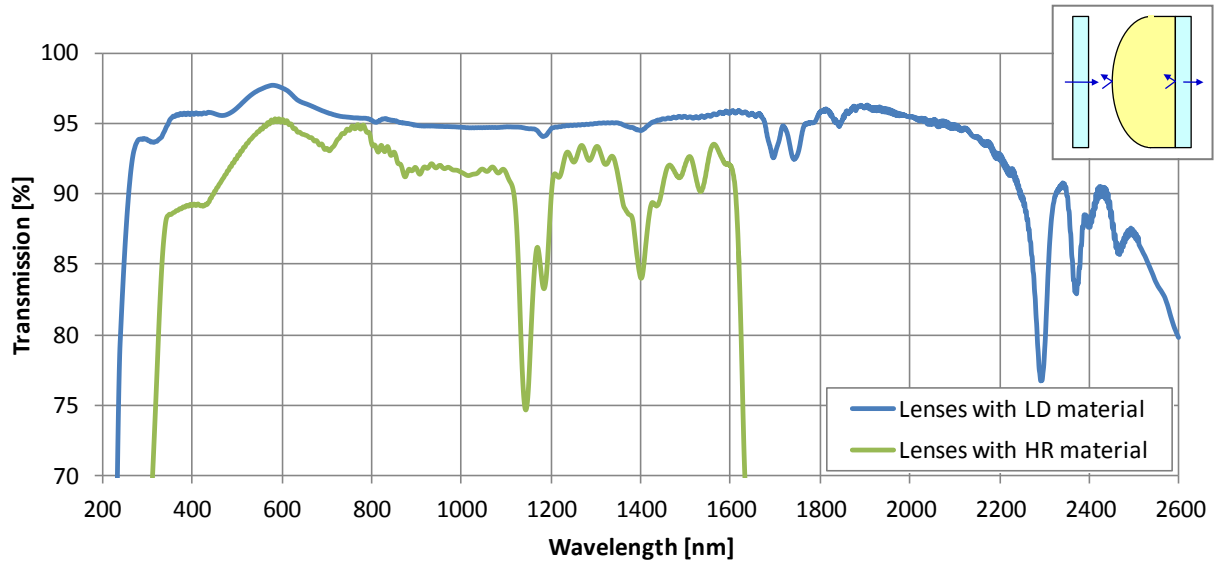


Figure 7: Transmission of the EL-10-30 assuming 100% transparent cover glasses

| Wavelength [nm] | EL-10-30-VIS-LD | EL-10-30-VIS-HR | EL-10-30-NIR-LD | EL-10-30-355-LD | EL-10-30-1064-LD | Lens with LD Material ³ | Lens with HR Material ³ |
|-----------------|-----------------|-----------------|-----------------|-----------------|------------------|------------------------------------|------------------------------------|
| 355 | 40.4 | 48.3 | 40.3 | 95.5 | 49.8 | 95.4 | 88.5 |
| 375 | 61.7 | 67.4 | 38.2 | 96.6 | 50.7 | 95.7 | 88.9 |
| 405 | 88.3 | 83.5 | 29.1 | 95.0 | 66.8 | 95.7 | 89.3 |
| 440 | 94.8 | 88.4 | 23.5 | 91.6 | 88.6 | 95.8 | 89.5 |
| 488 | 95.1 | 91.2 | 26.9 | 87.0 | 80.2 | 95.8 | 91.9 |
| 514 | 95.6 | 92.3 | 32.9 | 85.6 | 67.8 | 96.5 | 93.1 |
| 532 | 95.9 | 92.8 | 38.7 | 84.9 | 60.7 | 97.0 | 93.9 |
| 632 | 95.9 | 93.4 | 81.8 | 80.9 | 47.3 | 96.8 | 94.6 |
| 650 | 95.7 | 93.4 | 87.2 | 80.3 | 48.2 | 96.5 | 94.2 |
| 680 | 95.6 | 93.4 | 92.6 | 79.5 | 50.9 | 96.1 | 93.7 |
| 730 | 94.5 | 91.7 | 95.2 | 78.8 | 58.3 | 95.6 | 94.0 |
| 808 | 90.5 | 86.6 | 94.1 | 78.4 | 72.7 | 95.1 | 93.5 |
| 830 | 89.0 | 85.4 | 94.1 | 78.8 | 77.1 | 95.4 | 93.0 |
| 850 | 87.7 | 84.0 | 94.3 | 78.8 | 80.4 | 95.3 | 92.9 |
| 880 | 85.5 | 80.7 | 94.4 | 78.7 | 84.8 | 95.1 | 91.4 |
| 905 | 83.6 | 79.5 | 94.6 | 78.8 | 87.9 | 94.9 | 91.6 |
| 915 | 82.9 | 79.0 | 94.7 | 78.8 | 89.0 | 94.9 | 91.7 |
| 975 | 78.5 | 75.5 | 94.9 | 79.3 | 93.7 | 94.8 | 91.9 |
| 980 | 78.3 | 75.2 | 94.9 | 79.3 | 94.0 | 94.8 | 91.7 |
| 1030 | 74.9 | 72.8 | 94.4 | 79.6 | 95.4 | 94.7 | 91.4 |
| 1064 | 72.9 | 70.7 | 93.8 | 79.9 | 95.5 | 94.8 | 91.7 |
| 1070 | 72.7 | 70.3 | 93.7 | 80.0 | 95.4 | 94.8 | 91.9 |
| 1310 | 64.0 | 63.2 | 85.7 | 81.9 | 88.0 | 95.1 | 93.1 |
| 1540 | #N/A | #N/A | 78.9 | 83.5 | 81.5 | 95.6 | 90.4 |
| 1550 | #N/A | #N/A | 78.7 | 83.6 | 81.4 | 95.6 | 92.1 |

Table 1: Transmission values of the EL-10-30 for common lasers

³ The transmission of the „lens material only“ was put together from measurements of several lenses with differently coated cover glasses, whereas the three interfaces of „air to coverglass“ were removed.

Damage thresholds

The nominal specification of the lens materials used is 25kW/cm². However, this number was extrapolated from a small spot size. Good results have been achieved with the following lasers:

- 1070nm, 200W CW on a 3mm beam diameter (equivalent to 2.2kW/cm²)
- 1064nm, 20ns-pulsed at 50kHz, 10W average power on a 0.05mm beam diameter (10J/cm²)
- 355nm, 20ns-pulsed at 50kHz, 7W average power on a 0.05mm beam diameter (7J/cm²)
- 850nm, 140fs-pulsed at 80MHz, 3W average power on a 6mm beam diameter (0.13uJ/cm²)
- 345nm, 500fs-pulsed at 200kHz, 0.5W average power on a 3mm beam diameter (35uJ/cm²)

A known issue is failure of the cover glass material. For this reason Optotune is working on a version of the EL-10-30 with specialty coated glass at 1064nm, which can be expected in Q2 2011.

Another known issue is heating up of the lens as a result of reflections hitting absorbing surfaces. It is advised to calculate such reflections and preferably not use more than a 6mm beam size.

Wavefront quality

Optotune's focus tunable lenses exhibit a spherical lens shape (the nominal parameters can be found in the ZEMAX package, which is available for download on www.optotune.com).

As the materials used are elastic, the lens shape is influenced by gravity. With the lens lying horizontally (optical axis vertical) the RMS wavefront error of the EL-10-30 is currently in the order of 0.1 lambda. With the lens standing upright (optical axis horizontal) a coma Y term of about 0.3 lambda must be added.

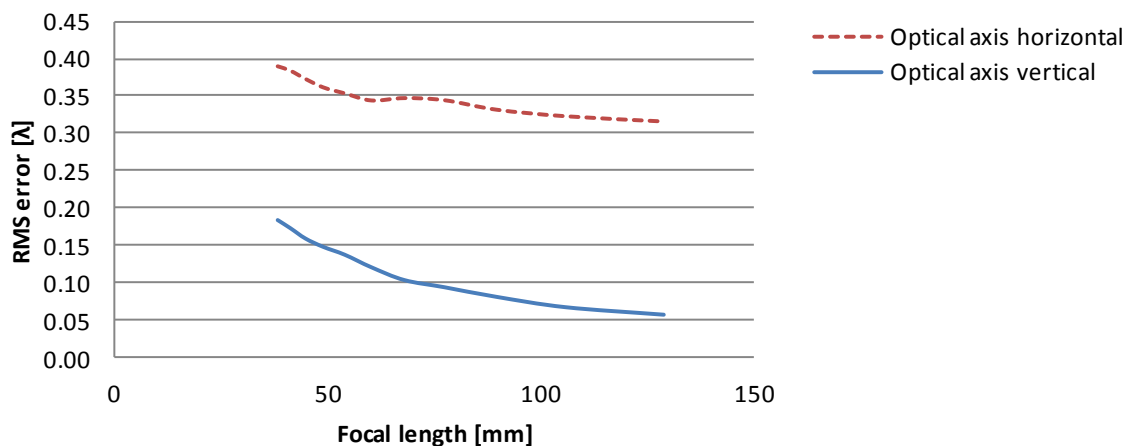


Figure 8: Wavefront measurement of an EL-10-30-VIS-LD (at 80% of clear aperture, defocus & tilt excluded)

This "sagging" effect depends on the size of the lens and several material parameters. While it hardly exists with lenses of apertures below 5mm, it can account for several lambda RMS error with lenses of e.g. 20mm aperture.

In general, a "stiffer" membrane can be used to significantly reduce this undesired effect, as the pressure inside the lens can be increased. However, that is at the expense of focal tuning range or power consumption. Optotune is working on improved materials and lens designs to reduce the dependence on gravity.

Temperature effects

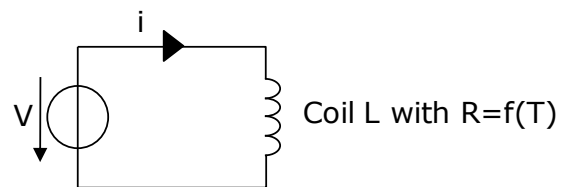
Heating up of the lens has two consequences: First, the refractive index of the optical fluid decreases. Second, the fluid expands in volume. While the first effect would increase the focal distance, the second effect reduces it. With the EL-10-30 design, the second effect prevails. The focal distance decreases by approximately 2% per 10°C temperature increase.

This temperature effect is systematic and reproducible. This means the focal length can be controlled if the temperature is known. The EL-10-30 actually has a built-in temperature sensor. The resistance of the coil (which pushes down on the lens) changes linearly with temperature. So measuring voltage and current can serve as a proxy for the temperature in the lens.

The heating up of the lens can occur at room temperature if driven at high currents or due to absorption of high power laser light. In such cases the lens is preferably mounted using heat-conducting metal clamps. For custom designs it is possible to balance the two temperature effects such that the focus shift becomes minimal at a certain focal length. Alternatively, if response time is not critical, mechanical designs like the ML-25-50 are available which do not heat up due to the controlling current.

Current control vs. voltage control

In principle, the EL-10-30 can be driven using a DC voltage (e.g. even a simple battery). However, as the lens incorporates an electromagnetic actuator, the force applied to the lens (and with that the focal distance) depends on the current flowing through the coil. As with all electronics, the resistance of the coil changes with temperature (12.5Ωm at 25°C). So if a voltage controller is used, the focal distance may not be reproducible or drift away. This is especially the case at currents >200mA where this effect can easily be in the range of 10%. Note that this temperature effect is visible in the order of a few seconds and has nothing to do with the expanding of the optical fluid described above, which is in the order of a few minutes.



Coil resistance = $f(T)$
EL-10-30-VIS-LD

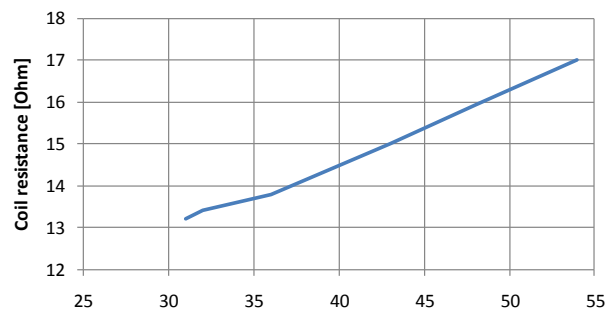


Figure 9: Coil resistance increases with temperature

Recommended drivers/power supplies

Here is a list of off-the-shelf products for current control:

- Precision constant current driver for laser diodes (e.g. Edmund Optics NT56-804, Thorlabs LD1255R)
- For high precision applications (0.1mA resolution) with manual control: TTI QL355
- For high precision applications (0.1mA resolution) with USB/RS232 computer control: TTI QL355P
- For low precision applications (1mA resolution) with manual control: TTI EL301R
- For low precision applications (1mA resolution) with USB computer control: Quakko HY3005DP

<http://shop.vendio.com/Evan2002/item/2041700966/?s=1282809362>

The lens can also be driven using pulse width modulation (PWM) with a frequency between 20 kHz and 50 kHz.

Response time

The 10-90% rise time on a full range step is about 10ms. The response time can be significantly improved by optimizing the current step function. An example is shown in the graph on the right, where a settling time of 15ms was achieved. To optimize the response time on the way back (e.g. when the current is turned off), a short pulse of negative current can be used.

While the actuator can actually move at several kHz, it remains to be analyzed what happens optically due to potential overshooting or wobbling effects. It also remains to be evaluated how the response time varies at different focal lengths. At this point, we expect the lens to be faster at short focal lengths due to the higher pressure of the fluid.

Optotune is working on a different lens design targeted to achieve a 1ms response time.

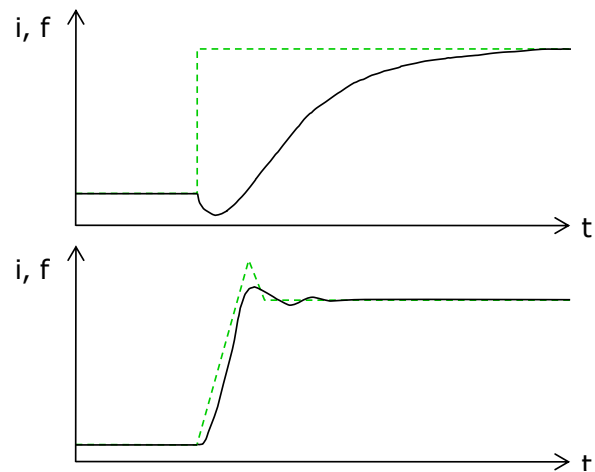


Figure 10: Typical step response (above) and improved response with an optimized step function (below)

Reproducibility

Unlike piezo systems, the EL-10-30 exhibits no hysteresis. The current through the coil induces a force, which is directly transferred onto the 100% elastic membrane. There is no friction in the system. This means that jumping between alternate current levels will always yield the same focal length. This could be confirmed after running 10 million full range cycles.

So basically the reproducibility is limited by the precision of the electronics. For high precision applications a controller with 12 bits is recommended. Assuming a linear relation between current and focal distance, this would mean that the focal distance of e.g. an EL-10-30-VIS-LD would be accurate to $(120\text{mm} - 45\text{mm}) / 4096 = 18\mu\text{m}$. What needs to be taken into account, though, is a potential heating up of the lens when it is operated at high currents over a long period of time.

Atmospheric pressure

By working principle, the atmospheric pressure has no influence on the lens. This has been validated by observing a constant focal length of the EL-10-30 in a vacuum chamber with pressure decreasing from 1 bar down to about 20mbar.

Autofluorescence

The EL-10-30 with LD material is not autofluorescent and can be used for fluorescence microscopy.

Life time

As the EL-10-30 has been released in June 2010, there is no useful lifetime information available. However, the lens has passed relevant environmental and accelerated aging tests as outline in the table below.

| Test | EL-10-30 |
|---|----------|
| Mechanical cycling: 40 million full-range cycles (0 to 300mA, at 10 Hz) | Passed |
| High temperature test: 85±2°C; rel.hum. <6% for 168 hours, non-operational | Passed |
| Temperature cycling test: -40°C / +85°C for 30 min each, 3 min transition time, 100 cycles | Passed |
| Damp heat cycling test: 25°C / 55°C at 90-100% relative humidity, 3 hour transition time, 24h per cycle (9h plus transition time each), 18 cycles | Passed |
| Shock test: 800g for 1ms duration, 5 pulses in each direction (30 pulses in total) | Passed |
| Solar radiation test: 1120 W per m2 (IEC 60068-2-5), 8 h irradiation & 16 h darkness, 10 cycles | Passed |

Table 2: Environmental tests performed on the EL-10-30

Customization

Optotune's lens technology can be adapted to your needs. The following table provides a range of possible parameters.

| | |
|-----------------------|--|
| Clear aperture (A) | From 2mm to 50mm |
| Range of focal length | From -A to infinity to +A |
| Response time | As little as 1ms |
| Lens shapes | Spherical, from convex to flat to concave, whereby the other side of the lens may be a static free form Cylindrical shapes are possible as well |
| Cover glasses | BK7, fused silica, sapphire, plastics (PC, PMMA, COC) |
| Coatings | For cover glasses only |

Table 3: Lens parameters that can be customized

Of course not all criteria can be met at once. For example, larger apertures based on the same EL-10-30 principle are slower and more power consuming. As an alternative, a mechanical design could be used similar to Optotune's ML-20-35 or ML-25-50, which requires no holding power and can easily be motorized.

Ordering information for custom versions of the EL-10-30

For custom versions, please follow the instructions below.

EL-C-10-30-AR-MAT- (F_{\min}/F_{\max})

C = custom design

AR = VIS : visible broad-band anti-reflection coating (400-700nm)
NIR : near broad-band infrared anti-reflection coating (700-1100nm)
355: narrow-band anti-reflection at 355nm
1064: narrow- band anti-reflection at 1064nm
NOC: No coating

MAT = HR : high refraction lens material ($n_b = 1.559$)
LD: low dispersion lens material ($n_b = 1.300$)

f_{\min} = minimum focal length

f_{\max} = maximum focal length

Example: EL-C-10-30-VIS-LD (+50/+150) refers to a custom electrical tunable lens of 10mm aperture packaged in a housing of 30mm diameter with anti-reflection coating for visible light, low dispersion lens material and a focal tunable range from +50 to +150mm.

For more information on optical, mechanical and electrical parameters, please contact sales@optotune.com.

DIGITAL HANDHELD OPTICAL POWER AND ENERGY METER CONSOLE

- ▶ Power and Energy Measurements for Free Space and Fiber Applications
- ▶ Designed for High Accuracy, Reliability, and Ease of Use
- ▶ Over 25 Compatible Sensors



PM100D



Multiple Display Options



Detector Options

Photodiode, Fiber, Integrating Sphere, Thermal, and Pyroelectric Sensors Available

Features

- Handheld Digital Power Meter Console
- Designed for Coherent and Incoherent Light Source Measurements
- Power and Energy Measurements for CW and Pulsed Source Detection
- Advanced Measurement Capabilities
- Large 4" LCD Display with Multiple Display Options
- Compatible with Over 25 Sensors (Shown Below)
- External 2 GB SD Memory Card for Storing and Transferring Data
- USB 2.0 Interface
- Long-Life Internal Li-Polymer Battery

The PM100D is the cornerstone of Thorlabs' optical power and energy meter consoles and is the digital counterpart to the PM100A Analog Power Meter Console. The console (and sensor, sold separately) is ideal for use as a CW and pulsed source power meter, incoherent optical source power meter, general light power meter, fiber power meter, and more. For a touchscreen version of the PM100D with more advanced spectral correction features, inputs for temperature and humidity sensors, data logging, and additional memory, we also offer the PM400 Capacitive Touchscreen Power and Energy Meter Console.

The PM100D is compatible with more than 25 photodiode, slim photodiode, integrating sphere, fiber, thermal, and pyroelectric sensors designed for use from the UV to the Mid-IR. See the *Sensor Selection* tab for further information. Thorlabs offers a variety of Power Meter Kits which include some of our most popular sensors bundled with the power meter console.

The PM100D is also available as a kit, bundled with our most popular sensors. Please visit our PM100D Kits page for more info. If you have any questions regarding these kits, or would like to suggest other kit options, please contact our tech support department for more details.

Console Design

The compact housing has a large, 4" backlit display with a resolution of 320 x 240 pixels and illuminated buttons, all of which make operation in dark labs easy. The LCD's clear GUI offers easy data readouts with an intuitive navigation scheme. Interactive tooltips help to operate the device by giving the user step-by-step operating instructions, displaying the next step on the screen.

The PM100D features four standard measurement screens. The first option is a numeric readout useful for standard power and energy readings. The second option is a tuning needle typically seen on analog devices, however, optimized to run as a digital readout on the display screen. Third is a tuning graph, which is very convenient for fine tuning CW and pulsed sources.

The unit can also be run in a data acquisition mode. Simply start the scan and the unit automatically starts recording data such as current power/energy, minimum, maximum, standard deviation, and other important statistics recorded over the acquisition period. The PM100D also features several user customizable displays and audio tuning for use when the detector is not within visual range. See the *Display Screens* tab for further information.

Connectivity

The sensor connector, shown to the right, enables "hot swappable" quick sensor exchange. The sensor connectors contain all the sensor information including NIST-traceable responsivity curves, sensor types, and model number.

A slot for an SD memory card (a 2 GB SD card is included) allows data recording even in stand-alone operation, giving the user large memory storage when recording data in the field or away from a computer in the lab. Data can also be recorded via the USB PC connection and the control software. The PM100D software is capable of handling up to eight consoles simultaneously. PC control software and features are highlighted in the *Software* tab, which also includes programming reference guides for LabVIEW™, Visual C++, Visual C#, and Visual Basic.

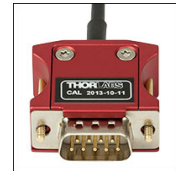
In addition to remote control operation and data logging/recording, the USB connection can also act as the charging system for the Li-Polymer battery. Also included is an AC battery charger which uses an intelligent charging management system to improve battery lifetime and reduce battery memory effects.

Sensor Upgrade Service

Thorlabs' current line of C-Series sensors and power meter consoles are not compatible with old power meter consoles and sensor heads, respectively. We offer a sensor upgrade service if you want to use your existing sensors with a new power meter console. Note: upgraded sensors will be incompatible with old power meter consoles and new sensors converted to work with older consoles will not be compatible with the PM100D. Please contact our tech support team for details.

| Item # | PM100D |
|--|---------------------------------------|
| Compatible Sensors | Photodiode, Thermal, and Pyroelectric |
| Optical Power Range ^a | 100 pW to 200 W |
| Optical Energy Range ^a | 3 μJ to 15 J |
| Available Sensor Wavelength Range ^a | 185 nm - 25 μm |
| Display Refresh Rate | 20 Hz |
| Bandwidth ^a | DC - 100 kHz |
| Photodiode Sensor Range ^b | 50 nA - 5 mA |
| Thermopile Sensor Range ^b | 1 mV - 1 V |
| Pyroelectric Sensor Range ^b | 100 mV - 100 V |

- Sensor Dependent
- Ranges Selectable in Watts (Photodiode and Thermopile) or Joules (Pyroelectric) and is dependent on the sensor used.



Click to Enlarge
Thorlabs' C-Series Power Meter Sensor Connectors Include the Sensor Calibration Data

| | |
|--|--|
| Item # | PM100D |
| Display | |
| Display Type | Graphical LCD 320 x 240 pixels, LED Backlight |
| Display Screens | Numerical, Bar Graph, Line Graph, Statistics, Simulated Analog Needle |
| Viewing Area | 81.4 mm x 61.0 mm (3.20" x 2.40") |
| Refresh Rate | 20 Hz |
| Audio | 1x Speaker |
| Sensor Interface | |
| Compatible Sensors | All Photodiodes, Thermopiles, and Pyros See Below for Full Sensor Specs |
| Time Constant Correction | <1 s |
| AD Converter | 16 bit |
| Trigger (Pulse Measurements, Pyroelectric Sensors) | Adjustable, 0.1 - 100% |
| Connector | DB9F, Left Side |
| Sensor Temperature Control | Thermistor |
| Temperature Range | -10 to 80 °C |
| Analog Outputs | |
| Signal | Amplified Input Signal (Not Corrected) |
| Voltage Range | 0 to 2 V |
| Accuracy | ±3% |
| Bandwidth | Up to 100 kHz, Dependent on Sensor and Settings |
| Connector | SMA, Left Side |
| Digital Outputs | |
| Memory | 2 GB Removable SD Card |
| Connector / Interface | Mini USB 2.0 |
| Power | |
| Battery | Li-Polymer, 3.7 V, 1300 mAh |
| Charger / DC Input | 5 V / 1 A |
| Dimensions and Mounting | |
| Dimensions (L x W x H) | 180 mm x 105 mm x 38 mm (7.09" x 4.13" x 1.50") |
| Weight | <0.5 kg (<1.1 lb) |
| Mounting Options | Kickstand; 1/4"-20 Post Thread |
| Operating Temperature | 0 to 40 °C |
| Storage Temperature | -40 to 70 °C |

Sensor Compatibility Specs

| Item # | PM100D | | |
|------------------------|--|--|--|
| Detector Compatibility | Photodiode Sensors: S1xxC Series Photodiodes (Max 5 mA) | Thermal Sensors: S3xxC Series Thermopiles (Max 1 V) | Pyroelectric Sensors: ESxxC Series Pyros (Max 100 V) |
| Measurement Ranges | 6 Decades; 50 nA - 5 mA Ranges Selectable in W, Sensor Dependent | 4 Decades; 1 mV - 1 V Ranges Selectable in W, Sensor Dependent | 4 Decades; 100 mV - 100 V Ranges Selectable in J, Sensor Dependent |
| Wavelength Ranges | 200 nm - 1800 nm | 190 nm - 25 µm | 185 nm - 25 µm |
| Power / Energy Ranges | 100 pW - 20 W | 100 µW - 200 W | 10 µJ - 15 J |
| Units | W, dBm, W/cm ² , A | W, dBm, W/cm ² , V | J, dBm, J/cm ² , V |
| Accuracy | ±0.2% of Full Scale (5 µA - 5 mA) ±0.5% of Full Scale (50 nA) | ±0.5% of Full Scale (10 mV - 1 V) ±1% of Full Scale (1 mV) | ±0.5% of Full Scale (100 mV - 100 V) |
| Display Resolution | 1 pA / Responsivity Value (A/W) | 1 µV / Responsivity Value (V/W) | 100 µV / Responsivity Value (V/W) |
| Bandwidth | DC - 100 kHz, Dependent on Sensor and Settings | DC - 10 Hz, Dependent on Sensor and Settings | DC - 30 Hz, Dependent on Sensor and Settings |
| Wavelength Correction | Sensor Dependent | Sensor Dependent | Sensor Dependent |

For a full list of the sensor head specifications please visit the Photodiode Power Sensors, Thermal Power Sensors, or Pyroelectric Energy Sensors pages. For other information, please contact tech support.

Features

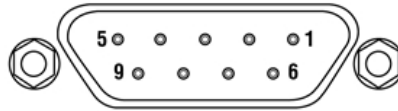
- Header line with sensor information, date/time and battery state
- Status line with warning annunciators Bar graph and configurable left and right sub display areas to display a minimum and a maximum value or a ratio of both values (numerical screen only)
- Tool tip text above the menu
- Easily accessible menu soft buttons

| GUI Overview | | | |
|--|---|--|--|
| <p>On the top bar, the sensor, date and time, and battery life indicator are shown.</p> | | <p>These menus at the bottom of the display access all the standard and customizable displays on the PM100D. The text display above the sub menus provides further assistance in navigating these menus.</p> | <p>Power and energy range, wavelength, measurement configuration, units, audio tuning, measurement views, and the system menu are all accessible from this bottom menu.</p> |
| <p>The main window contains one of the six standard display views described below. Here, the numerical readout is shown along with min and max values.</p> | | <p>Below the main window is a bar graph displaying relative and absolute changes in power and energy.</p> | <p>The bottom menu also allows customization of the display screen to include frequency, power density, and min and max values.</p> |
| Numeric Screen (Power Mode) | | Statistics Screen (Power Mode) | |
| | <p>This display combines a clear numerical 4-digit read out of the optical power, a bar-graph function with zooming capabilities, and configurable sub displays.</p> | | <p>The statistics display shows the actual, minimum, maximum and mean power values in linear and logarithmic representation; further the standard deviation, the max/min ratio, the number of samples and the elapsed time.</p> |
| Trend Graph (Power Mode) | | Needle Tuning (Power Mode) | |
| | <p>For laser tuning and beam alignment to visualize changes and trends together with an additional 4-digit numerical value of the absolute power.</p> | | <p>A display imitating an analog needle together with an additional 4-digit numerical value for laser tuning tasks. A special feature is a resettable max hold indicator and a shiftable tuning sound.</p> |
| Pulsed Numeric Screen (Energy Mode) | | Pulsed Statistics Screen (Energy Mode) | |
| | <p>This display combines a clear numerical 4-digit read out of the optical energy, a bar-graph function with zooming capabilities, and configurable sub displays.</p> | | <p>The statistics display shows the actual, minimum, maximum and mean energy values in linear and logarithmic representation; further the standard deviation, the max/min ratio, the number of samples and the elapsed time.</p> |
| Pulse Bar Graph (Energy Mode) | | | |
| | <p>Like the Trend Graph (Power Mode) this easily shows changes and trends together with an additional 4-digit numerical value of the absolute energy of incident beam pulses.</p> | | |

The user can customize the display screen by selecting various measurement tasks to be shown on the screen. Some screens are partly configurable by the user, for example, the user can display the min and max values within a certain time period or enable visual and audible peak indicator as a tuning aid.

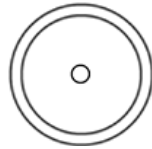
PM100D Sensor Connectors

D-type Female



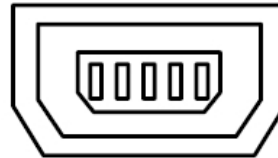
| Pin | Connection |
|-----|--|
| 1 | +5 V (Drive max 50 mA from this pin) |
| 2 | EEPROM Digital I/O |
| 3 | Photodiode Ground (Anode), Thermal and Pyro Sensor Ground, Analog Ground |
| 4 | Photodiode Cathode |
| 5 | Pyro-Electric Sensor + |
| 6 | DGND |
| 7 | PRESENT (Connect this pin via a 1k Ω - 10k Ω resistor to Pin 3 (AGND)) |
| 8 | Thermal Sensor + |
| 9 | N.C. |

**Analog Output
SMA Female**



0 ... 2 V

**Computer Connection
USB Type Mini-B**



USB Type Mini-B to Type A Cable Included

Standard Photodiode Power Sensors

- ▶ For General Purpose Optical Power Measurements
- ▶ Integrated Viewing Target for Easy Sensor Alignment
- ▶ Ø9.5 mm Sensor Aperture
- ▶ Sensor, Protective Cap, IR Target, and Thread Adapter Included
- ▶ Fiber Adapters Available Separately (See Table Below)
- ▶ See the Full Web Presentation for More Information



Click to Enlarge
S120C and CP90F Quick-Release Mount

These Standard Photodiode Power Sensors are ideal for metering low power coherent and incoherent sources from the UV to the NIR. Each NIST-Traceable, calibrated sensor features an integrated viewing target for easy alignment, enhanced shielding against electromagnetic interference, an over-temperature-alert device, and a large Ø9.5 mm sensor aperture. The sensors are compatible with 30 mm cage systems, Ø1/2" posts, and SM1 (1.035"-40) lens tubes, and are ideal for free-space and fiber-coupled sources.

| Item # ^a | S120VC | S120C | S121C | S122C |
|--|--|---|----------------------------------|----------------------------|
| Sensor Image (Click the Image to Enlarge) | | | | |
| Aperture Size | Ø9.5 mm | | | |
| Wavelength Range | 200 - 1100 nm | 400 - 1100 nm | 400 - 1100 nm | 700 - 1800 nm |
| Power Range | 50 nW - 50 mW | | 500 nW - 500 mW | 50 nW - 40 mW |
| Detector Type | Si Photodiode (UV Extended) | Si Photodiode | | Ge Photodiode |
| Linearity | ±0.5% | | | |
| Resolution ^b | 1 nW | | 10 nW | 2 nW |
| Measurement Uncertainty ^c | ±3% (440 - 980 nm) ±5% (280 - 439 nm) ±7% (200 - 279 nm, 981 - 1100 nm) | ±3% (440 - 980 nm) ±5% (400 - 439 nm) ±7% (981 - 1100 nm) | | ±5% |
| Coating/Diffuser | Reflective ND (OD1.5) ^d | Reflective ND (OD1) ^e | Reflective ND (OD2) ^f | Absorptive ND (Schott NG9) |
| Head Temperature Measurement | NTC Thermistor 4.7 kΩ | | | |
| Housing Dimensions | Ø30.5 mm x 12.7 mm | | | |
| Cable Length | 1.5 m | | | |
| Post Mounting ^{d,e,f} | Universal 8-32 / M4 Tap, Post Not Included | | | |
| Aperture Thread | External SM1 (1.035"-40) | | | |
| Compatible Fiber Adapters | S120-FC, S120-SMA, S120-ST, S120-LC, and S120-SC (Not Included) | | | |
| Compatible Consoles | PM400, PM200, PM100D, PM100A, PM100USB, and PM320E | | | |

- For complete specifications, please see the *Specs* tab here.
- Measured with PM100D console in low bandwidth setting.
- Beam diameter > 1 mm.
- For the S120VC, these specifications are valid for devices with serial numbers 1203xxx or higher. Older versions had a reflective ND diffuser (OD1). Additionally, they came with an 8-32 tap and M4 adapter. For additional information, please contact technical support.
- For the S120C, these specifications are valid for devices with serial numbers 1203xxx or higher. Older versions had an absorptive ND diffuser (Schott NG3). Additionally, they came with an 8-32 tap and M4 adapter. For additional information, please contact technical support.
- For the S121C, these specifications are valid for devices with serial numbers 1203xxx or higher. Older versions had an absorptive ND diffuser (Schott NG9). Additionally, they came with an 8-32 tap and M4 adapter. For additional information, please contact technical support.

| Part Number | Description | Price | Availability |
|-------------|---|----------|--------------|
| S120VC | Standard Photodiode Power Sensor, Si, 200 - 1100 nm, 50 mW | 378,00 € | Today |
| S120C | Standard Photodiode Power Sensor, Si, 400 - 1100 nm, 50 mW | 273,00 € | Today |
| S121C | Standard Photodiode Power Sensor, Si, 400 - 1100 nm, 500 mW | 296,00 € | 2-3 Days |
| S122C | Standard Photodiode Power Sensor, Ge, 700 - 1800 nm, 40 mW | 545,00 € | Today |

DIGITAL CAMERA

ORCA[®]-Flash4.0 V2

Versatile by design

A game changer from inception and a proven performer since its initial release, the ORCA-Flash4.0 V2 offers unrivaled flexibility across a wide range of imaging applications. Easily change from USB to Camera Link connectivity. Switch from a blazing fast scan to a virtually noiseless slow scan by a simple click in software. Use our Lightsheet Readout Mode™ for seamless integration with light sheet microscopy systems. Robust triggering allows the ORCA-Flash4.0 V2 to drive other devices or be driven by them. And then there's the highest QE of any sCMOS camera on the market.

Exceptional quantum efficiency

Over 70 %
at 600 nm

Low noise

1.3 electrons median 1.9 electrons rms
Standard scan at 100 frames/s

0.9 electrons median 1.5 electrons rms
Slow scan at 30 frames/s

High-speed readout

100 frames/s
Camera Link at 4.0 megapixels



HAMAMATSU
PHOTON IS OUR BUSINESS

High sensitivity means extreme versatility

The ORCA-Flash4.0 V2 is changing the game of scientific imaging. For years, cooled CCDs have been the go-to technology for fluorescence applications such as GFP or multi-channel imaging that require high signal to noise, high contrast images. EM-CCDs have been scientists' choice for low-light, often high speed applications such as TIRF or spinning disk confocal. For lack of a better choice, the same technology has been adopted for localization microscopy. The ORCA-Flash4.0 V2 offers such a multitude of benefits that it not only easily accomplishes each of these applications -- it may do them better.

Fan Long, Shaoqun Zeng, and Zhen-Li Huang. "Localization-based super-resolution microscopy with an sCMOS camera Part II: Experimental methodology for comparing sCMOS with EMCCD cameras," *Optics Express*, Vol. 20, Issue 16, pp. 17741-17759 (2012) <http://dx.doi.org/10.1364/OE.20.017741>

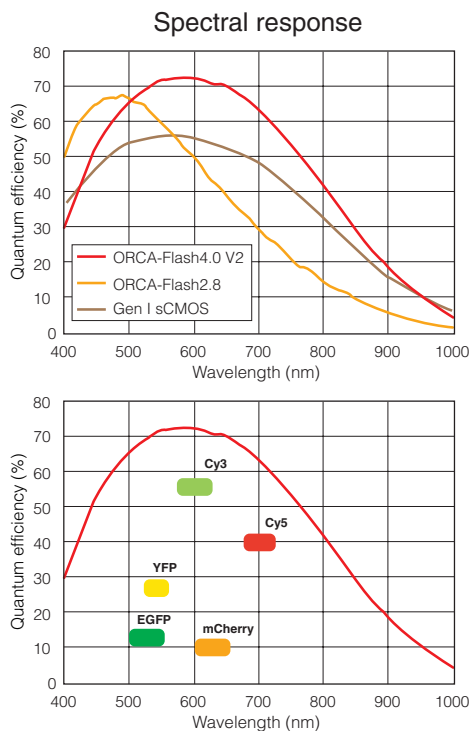
Quantum efficiency: higher than 70 % at 600 nm and 50 % at 750 nm

The ORCA-Flash4.0 V2 is engineered to outperform all other cameras for fluorescence microscopy. With carefully designed pixels and on-chip lens technology, its Gen II sCMOS sensor provides high QE across the range of wavelengths most commonly used in fluorescence microscopy.

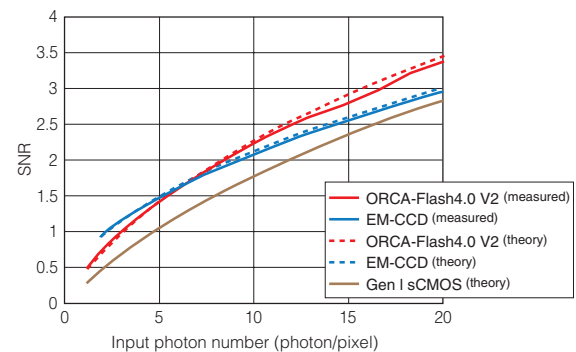
Low noise

The ORCA-Flash4.0 V2 has the lowest read noise at 100 frames/s of any CCD or sCMOS camera. Even EM-CCDs trade off "relative" low read noise for multiplicative noise by using on-chip gain. But the ORCA-Flash4.0 V2 requires no tradeoffs. Our "quiet" electronics successfully lower the limit of detection, allowing you to take full advantage of high frame rates and see your signal with fewer photons.

The unique combination of high quantum efficiency and low noise, in the absence of EM-CCD multiplicative noise, means that your images are not limited by the camera. Detect signal at low light levels, compare small changes in intensity, and discriminate small signals amid large backgrounds—with ease.



SNR Comparison of ORCA-Flash4.0 V2, Gen I sCMOS and EM-CCD



The ORCA-Flash4.0 V2 SNR exceeds that of EM-CCDs at about 6 photons/pixel. The solid lines show measured data at 533 nm. This measurement aligns well with predicted values (dotted line) for EM-CCD and ORCA-Flash4.0 V2. For comparison, the theoretical line for the Gen I type sensor is shown. Due to low QE and higher read noise, the Gen I camera does not compete with EM-CCD or Gen II ORCA-Flash4.0 V2 at these low light levels.

ORCA-Flash4.0 V2: QE = 70 %, Nr = 1.6 electrons rms as measured for this camera
 EM-CCD: QE = 91 %, Nr = 0.2 electrons rms
 Gen I sCMOS: QE = 52 %, Nr = 2 electrons rms as reported in literature

→ **High speed** Up to 40 min. of continuous full speed, full resolution acquisition*1

*1 This was tested with Dell T5500 (E5640 2.66GHz) + RAID0 (LSI MegaRAID SAS 9260-4i) and 4 pcs SATA SSD drives (SAMSUNG MZ-7PC512) Windows7 64 bit

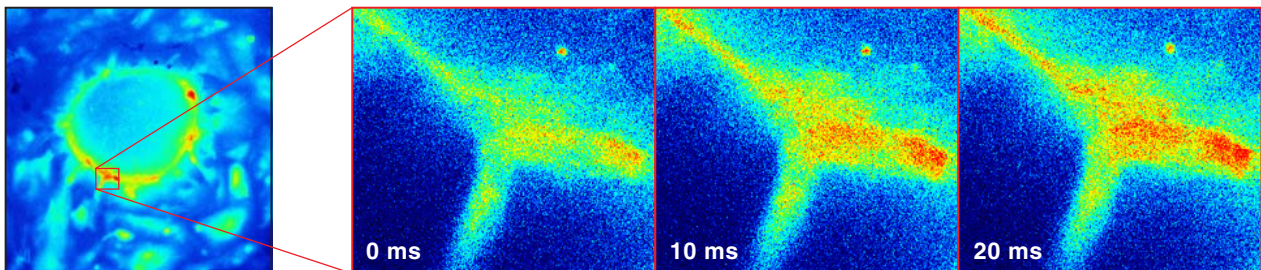
Allegro or presto? You be the Conductor.

When conducting imaging with a camera that has 4 194 304 pixels with 16-bit data depth, a single image is 8 megabytes. But capturing a single frame is child's play. What really matters is sustained, sequential image capture. Hamamatsu's ImageConductor gives you control over which speed works for you. In the default configuration, the ORCA-Flash4.0 V2 comes with a USB 3.0 card and cable and will deliver 30 frames/s of full frame acquisition. If you choose, upgrade to our fully supported FireBird PCI Express Gen II 8x Camera Link card, and that very same camera, without any additional modifications, can achieve 100 frames/s full resolution speed. Combining the Camera Link version with our recommended solid state drive and high-speed computer keeps your data flowing, for up to 40 minutes of full speed, full resolution recording. Both camera configurations facilitate fine tuning of frame rates by allowing flexible region of interest, letting you select the area that matters. At all speeds, in every configuration, the ORCA-Flash4.0 V2 has just 1.9 electrons rms (1.3 electrons median) read noise for the ultimate in versatility and performance.

Low noise and fast readout time simultaneously

| Readout speed | | Camera Link | | USB 3.0 | | |
|---------------|------|--------------------------|-------------------------|--------------------|--------|-------------------------|
| | | Horizontal pixel | Binning 2 × 2, 4 × 4 | Horizontal pixel | | Binning 2 × 2, 4 × 4 |
| | | 2048 / 1536 / 1024 / 512 | | 2048 / 1536 / 1024 | 512 | |
| Vertical line | 2048 | 100 | | 30 | 100 | 100 |
| | 1024 | 200 | | 60 | 200 | 200 |
| | 512 | 400 | | 120 | 400 | 400 |
| | 256 | 801 | | 240 | 801 | 801 |
| | 128 | 1603 | | 481 | 1603 | 1603 |
| | 64 | 3206 | | 968 | 3206 | 3206 |
| | 8 | 25 655 | | 7894 | 25 655 | 25 655 |

Readout speed at center position (frames/s, typ.)



High-speed Ca²⁺ imaging of cardiomyocyte derived from human iPS cell stained with Fluo8-AM. Sequential images were obtained every 10 ms. Left: whole FOV of the ORCA-Flash4.0 V2 image. Right: magnified images show rapid and finely localized changes in intracellular Ca²⁺ concentration associated with cardiomyocyte contractions.

 Specifications

| | | |
|------------------------------------|---------------------------------------|---|
| Product number | | C11440-22CU (ORCA-Flash4.0 V2) |
| Imaging device | | Scientific CMOS sensor FL-400 |
| Effective number of pixels | | 2048(H) × 2048(V) |
| Cell size | | 6.5 μm × 6.5 μm |
| Effective area | | 13.312 mm × 13.312 mm |
| Full well capacity (typ.) | | 30 000 electrons |
| Readout time | Standard scan (at 100 frames/s) | 10 ms |
| | Slow scan (at 30 frames/s) | 33 ms |
| Readout noise | Standard scan (at 100 frames/s, typ.) | 1.9 electrons rms (1.3 electrons median) |
| | Slow scan (at 30 frames/s, typ.) | 1.5 electrons rms (0.9 electrons median) |
| Dynamic range (typ.)* ² | | 33 000:1 |
| Quantum efficiency | | Higher than 70 % at 600 nm and 50 % at 750 nm |

| Cooling method | Dark current (typ.) | Sensor temperature (nominal) |
|--------------------------------|------------------------|------------------------------|
| Forced air (Ambient at +20 °C) | 0.5 electrons/pixel/s | -10 °C |
| Water (+20 °C) | 0.15 electrons/pixel/s | -20 °C |
| Water (+15 °C) | 0.05 electrons/pixel/s | -30 °C |

| Readout speed | Camera Link | USB 3.0 |
|----------------------------------|-----------------|-----------------|
| Full resolution | 100 frames/s | 30 frames/s |
| 2048 × 1024 (at center position) | 200 frames/s | 60 frames/s |
| 2048 × 8 (at center position) | 25 655 frames/s | 7894 frames/s |
| 512 × 8 (at center position) | - | 25 655 frames/s |

| Lightsheet Readout Mode™ (Camera Link only) | |
|---|---|
| Readout format | Seamless readout |
| Readout direction | Top to bottom / Bottom to top |
| Readout time | 20 ms to 204.8 s (at full area readout) |
| Scan mode | Full area, Sub-array |

| | | |
|-----------------------------|--|------------------|
| A/D conversion | 16 bit output | |
| Readout modes | Digital binning 2 × 2 / 4 × 4 | |
| | Sub-array readout mode | |
| Exposure time* ³ | Internal trigger mode (at full resolution) | 1 ms to 10 s |
| | Internal trigger mode with sub-array readout | 38.96 μs to 10 s |
| | External trigger mode with sub-array readout | 1 ms to 10 s |
| Digital interface | Camera Link full configuration Deca mode / USB 3.0 | |
| Lens mount | C-mount | |
| Power requirement | AC 100 V to AC 240 V, 50 Hz/60 Hz | |
| Power consumption | Approx. 70 VA | |

| Trigger in | |
|---------------------------------|--|
| External trigger mode | Edge, Level, Synchronous readout and Start trigger |
| External trigger signal routing | SMA connector or Camera Link I/F |
| External trigger delay function | 0 to 10 s in 10 μs steps |

| Trigger out | |
|--------------------------------|---|
| External signal output | 3 programmable timing outputs |
| | Global exposure timing and Trigger ready output |
| External signal output routing | SMA connector |

| Software | |
|--------------------|---|
| Software interface | PC-based acquisition package included |
| | DCAM-SDK, commercially available software |

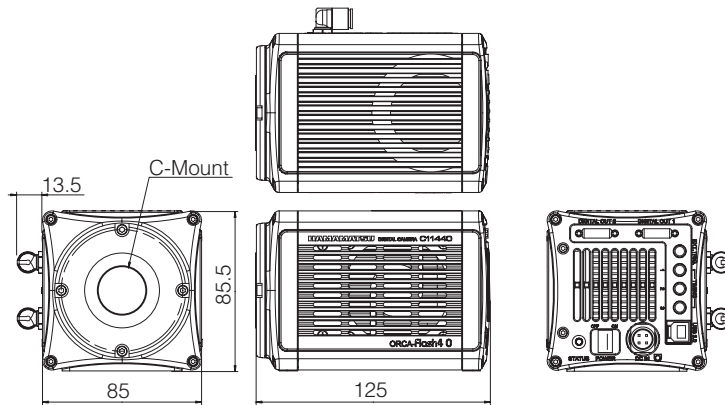
*² Full well capacity / Readout noise median in slow scan

*³ Minimum exposure time in internal trigger mode varies depending on sub-array setting. Minimum exposure time is in standard scan.

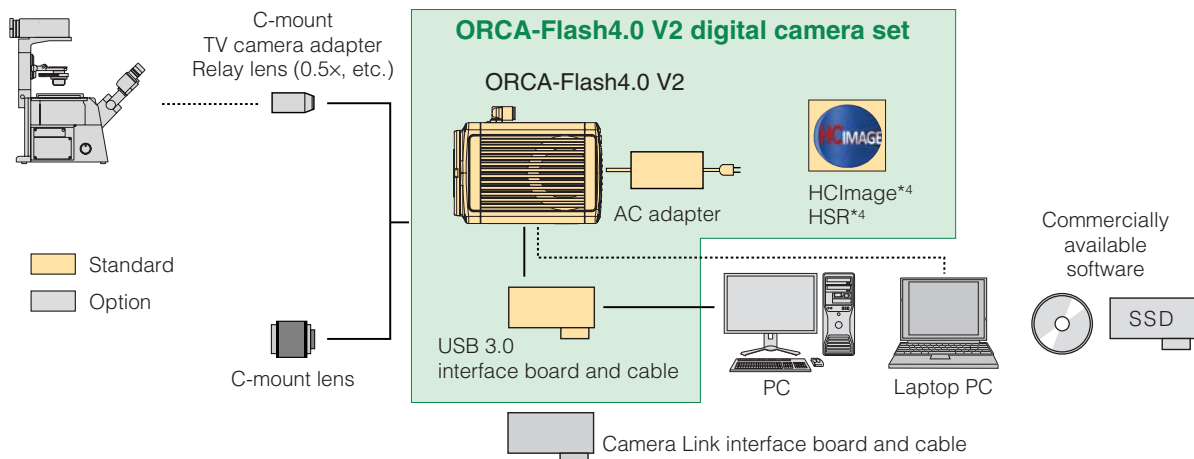
Dimensional outlines

Camera head (approx. 2.0 kg)

Unit: mm



Configuration example



*4 HImage/HSR software provides standard image measurement functions.

Please contact your local Hamamatsu Sales Office or distributor regarding actual configuration.

Cover image:
Rat hippocampal neurons and glial fixed and immunostained
with antibodies against HDAC6, GFAP and Synapsin1&2.
Courtesy of Qi Zhang, Ph.D., Vanderbilt University
<http://www.mc.vanderbilt.edu/labs/nano-neurosci/>

ORCA is registered trademark of Hamamatsu Photonics K.K. (France, Germany, Japan, U.K., U.S.A.)
HIMAGE is registered trademark of PHOTONICS MANAGEMENT CORP. (Australia, China, EU, Japan, Norway, Singapore, Switzerland, U.S.A.)
Product and software package names noted in this documentation are trademarks or registered trademarks of their respective manufacturers.

● Subject to local technical requirements and regulations, availability of products included in this promotional material may vary. Please consult your local sales representative.
● Information furnished by HAMAMATSU is believed to be reliable. However, no responsibility is assumed for possible inaccuracies or omissions.
Specifications and external appearance are subject to change without notice.

© 2013 Hamamatsu Photonics K.K.

HAMAMATSU PHOTONICS K.K. www.hamamatsu.com

HAMAMATSU PHOTONICS K.K., Systems Division

812 Joko-cho, Higashi-ku, Hamamatsu City, 431-3196, Japan, Telephone: (81)53-431-0124, Fax: (81)53-435-1574, E-mail: export@sys.hpk.co.jp

U.S.A.: Hamamatsu Corporation: 360 Foothill Road, P. O. Box 6910, Bridgewater, N.J. 08807-0910, U.S.A., Telephone: (1)908-231-0960, Fax: (1)908-231-1218 E-mail: usa@hamamatsu.com

Germany: Hamamatsu Photonics Deutschland GmbH: Arzbergerstr. 10, D-82211 Herrsching am Ammersee, Germany, Telephone: (49)8152-375-0, Fax: (49)8152-2658 E-mail: info@hamamatsu.de

France: Hamamatsu Photonics France S.A.R.L.: 19, Rue du Saule Trapu, Parc du Moulin de Massy, 91882 Massy Cedex, France, Telephone: (33)1 69 53 71 00, Fax: (33)1 69 53 71 10 E-mail: infos@hamamatsu.fr

United Kingdom: Hamamatsu Photonics UK Limited: 2 Howard Court, 10 Tewin Road Welwyn Garden City Hertfordshire AL7 1BW, United Kingdom, Telephone: 44-(0)1707-294888, Fax: 44-(0)1707-325777 E-mail: info@hamamatsu.co.uk

North Europe: Hamamatsu Photonics Norden AB: Thorshamnsgatan 35 SE-164 40 Kista, Sweden, Telephone: (46)8-509-031-00, Fax: (46)8-509-031-01 E-mail: info@hamamatsu.se

Italy: Hamamatsu Photonics Italia: S.R.L.: Strada della Moia, 1/E, 20020 Arese, (Milano), Italy, Telephone: (39)02-935 81 733, Fax: (39)02-935 81 741 E-mail: info@hamamatsu.it

China: Hamamatsu Photonics (China) Co., Ltd.: 1201 Tower B, JIaming Center, 27 Dongsanhuan Road North, Chaoyang District, Beijing 100020, China, Telephone: (86)10-6586-6006, Fax: (86)10-6586-2866 E-mail: hpc@hamamatsu.com.cn

Cat. No. SCAS0081E07
JAN/2013 HPK Created in Japan

A. Appendix 3: Interferometry

Project Report

This project was done under the supervision of the *Prof. Atchison* at the optics laboratories of the Queensland University of Technology (Brisbane, Queensland, Australia).

A.1 Introduction

One of the most important parts of the human eye is the retina (Figure A.1.1). The retina is a photo-sensor tissue of the eye that transforms the light information into neuronal impulses and sends them to the brain passing through the optical nerve. Basically, it is the main responsible of sight. Due to its importance, it has been developed and improved all the instrumentation and techniques to image and to obtain information of the living human retina.

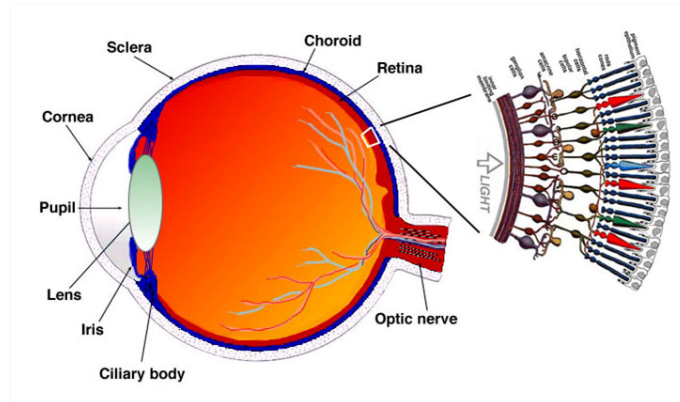


Figure A.1.1: A drawing of a section through the human eye with a schematic enlargement of the retina (Source: [146]).

Williams published a detailed review in this issue at 2011 [147]. The review starts presenting the ophthalmoscope, invented by Helmholtz [148] and ends with adaptive optics scanning laser ophthalmoscopy [149] and the main advantages of it, passing through imaging interference fringes on the retina [150, 151], the scanning laser ophthalmoscope [152] and OCT (Optical Coherence Tomography) [153].

The same way than in the vision correction topic, adaptive optics is presented as the most useful tool to overcome the limits in retinal imaging [147]. Nevertheless, the purpose of this study is to verify if there is some information that can be extracted imaging interference fringes on the retina and process them using superresolution techniques [154][9], or, in the contrary, if it is necessary to use adaptive optics.

A.2 Methods

Regarding the fact that two small coherent light sources, or images of such sources, have to be focused on the pupil's plane of the eye to create a fringe interference pattern on the retina [155], different experimental set-ups and modification of an instrument had been attempted to image it.

A.2.1 Experimental Set-Up: Configuration 1

The configuration 1 of the experimental set-up (Figure A.2.1) was composed of:

- Laser [$\lambda = 743.5nm$] and laser expander (1)
- 2 Circular apertures (2) (Details in Figure A.2.2)
- Dove prism (3)
- Pellicle Beamsplitter (PBS) [Thorlabs *BP245B345/55*] (5)
- Achromatic doublet [$f' = 30mm$] (6)
- Artificial eye (7)
- Camera lens (8)
- PixelLink Camera [*PL – A741*] (9)

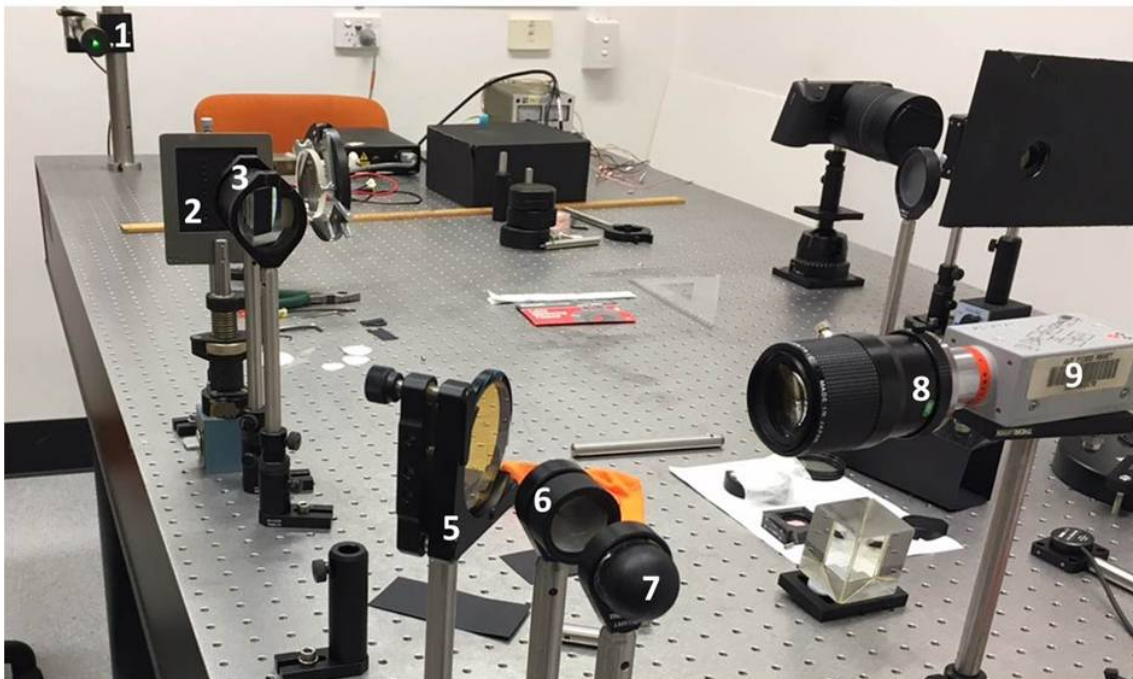


Figure A.2.1: Configuration 1; Laser (1), Circular Apertures (2), Dove Prism (3), FBS (5), Achromatic Doublet (6), Eye (7), Camera Lens (8) and Camera (9).

In order to create the interference pattern in the retina's plane of the eye (7), the laser beam passes first to the beam's expander (1) resulting in a $20mm$ diameter collimated beam. This beam is

divided into two spots of 1mm diameter by the circular apertures (2). A Dove prism (3) is after the apertures to change the orientation of the fringes. After this, there is the PBS (5) and an achromatic doublet (6), just in front of the eye, which focuses the two spots on the pupil's plane to create the interference pattern on the retina's plane. The retina is image by the beamsplitter and camera lens (8) onto the camera image plane (9).

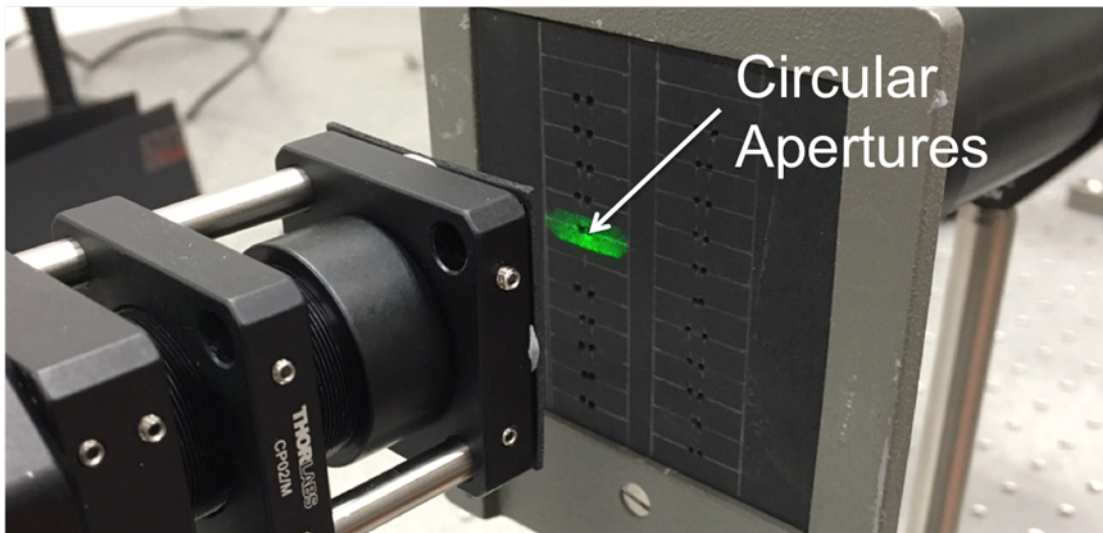


Figure A.2.2: Circular apertures.

A.2.2 Experimental Set-Up: Configuration 2

The configuration 2 was developed to have a system as similar as possible as that described in Lotmar's paper [155] to try to get the expected interference pattern.

This differs from configuration 1 by the light not being collimated before the achromatic doublet. To do that, a divergent lens was placed between the two circular apertures and the achromatic doublet (Figure A.2.3). A cube beamsplitter was used instead of the PBS to compare them and choose the best option for the system.

The two spots are focused on the pupil's plane of the eye (7) after passing through the divergent lens (4), the cube beamsplitter (5) and the achromatic doublet (6). Then the reflection of the retina is captured by the camera (9) which is focused on the retina's plane of the eye thanks to the oriented cube beamsplitter (5) and the camera lens (8). The Dove prism (3) is placed before the divergent lens since it can only work with collimated light [155].

A.2.3 Experimental Set-Up: Configuration 3

Due to several problems found with configuration 1 and 2 commented in the results section of this report, a configuration 3 was built up. In this case, a flat beamsplitter (50/50) and 3 mirrors (Figure A.2.4) were used instead of the circular apertures and the Dove prism. As a consequence, after the beam expander (1), the 20mm spot passed through the flat beam splitter (2) that reflected the 50% of the light to mirror 1 (3) and refracted the other 5% to mirror 2. Mirror 2 (4) reflected the 20mm spot to mirror 3 (5). Mirror 1 and 3 reflected the two 20mm spots to the achromatic

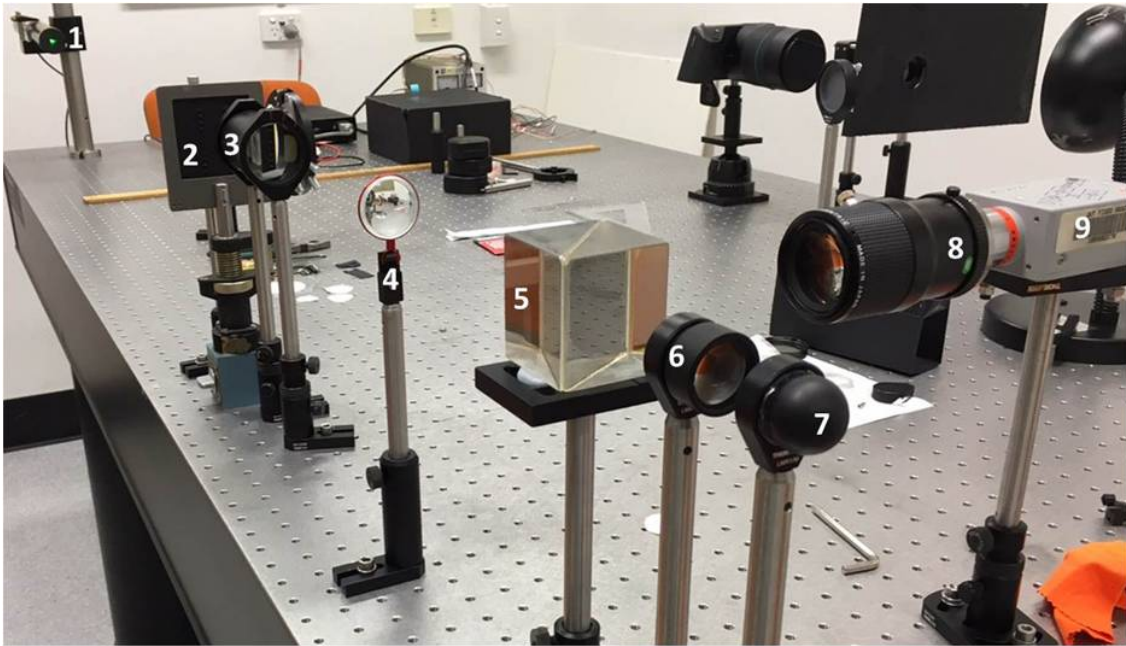


Figure A.2.3: Configuration 2; Laser (1), Circular Apertures (2), Dove Prism (3), Divergent lens (4), Cube beamsplitter (5), Achromatic Doublet (6), Eye (7), Camera Lens (8) and Camera (9).

doublet ($f' = 30\text{mm}$) going through the pellicle beamsplitter. The same way as in configuration 1, the achromatic doublet focused both spots on the pupil's plane of the eye. Then, the interference pattern created on the retina was imaged by the camera, thanks to the pellicle beamsplitter and the camera lens (Figure A.2.1).

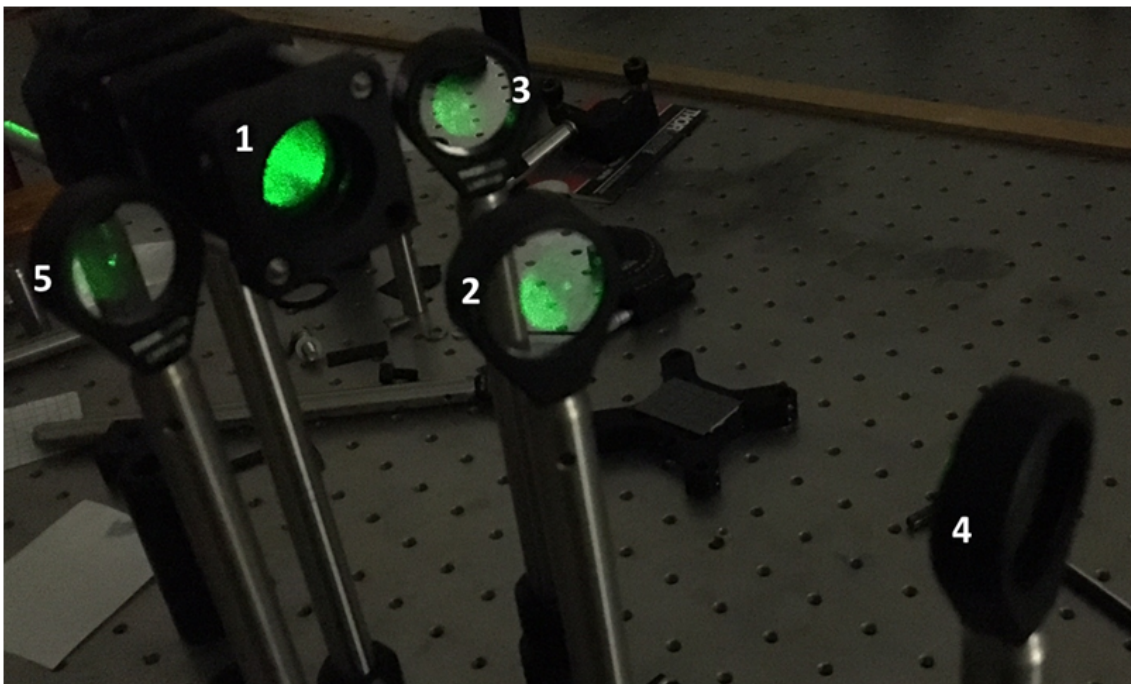


Figure A.2.4: First part of configuration 3; Beam expander (1), flat beamsplitter (2), mirror 1 (3), mirror 2 (4) and mirror 3 (5).

A.2.4 Modified Lotmar Interferometer

After all the unsuccessful attempts to create an appropriate fringe pattern on the retina with previous explained configurations, we decided to modify the Lotmar interferometer to get images of the fringe pattern that the system creates on the retina by a camera and to have enough intensity of light to image it.

Different sources as superluminescent LEDs, incandescent bulb or white light conducted by an optical fibre were tested. But only the laser of 637nm of wavelength (Laser Source THORLABS SFC635 (Power range from 0 to 8.04mW/ $\lambda = 637nm$)) had enough intensity to image the fringe pattern on the retina by a camera. As a consequence, the original illumination system was replaced by the optical fibre and lens that focus the light at the entrance pupil plane of the system (Figure A.2.5), which is placed after the lens.



Figure A.2.5: Image of the new illumination system composed by the optical fiber of the laser and the achromatic doublet.

A cube beamsplitter (50/50) and the camera used in the previous set-ups were added to get the images (Figure A.2.6). The beamsplitter orientation was manipulated to ensure that reflections from its walls did not enter the camera. A beam trap was also placed in the opposite direction of the camera to avoid the entrance of the light reflection of the wall of the first reflection light of the beamsplitter in it. Of course, this does not stop light being reflected from the side of the beamsplitter closest to the eye or to the wall.

Background images were taken. These may be used in processing, but this has not yet been done. Once all the modifications were added in the Lotmar interferometer, different tests were performed to check the safety power range of the laser and the availability of the system to get the images. In order to check the safety power range of the laser, a power meter sensor was placed 50mm away from the exit of the instrument (45mm away from the cube beamsplitter), since is where the eye has to be positioned. According to the results, although the maximum power of the laser was 8.03mW, only 30 μ W were arriving at cornea's plane, which is the half power of the safe limit (60 μ W). Then, the availability was also checked getting several images of the fringe pattern on the retina of a model eye and on the retina of two different human eyes.

Post-processing of images was done with Photoshop. This includes a pseudo-exposure control,

the gamma correction (is a nonlinear processing about the luminance of the image), levels (that you use to correct the tonal range and color balance of an image by adjusting intensity levels of image shadows, midtones, and highlights) and contrast values.

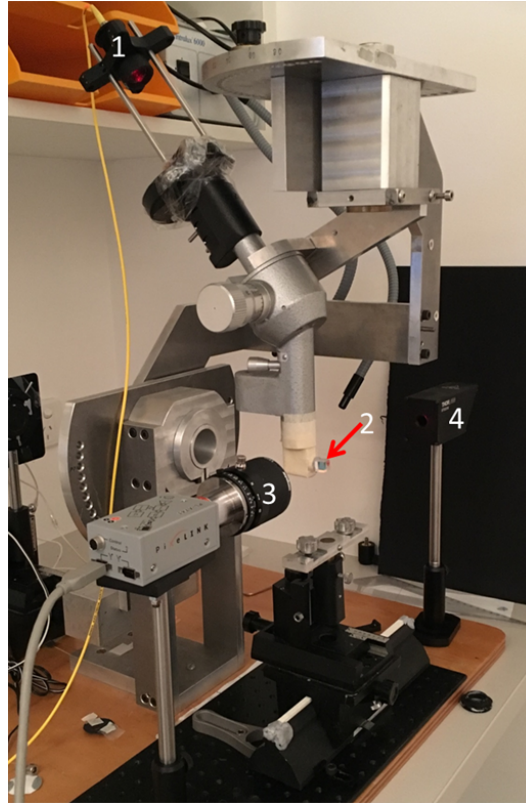


Figure A.2.6: Modified Lotmar interferometer; Illumination system (1), cube beamsplitter (2), camera lens (telecentric) + camera (3), beam trap (4).

A.2.4.1 Participants and Measurement Conditions

Right eyes of two participants of 22 and 31 years old were assessed. Some images were collected on a third participant (not reported here). The participants were stabilized by a bitebar and aligned with a xyz translation stage.

Part of the images was taken with dilated pupils. In this case, one drop of tropicamide 1% was inserted in the right eye of the participants 15min before the measurements. Both participants had a pupil's diameter of 7mm in this condition. The other part was taken with no dilation. In this case, the 31 years old participant had a pupil's diameter of 3mm and the 22 years old participant had a 4mm diameter of the pupil under the illumination conditions of the experiment. The only illumination was the own illumination of the instrument. The intensity of the light was high enough to cause near the maximum response of the pupil. Consequently, both participants had nearly their own minimum pupil's diameter when no dilated acquisitions were performed.

Taking into account that Lotmar interferometer has a range of frequency of the fringe pattern from 1cycle/degree to 75cycles/degree and 4 different orientations of the fringes (45, 90, 135and180degrees), a large number of images of different frequencies and orientations were gotten per each participant

in both conditions. The field angle was 3.5degrees . Different exposure times and laser power were used in different images. The camera focus was adjusted for each participant.

A.3 Results

As it was commented in the previous section, only with the modified Lotmar interferometer was possible to produce and image a fringe pattern on the retina. Configurations 1 and 2 of the set-up were imaging the two circular spots mask. This means that the spots never overlapped on the retina and, as a consequence, none appropriate interference pattern was formed (Figure A.3.1).

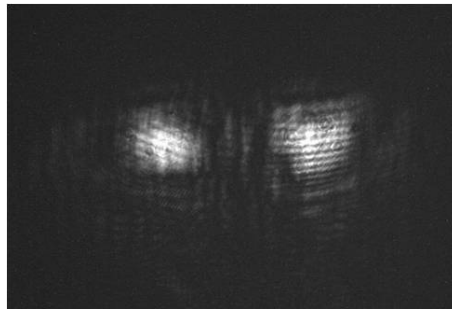


Figure A.3.1: Retinal plane image of configuration 1.

The two 20mm spots of configuration 3 were overlapped on the retina, but not the interference pattern that we were looking for was formed (Figure A.3.2). The problem with this configuration was the limited accuracy that the system had to align perfectly the two spots.

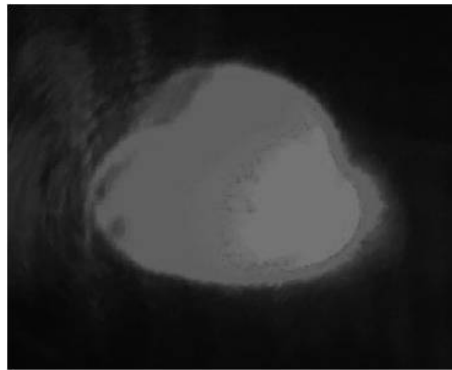


Figure A.3.2: Retinal plane image of configuration 3.

Several examples of model eye (Figure A.3.3) and the participants' images (Figure A.3.4 and A.3.5) are presented below. The orientation for the images is that of the images – it is possible that the subject's view is flipped about the vertical/horizontal axis and this needs checking.

A.4 Discussion

The quality of the images from 31 years old participant is quite better than the ones from the 22 years old participant. So, it might be recommendable to get more images from the 31 years old participant if it would be necessary have more images.

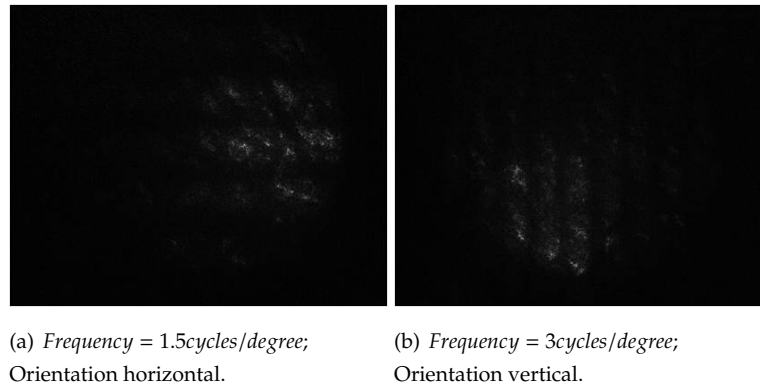


Figure A.3.3: Images of the retina plane of the model eye (*Exposuretime = 240ms; LaserPower = 8.03mW*)

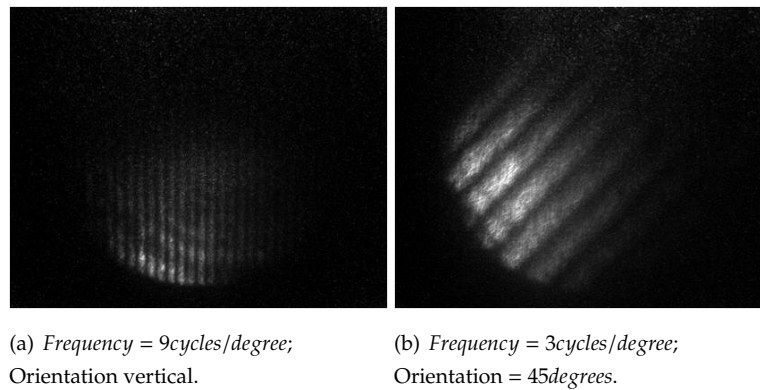


Figure A.3.4: Images of the retina plane of the no-dilated right eye of the 31 years old participant (*Exposuretime = 570ms; LaserPower = 8.03mW*) [Images had been modified in Photoshop].

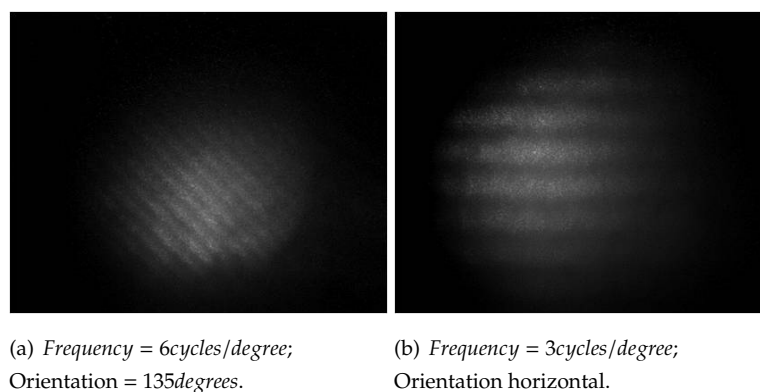


Figure A.3.5: Images of the retina plane of the dilated right eye of the 22 years old participant (*Exposuretime = 130ms* (a) and *230ms* (b); *LaserPower = 8.03mW*) [Images had been modified in Photoshop].

Further manipulation of the imaging parameters can be considered e.g. shorter exposure to reduce problems associated with eye movement combined with gains higher than 0 (all the images taken for this project have a gain of 0).

A.4. DISCUSSION

At this point of the project, it is possible to confirm that the modified Lotmar interferometer can be used to get images of the interference pattern that form on the retina of eyes. Due to this, the next steps should be process the images by superresolution techniques and prove it is possible, or not, to extract information about the distribution of the photoreceptors of the retina. If the conclusion is that is not possible, then the addition of adaptive optics can be considered as a solution.

Bibliography

- [1] R. B. Rabbets, *Clinical Visual Optics*, 4th ed., Elsevier, Ed. Philadelphia: Butterworth Heinemann, 2007.
- [2] Discovery Eye Foundation, "The Optic Nerve And Its Visual Link To The Brain," 2015. [Online]. Available: <http://discoveryeye.org/optic-nerve-visual-link-brain/>
- [3] A. Glasser and M. C. Campbell, "Presbyopia and the optical changes in the human crystalline lens with age." *Vision research*, vol. 38, no. 2, pp. 209–29, 1 1998. [Online]. Available: <http://www.ncbi.nlm.nih.gov/pubmed/10343784>
- [4] J. F. Koretz, C. A. Cook, and P. L. Kaufman, "Accommodation and Presbyopia in the Human Eye Changes in the Anterior Segment and Crystalline Lens With Focus," *Invest. Ophthalmology and Vision Science*, vol. 38, pp. 569–578, 1997.
- [5] Adithyakiran, "Progressive lenses- what's hidden besides the line," 2013. [Online]. Available: <https://adithyakiran.wordpress.com/2013/01/>
- [6] J. E. Sheedy, M. Buri, I. L. Bailey, and J. Azus, "Optics of progressive addition lenses," *American journal of Optometry & Physiological Optics*, vol. 64, no. 2, pp. 90–99, 1987.
- [7] E. S. Bennett, "Contact lens correction of presbyopia." *Clinical & experimental optometry : journal of the Australian Optometrical Association*, vol. 91, no. 3, pp. 265–78, 5 2008. [Online]. Available: <http://www.ncbi.nlm.nih.gov/pubmed/18201225>
- [8] R. Gil-Cazorla, S. Shah, S. A. Naroo, D. Shehzad, and A. Naroo, "A review of the surgical options for the correction of presbyopia," *Br J Ophthalmol*, vol. 100, pp. 62–70, 2016.
- [9] C. Owsley, B. Stalvey, J. Wells, and M. Sloane, "Older Drivers and Cataract: Driving Habits and Crash Risk," *Journal of Gerontology: MEDICAL SCIENCES*, vol. 54, no. 4, pp. 203–211, 1999.
- [10] World Health Organization, "Prevention of Blindness and Visual Impairment," World Health Organization, Geneva, Tech. Rep., 2002. [Online]. Available: <http://www.who.int/blindness/causes/en/>
- [11] Mark A. Latina M.D., "Cataracts." [Online]. Available: <https://marklatina.com/eye-care-services/cataracts/>
- [12] T. Ferrer-Blasco and D. Madrid-Costa, "Stereoacuity with Simultaneous Vision Multifocal Contact Lenses," *Optometry and Vision Science*, vol. 87, no. 9, pp. E663–E668, 2010.
- [13] G. Ravalico, F. Parentin, P. Sirotti, and F. Baccara, "Analysis of light energy distribution by multifocal intraocular lenses through an experimental optical model." *Journal of cataract and refractive surgery*, vol. 24, no. 5, pp. 647–652, 1998. [Online]. Available: [http://dx.doi.org/10.1016/S0886-3350\(98\)80259-9](http://dx.doi.org/10.1016/S0886-3350(98)80259-9)

BIBLIOGRAPHY

- [14] S. G. Kang and J. H. Lee, "The change of visual acuity and visual field by diminished illumination in eyes with multifocal intraocular lenses," *Korean Journal Ophthalmology*, vol. 8, pp. 72–76, 1994.
- [15] J. Gispets, M. Arjona, J. Pujol, M. Vilaseca, and G. Cardona, "Task oriented visual satisfaction and wearing success with two different simultaneous vision multifocal soft contact lenses," *Journal of Optometry*, vol. 4, no. 3, pp. 76–84, 2011.
- [16] P. de Gracia, C. Dorronsoro, A. Sanchez-Gonzalez, L. Sawides, and S. Marcos, "Experimental simulation of simultaneous vision," *Investigative Ophthalmology and Visual Science*, vol. 54, no. 1, pp. 415–422, 2013.
- [17] S. Manzanera, P. M. Prieto, D. B. Ayala, J. M. Lindacher, and P. Artal, "Liquid crystal Adaptive Optics Visual Simulator: Application to testing and design of ophthalmic optical elements," *OPTICS EXPRESS*, vol. 15, no. 24, pp. 16 177–16 188, 2007.
- [18] M. Vinas, C. Dorronsoro, V. Gonzalez, D. Cortes, A. Radhakrishnan, and S. Marcos, "Testing vision with angular and radial multifocal designs using Adaptive Optics," *Vision Research*, 2016.
- [19] M. Aldaba, A. Giner, J. L. Güell, and J. Pujol, "Visual performance evaluation of a new multifocal intraocular lens design before implantation," in *XXXII Congress of the ESCRS: Poster Abstracts*, London, 2014.
- [20] W. N. Charman, R. Montés-Micó, and H. Radhakrishnan, "Problems in the Measurement of Wavefront Aberration for Eyes Implanted with diffractive bifocal and multifocal intraocular lenses," *Journal of refractive surgery (Thorofare, N.J. : 1995)*, vol. 24, no. March, pp. 280–286, 2008.
- [21] H. S. Hwang, H. Y. Shin, and C. K. Joo, "Double-pass system (optical quality analysis system) for analysis of the multifocal function of a diffractive multifocal intraocular lens (Acrysof ReSTOR®) compared to a monofocal intraocular lens (Acrysof IQ®)," *Journal of the Optical Society of Korea*, vol. 18, no. 2, pp. 110–117, 2014.
- [22] G. Heiting and M. Mattison-Shupnick, "Bifocal and trifocal options for vision after age 40," 2016. [Online]. Available: <http://www.allaboutvision.com/over40/segmented.htm>
- [23] D. J. Meister and S. W. Fisher, "Progress in the spectacle correction of presbyopia. Part 1: Design and development of progressive lenses," *Clinical and Experimental Optometry*, vol. 91, no. 3, pp. 240–250, 2008.
- [24] M. Fransoy, L. Guissasola, and M. Vera, *Tecnología Óptica*, 1st ed., Edicions UPC, Ed. Terrassa: Universitat Politècnica de Catalunya, 2001.
- [25] E. Szasz and A. Szasz, "Progressive lenses: How to get used easier with." [Online]. Available: <http://www.perfect-eyeglasses-guide.com/progressive-lenses.html>
- [26] ZEISS AG, "Power design of progressive lenses." [Online]. Available: https://www.zeiss.com/vision-care/en_us/eye-care-professionals/optical-knowledge/optical-basics/optical-designs/power-design-of-progressive-lenses-pal.html

BIBLIOGRAPHY

- [27] S. C. Han, A. D. Graham, and M. C. Lin, "Clinical Assessment of a Customized Free-Form Progressive Add Lens Spectacle," *Optometry and Vision Science*, vol. 88, no. 2, pp. 234–243, 2011.
- [28] ProCornea Speziallinser, "Menicon Z Executive." [Online]. Available: <http://procornea.no/menicon-z-executive.aspx>
- [29] CONOPTICA S.L., "BICON: Lente permeable bifocal." [Online]. Available: <http://www.conoptica.es/es/productos/lentes-de-contacto/presbicia/136-bicon>
- [30] K. S. Ames, P. Erickson, L. Godio, and L. Medici, "Factors influencing vision with rigid gas permeable alternating bifocals," *Optometry and Vision Science*, vol. 66, no. 2, pp. 92–97, 1989.
- [31] J. G. Oster, "Multifocal IOL vs. Monofocal IOL: What you need to know." [Online]. Available: http://www.grandvalleylasik.com/informed_decision.html
- [32] L. Werner, "Glistenings and surface light scattering in intraocular lenses." *Journal of cataract and refractive surgery*, vol. 36, no. 8, pp. 1398–420, 8 2010.
- [33] Abbott Medical Optics Inc., "The TECNIS multifocal family of IOLs," Tech. Rep., 2015. [Online]. Available: <http://abbottmedicaloptics.com/pdf/AMO-Tecnis-Multifocal-IOL-Family-SpecSheet.pdf>
- [34] M. B. Baamonde, "El inicio: LIO difractiva 815LE de 3M," in *Lentes intraoculares bifocales, multifocales y acomodativas en cirugía del cristalino*, 1st ed., S. E. d. I. C. O. Implanto-Refractiva, Ed. MAC LINE S.L., 2007, ch. 8, pp. 77–80.
- [35] M. Orchowsky, "Multifocal intraocular lenses," in *Lentes intraoculares bifocales, multifocales y acomodativas en cirugía del cristalino*, 1st ed., S. E. d. C. Implanto-Refractiva, Ed. MAC LINE S.L., 2007, ch. 3, pp. 35–42.
- [36] N. E. de Vries and R. M. M. a. Nuijts, "Multifocal intraocular lenses in cataract surgery: literature review of benefits and side effects." *Journal of cataract and refractive surgery*, vol. 39, no. 2, pp. 268–78, 2 2013.
- [37] Abbott Medical Optics Inc., "TECNIS Symphony: Extended range of vision IOL," 2014. [Online]. Available: <http://www.tecnisiol.com/eu/tecnis-symfony-iol.htm>
- [38] U.S. Food and Drug Administration, "FDA approves first intraocular lens with extended range of vision for cataract patients For Immediate Release," Tech. Rep., 2016.
- [39] Rayner, "M-flex Multifocal and M-flex T Multifocal." [Online]. Available: <http://www.rayner.com/en/m-flex-and-m-flex-t>
- [40] Oculentis, "LENTIS MPlus LS-313 MF30," Tech. Rep. [Online]. Available: <http://www.oculentis.com/Downloads/LENTIS-Mplus-LS-313-MF30-DE.PDF>
- [41] OPHTEC BV, "CE-Mark for Precizon Presbiopic IOL," 2017. [Online]. Available: http://www.ophtec.com/company/news?news_id=565266

BIBLIOGRAPHY

- [42] Alcon Novartis Co., "ACRYSOF IQ RESTOR MULTIFOCAL IOL." [Online]. Available: <https://www.myalcon.com/products/surgical/acrysof-iq-restor-multifocal-iol/specifications.shtml>
- [43] D. Madrid-Costa, A. Cerviño, T. Ferrer-Blasco, S. García-Lázaro, and R. Montés-Micó, "Visual and optical performance with hybrid multifocal intraocular lenses," *Clinical and Experimental Optometry*, vol. 93, no. 6, pp. 426–440, 2010.
- [44] P. B. Morgan, N. Efron, and C. A. Woods, "An international survey of contact lens prescribing for presbyopia," *Clinical and Experimental Optometry*, vol. 94, no. 1, pp. 87–92, 2011.
- [45] J. Santodomingo-Rubido, C. Villa, and P. B. Morgan, "Lentes de contacto adaptadas en España en 2014," *Gaceta de Optometría y Óptica Oftálmica*, vol. Xaneiro, no. 499, pp. 10–15, 2015.
- [46] N. Efron, J. J. Nichols, C. A. Woods, and P. B. Morgan, "Trends in US Contact Lens Prescribing 2002 to 2014." *Optometry and vision science : official publication of the American Academy of Optometry*, vol. 92, no. 7, pp. 758–67, 2015.
- [47] Julie, "What are multifocal contact lenses and should you order them online?" 2015. [Online]. Available: <http://contactsadvice.com/what-are-multifocal-contact-lenses-and-should-you-order-them-online>
- [48] Alcon Novartis Co., "Air Optix Aqua Multifocal." [Online]. Available: <http://www.airoptix.com/contact-lenses/multifocal.shtml>
- [49] J. M. Artigas, P. Capilla, A. Felipe, and J. Pujol, *Óptica fisiológica. Psicofísica de la visión.*, 1995.
- [50] "BERNELL (USA)." [Online]. Available: <https://www.bernell.com/category/674>
- [51] "Precision Vision (IL, USA)." [Online]. Available: <http://www.precision-vision.com/product/pvnumbersacuitychartfor4meters/>
- [52] C. Fedtke, R. C. Bakaraju, K. Ehrmann, J. Chung, V. Thomas, and B. A. Holden, "Visual performance of single vision and multifocal contact lenses in non-presbyopic myopic eyes," *Contact Lens and Anterior Eye*, vol. 39, pp. 38–46, 2016.
- [53] J. Woods, C. Woods, and D. Fonn, "Visual Performance of a Multifocal Contact Lens versus Monovision in Established Presbyopes," *Optometry and Vision Science*, vol. 92, no. 2, pp. 175–182, 2014.
- [54] S. Cillino, A. Casuccio, F. Di Pace, R. Morreale, F. Pillitteri, G. Cillino, and G. Lodato, "One-Year Outcomes with New-Generation Multifocal Intraocular Lenses," *Ophthalmology*, vol. 115, pp. 1508–1516, 2008.
- [55] "Contrast Sensitivity Testing." [Online]. Available: <http://www.allaboutvision.com/eye-exam/contrast-sensitivity.htm>
- [56] "Standardized Contrast Sensitivity Tests." [Online]. Available: <http://www.vectorvision.com/csv1000-contrast-sensitivity/>

- [57] S. García-Lázaro, T. Ferrer-Blasco, D. Madrid-Costa, C. Albarrán-Diego, and R. Montés-Micó, "Visual Performance of Four Simultaneous-Image Multifocal Contact Lenses Under Dim and Glare Conditions."
- [58] R. Montés-Micó and J. L. Alió, "Distance and near contrast sensitivity function after multifocal intraocular lens implantation," *Journal of Cataract & Refractive Surgery*, vol. 29, no. 4, pp. 703–711, 4 2003.
- [59] "TNO Stereo Test." [Online]. Available: <http://www.graftonoptical.com/products/775-tno-stereo-test.html>
- [60] E. p. Estudiantes, "La Estereopsis," 2012. [Online]. Available: <http://estrabismoparaestudiantes.blogspot.com.es/2012/07/la-estereopsis-en-podemos-definir.html>
- [61] Bernell, "Random Dot 2 Test." [Online]. Available: <http://www.bernell.com/product/VA1007/Depth-Perception-Tests>
- [62] GIMA, "Lang Stereotest II." [Online]. Available: http://www.gimaitaly.com/prodotti.asp?sku=31295&dept_selected=521&dept_id=5210
- [63] K. Richdale, G. L. Mitchell, and K. Zadnik, "Comparison of Multifocal and Monovision Soft Contact Lens Corrections in Patients With Low-Astigmatic Presbyopia," *Optometry and Vision Science*, vol. 83, no. 5, pp. 266–273, 2006.
- [64] A. Sivardeen, D. Laughton, and J. S. Wolffsohn, "Randomized Crossover Trial of Silicone Hydrogel Presbyopic Contact Lenses," *Optometry and Vision Science*, vol. 93, no. 2, pp. 141–149, 2015.
- [65] K. Hayashi, M. Yoshida, A. Hirata, and K. Yoshimura, "Short-term outcomes of combined implantation of diffractive multifocal intraocular lenses with different addition power," *Acta Ophthalmologica*, vol. 93, no. 4, pp. e287–e293, 2015.
- [66] C. Dorrnsoro and S. Marcos, "Instrument for simulating multifocal ophthalmic corrections," pp. 1–25, 2010.
- [67] C. Dorrnsoro, A. Radhakrishnan, J. R. Alonso-Sanz, D. Pascual, M. Velasco-Ocana, P. Perez-Merino, and S. Marcos, "Portable simultaneous vision device to simulate multifocal corrections," *Optica*, vol. 3, no. 8, pp. 918–924, 2016.
- [68] C. Dorrnsoro and S. Marcos, "Miniaturized simultaneous vision simulator with mask generator," 2015.
- [69] 2Eyes Vision S.L., "SimVis," 2016. [Online]. Available: <http://www.2eyesvision.com/>
- [70] R. Tyson, *Principle of adaptive optics*, 3rd ed., CRC Press, Ed. Taylor & Francis Group, 2011.
- [71] D. R. Williams, "Imaging single cells in the living retina," *Vision Research*, vol. 51, pp. 1379–1396, 2011.

BIBLIOGRAPHY

- [72] P. Prieto, E. Fernández, S. Manzanera, and P. Artal, "Adaptive optics with a programmable phase modulator: applications in the human eye." *Optics Express*, vol. 12, no. 17, pp. 4059–4071, 2004.
- [73] "VOPTICA (Murcia, SPain)." [Online]. Available: <http://voptica.com/product/>
- [74] E. J. Fernández, I. Iglesias, and P. Artal, "Closed-loop adaptive optics in the human eye," *OPTICS LETTERS*, vol. 26, no. 10, pp. 746–748, 2001.
- [75] E. J. Fernández, S. Manzanera, P. Piers, and P. Artal, "Adaptive optics visual simulator," *Journal of Refractive Surgery*, vol. 18, no. September/October, pp. S634 – S638, 2002.
- [76] C. Otero, M. Vilaseca, M. Arjona, J. A. Martínez-Roda, and J. Pujol, "Repeatability of aberrometric measurements with a new instrument for vision analysis based on adaptive optics," *Journal of Refractive Surgery*, vol. 31, no. 3, pp. 188–194, 2015.
- [77] "VirtIOL: See the difference," 2014. [Online]. Available: <http://virtiol.wixsite.com/virtiol/technology>
- [78] A. Giner, M. Aldaba, M. Arjona, and J. Pujol, "On the evaluation of multifocal IOLs by means of a vision simulator," in *Proceedings of the VII European/I World Meeting in Visual and Physiological Optics VPOptics*, Wroclaw, 2014, pp. 98–101.
- [79] A. Giner, M. Aldaba, S. O. Luque, M. Borrat, M. Arjona, A. Salvador, and J. Pujol, "Analysis of the visual quality with multifocal intraocular lenses before surgery," in *ARVO 2015: annual meeting abstracts*. Denver: Investigative Ophthalmology & Visual Science, 2015, p. 2983.
- [80] ISO, "ISO 11979-2:2014 Ophthalmic implants – Intraocular lenses – Part 2: Optical properties and test methods," pp. 1–22, 2014.
- [81] F. Díaz-Doutón, A. Benito, J. Pujol, M. Arjona, J. L. Güell, and P. Artal, "Comparison of the retinal image quality with a Hartmann-Shack wavefront sensor and a double-pass instrument." *Investigative ophthalmology & visual science*, vol. 47, no. 4, pp. 1710–6, 4 2006.
- [82] M. Vilaseca, A. Padilla, J. C. Ondategui, M. Arjona, J. L. Güell, and J. Pujol, "Effect of laser in situ keratomileusis on vision analyzed using preoperative optical quality," *Journal of Cataract Refractive Surgery*, vol. 36, pp. 1945–1953, 2010.
- [83] L. N. Thibos, A. Bradley, and R. A. Applegate, "Accuracy and precision of objective refraction from wavefront aberrations," *Journal of Vision*, vol. 4, pp. 329–351, 2004.
- [84] T. Terwee, H. Weeber, M. van der Mooren, and P. Piers, "Visualization of the retinal image in an eye model with spherical and aspheric, diffractive, and refractive multifocal intraocular lenses." *Journal of refractive surgery (Thorofare, N.J. : 1995)*, vol. 24, no. 3, pp. 223–232, 3 2008.
- [85] American Air Force, "Military Standardization Report," American Air Force, Tech. Rep., 1959.

- [86] M. Inoue, T. Noda, T. Mihashi, K. Ohnuma, H. Bissen-Miyajima, and A. Hirakata, "Quality of image of grating target placed in model of human eye with corneal aberrations as observed through multifocal intraocular lenses." *American journal of ophthalmology*, vol. 151, no. 4, pp. 644–652, 4 2011.
- [87] F. Alba-Bueno, F. Vega, and M. S. Millán, "Design of a Test Bench for Intraocular Lens Optical Characterization," *Journal of Physics: Conference Series*, vol. 274, p. 012105, 1 2011.
- [88] —, "Energy balance in apodized diffractive multifocal intraocular lenses," *SPIE*, vol. 8011, pp. 80 119G–80 119G–10, 8 2011.
- [89] J. M. Artigas, J. L. Menezo, C. Peris, A. Felipe, and M. Díaz-Llopis, "Image quality with multifocal intraocular lenses and the effect of pupil size: comparison of refractive and hybrid refractive-diffractive designs." *Journal of cataract and refractive surgery*, vol. 33, no. 12, pp. 2111–7, 12 2007.
- [90] T. Kawamorita and H. Uozato, "Modulation transfer function and pupil size in multifocal and monofocal intraocular lenses in vitro." *Journal of cataract and refractive surgery*, vol. 31, no. 12, pp. 2379–85, 12 2005.
- [91] T. Kawamorita, H. Uozato, D. Aizawa, K. Kamiya, and K. Shimizu, "Optical Performance in ReZoom and Array Multifocal Intraocular Lenses In Vitro," *Journal of Refractive Surgery*, vol. 25, no. May, pp. 467–469, 2009.
- [92] TRIOPTICS GmbH, "OptiSpheric IOL." [Online]. Available: <http://www.trioptics.com/products/optical-test-instruments/optispheric/optispheric-iol/>
- [93] M. Soda and S. Yaguchi, "Effect of decentration on the optical performance in multifocal intraocular lenses," *Ophthalmologica*, vol. 227, no. 4, pp. 197–204, 2012.
- [94] M. Flamant, "Etude de la repartition de lumiere dans l'image retinienne d'une fente," *Rev. Opt.*, vol. 34, pp. 433–459, 1955.
- [95] J. Santamaría, P. Artal, and J. Bescos, "Determination of the point spread function of human eyes using a hybrid optic all-digital method," *Journal of the Optical Society of America. A, Optics, image science, and vision*, vol. 4, pp. 1109–1114, 1987.
- [96] P. Artal, I. Iglesias, N. López-Gil, and D. G. Green, "Double-pass measurements of the retinal-image quality with unequal entrance and exit pupil sizes and the reversibility of the eye's optical system." *Journal of the Optical Society of America. A, Optics, image science, and vision*, vol. 12, no. 10, pp. 2358–66, 10 1995.
- [97] C. E. García-Guerra, M. Aldaba, M. Arjona, and J. Pujol, "Binocular open-view system to perform estimations of aberrations and scattering in the human eye," *Applied optics*, vol. 54, no. 32, pp. 9504–9508, 2016.
- [98] M. Aldaba, M. Vilaseca, M. Arjona, and J. Pujol, "Age-related changes in accommodation measured with a double-pass system." *Ophthalmic & physiological optics : the journal of the British College of Ophthalmic Opticians (Optometrists)*, pp. 1–8, 3 2013.

BIBLIOGRAPHY

- [99] F. Sanàbria, F. Díaz-Doutòn, M. Aldaba, and J. Pujol, "Spherical refractive correction with an electro-optical liquid lens in a double-pass system," *Journal of the European Optical Society*, vol. 8, pp. 13 062–4, 2013.
- [100] F. Sanabria, M. Aldaba, F. Díaz-Doutón, C. E. García-Guerra, and J. Pujol, "Technical improvements applied to a double-pass setup for performance and cost optimization," *Optical Engineering*, vol. 53, no. 6, pp. 061 710–8, 2014.
- [101] M. Vilaseca, E. Peris, J. Pujol, R. Borrás, and M. Arjona, "Intra-and Intersession Repeatability of a Double-Pass Instrument," *Optometry and Vision Science*, vol. 87, no. 9, pp. 675–681, 2010.
- [102] Visiometrics (an Halma company), "HD Analyzer." [Online]. Available: <http://www.visiometrics.com/hd-analyzer/>
- [103] J. Gispets, M. Arjona, and J. Pujol, "Image quality in wearers of a center distance concentric design bifocal contact lens," *Ophthalmic Physiological Optics*, vol. 3, pp. 221–233, 2002.
- [104] J. Pujol, J. Gispets, and M. Arjona, "Optical performance in eyes wearing two multifocal contact lens designs," *Ophthalmic physiological optics*, vol. 23, pp. 347–360, 2003.
- [105] J. L. Alió, A. B. Plaza-Puche, J. Javaloy, and M. J. Ayala, "Comparison of the visual and intraocular optical performance of a refractive multifocal IOL with rotational asymmetry and an apodized diffractive multifocal IOL." *Journal of refractive surgery (Thorofare, N.J. : 1995)*, vol. 28, no. 2, pp. 100–5, 2 2012.
- [106] H. Lee, K. Lee, J. M. Ahn, E. K. Kim, B. Sgrignoli, and T. I. Kim, "Evaluation of optical quality parameters and ocular aberrations in multifocal intraocular lens implanted eyes," *Yonsei Medical Journal*, vol. 55, no. 5, pp. 1413–1420, 2014.
- [107] H. Zuluaga, S. O. Luque, M. Vilaseca, M. Arjona, J. Pujol, A. de la Torre, and T. Salvador, "Measurements of optical quality in multifocal intraocular lenses by means of a double-pass system," in *4th European Meeting in Visual Optics and Physiological Optics*, Creta, 2008.
- [108] P. M. Prieto, F. Vargas-Martín, S. Goelz, and P. Artal, "Analysis of the performance of the Hartmann–Shack sensor in the human eye," *Journal of the Optical Society of America A: Optics and Image Science, and Vision*, vol. 17, no. 8, pp. 1388–1398, 2000.
- [109] M. Aldaba, M. Vilaseca, F. Díaz-Doutón, M. Arjona, and J. Pujol, "Measuring the accommodative response with a double-pass system: comparison with the Hartmann-Shack technique." *Vision research*, vol. 62, pp. 26–34, 6 2012. [Online]. Available: <http://www.ncbi.nlm.nih.gov/pubmed/22487720>
- [110] L. N. Thibos, "Principles of Hartmann-Shack aberrometry," *OSA tops*, vol. 35, pp. 163–169, 2000.
- [111] J. Liang, B. Grimm, S. Goelz, and J. F. Bille, "Objective measurement of wave aberrations of the human eye with the use of a Hartmann-Shack wave-front sensor," *J. Opt. Soc. Am. A*, vol. 11, no. 7, pp. 1949–1957, 1994.

BIBLIOGRAPHY

- [112] C. Fedtke, K. Ehrmann, D. Falk, R. C. Bakaraju, and B. A. Holden, "The BHVI-EyeMapper: Peripheral Refraction and Aberration Profiles," *Optometry and Vision Science*, vol. 91, pp. 1199–1207, 2014.
- [113] Topcon Medical Instrument Inc, "KR-1W." [Online]. Available: <http://www.topconmedical.com/products/kr1w.htm>
- [114] S. Patel, M. Fakhry, and J. Alio, "Objective assessment of aberrations induced by multifocal contact lenses in vivo," *Contact lens and anterior eye*, vol. 28, no. 4, pp. 196–201, 2002.
- [115] J. L. Alió, A. B. Plaza-Puche, R. Montalban, and J. Javaloy, "Visual outcomes with a single-optic accommodating intraocular lens and a low-addition-power rotational asymmetric multifocal intraocular lens." *Journal of cataract and refractive surgery*, vol. 38, no. 6, pp. 978–85, 6 2012.
- [116] D. Ortiz, J. L. Alió, G. Bernabéu, and V. Pongo, "Optical performance of monofocal and multifocal intraocular lenses in the human eye," *Journal of Cataract and Refractive Surgery*, vol. 34, pp. 755–762, 2008.
- [117] Molebny, V. Vasyi, Dsc, Panagopoulou, I. Sophia, Bsc, V. Sergiy, Msc, Wakil, M. S. Youssef, and Pal, "Principles of Ray Tracing Aberrometry," *Journal of Refractive Surgery*, vol. 16, no. 5.
- [118] R. Navarro and E. Moreno-Barriuso, "Laser ray-tracing method for optical testing," *OPTICS LETTERS*, vol. 24, no. 14, pp. 951–953, 1999.
- [119] B. Vasudevan, M. Flores, and S. Gaib, "Objective and subjective visual performance of multifocal contact lenses: Pilot study," *Contact Lens and Anterior Eye*, vol. 37, no. 3, pp. 168–174, 2014.
- [120] A. Gasson and J. A. Morris, "Soft lens fitting characteristics," in *The contact lens manual*, 3rd ed., A. Gasson and Morris Judith A., Eds. London: Butterworth-Heinemann Elsevier, 2010, ch. 16, pp. 187–198.
- [121] J. J. Walline, K. O. Lorenz, and J. J. Nichols, "Long-term contact lens wear of children and teens." *Eye & contact lens*, vol. 39, no. 4, pp. 283–9, 7 2013. [Online]. Available: <http://www.ncbi.nlm.nih.gov/pubmed/23771010>
- [122] L. Sorbara, B. A. Holden, and R. Wong, "Centrally fitted versus upper lid-attached rigid gas permeable lenses, Part II: A comparison of the clinical performance," *International Contact Lens Clinical*, vol. 23, no. 96, pp. 121–127, 1996.
- [123] N. C. Strang, L. S. Gray, B. Winn, and J. R. Pugh, "Clinical evaluation of infrared autorefractors for use in contact lens over-refraction." *Contact lens & anterior eye : the journal of the British Contact Lens Association*, vol. 20, no. 4, pp. 137–42, 1 1997. [Online]. Available: <http://www.ncbi.nlm.nih.gov/pubmed/16303360>
- [124] J. Ruiz-Alcocer, D. Madrid-Costa, H. Radhakrishnan, T. Ferrer-Blasco, and R. Montés-Micó, "Changes in accommodation and ocular aberration with simultaneous vision multifocal contact lenses." *Eye & contact lens*, vol. 38, no. 5, pp. 288–94, 9 2012. [Online]. Available: <http://www.ncbi.nlm.nih.gov/pubmed/22878382>

BIBLIOGRAPHY

- [125] H. Bissen-Miyajima, K. Minami, M. Yoshino, M. Nishimura, and S. Oki, "Autorefracton after implantation of diffractive multifocal intraocular lenses." *Journal of cataract and refractive surgery*, vol. 36, no. 4, pp. 553–6, 4 2010. [Online]. Available: <http://www.ncbi.nlm.nih.gov/pubmed/20362844>
- [126] G. Muñoz, C. Albarrán-Diego, and H. F. Sakla, "Validity of autorefracton after cataract surgery with multifocal ReZoom intraocular lens implantation." *Journal of cataract and refractive surgery*, vol. 33, no. 9, pp. 1573–8, 9 2007. [Online]. Available: <http://www.ncbi.nlm.nih.gov/pubmed/17720072>
- [127] D. Madrid-Costa, S. García-Lázaro, C. Albarrán-Diego, T. Ferrer-Blasco, and R. Montés-Micó, "Visual performance of two simultaneous vision multifocal contact lenses." *Ophthalmic & physiological optics : the journal of the British College of Ophthalmic Opticians (Optometrists)*, vol. 33, no. 1, pp. 51–6, 1 2013. [Online]. Available: <http://www.ncbi.nlm.nih.gov/pubmed/23252854>
- [128] R. Legras, Y. Benard, and H. Rouger, "Through-focus visual performance measurements and predictions with multifocal contact lenses." *Vision research*, vol. 50, no. 12, pp. 1185–93, 6 2010. [Online]. Available: <http://www.ncbi.nlm.nih.gov/pubmed/20371368>
- [129] A. L. Sheppard and L. N. Davies, "Clinical evaluation of the Grand Seiko Auto Ref/Keratometer WAM-5500." *Ophthalmic & physiological optics : the journal of the British College of Ophthalmic Opticians (Optometrists)*, vol. 30, no. 2, pp. 143–51, 3 2010. [Online]. Available: <http://www.ncbi.nlm.nih.gov/pubmed/20444118>
- [130] E. a. Mallen, J. S. Wolffsohn, B. Gilmartin, and S. Tsujimura, "Clinical evaluation of the Shin-Nippon SRW-5000 autorefractor in adults." *Ophthalmic & physiological optics : the journal of the British College of Ophthalmic Opticians (Optometrists)*, vol. 21, no. 2, pp. 101–7, 3 2001. [Online]. Available: <http://www.ncbi.nlm.nih.gov/pubmed/11261343>
- [131] I. L. Bailey and J. E. Lovie, "New design principles for visual acuity letter charts," *American journal of optometry and physiological optics*, vol. 53, pp. 740–745, 1976.
- [132] L. N. Thibos, W. Wheeler, and D. Horner, "Power vectors: an application of Fourier analysis to the description and statistical analysis of refractive error," *Optometry and Vision Science*, vol. 74, no. 6, pp. 367–375, 1997.
- [133] J. M. Bland and D. G. Altman, "Statistical methods for assessing agreement between two methods of clinical measurement." *Lancet*, vol. 1, no. 8476, pp. 307–10, 2 1986. [Online]. Available: <http://www.ncbi.nlm.nih.gov/pubmed/2868172>
- [134] A. Giner, M. Aldaba, M. Arjona, and J. Pujol, "Evaluation of an auto-refractor for over-refraction with multifocal contact lenses patients," in *ARVO Annual Meeting Proceedings*, ARVO, Ed. Seattle: Investigative Ophthalmology & Visual Science, 2013, p. 5481.
- [135] A. Giner, M. Aldaba, M. Arjona, M. Vilaseca, and J. Pujol, "Assessment of multifocal contact lens over-refraction using an infrared, open-field autorefractor: A preliminary study," *Contact Lens and Anterior Eye*, vol. 38, no. 5, pp. 322–326, 2015.

- [136] J. L. Alió, A. B. Plaza-Puche, D. P. Piñero, F. Amparo, R. Jiménez, J. L. Rodríguez-Prats, J. Javaloy, and V. Pongo, "Optical analysis, reading performance, and quality-of-life evaluation after implantation of a diffractive multifocal intraocular lens." *Journal of cataract and refractive surgery*, vol. 37, no. 1, pp. 27–37, 1 2011. [Online]. Available: <http://www.ncbi.nlm.nih.gov/pubmed/21183097>
- [137] J. F. Alfonso, L. Fernández-Vega, J. I. Blázquez, and R. Montés-Micó, "Visual function comparison of 2 aspheric multifocal intraocular lenses," *Journal of Cataract and Refractive Surgery*, vol. 38, no. 2, pp. 242–248, 2012.
- [138] C. McAlinden and J. E. Moore, "Multifocal intraocular lens with a surface-embedded near section: Short-term clinical outcomes." *Journal of cataract and refractive surgery*, vol. 37, no. 3, pp. 441–5, 3 2011. [Online]. Available: <http://www.ncbi.nlm.nih.gov/pubmed/21333867>
- [139] M. Rosenfield and K. J. Ciuffreda, "Effect of surround propinquity on the open-loop accommodative response," *Investigative Ophthalmology and Visual Science*, vol. 32, no. 1, pp. 142–147, 1991.
- [140] H. Hofer, P. Artal, B. Singer, J. L. Aragón, and D. R. Williams, "Dynamics of the eye's wave aberration," *Journal of the Optical Society of America A: Optics and Image Science, and Vision*, vol. 18, no. 3, pp. 497–506, 2001. [Online]. Available: <https://www.scopus.com/inward/record.url?eid=2-s2.0-0035289737&partnerID=40&md5=59dabd90d13be2c53e419ce89463ad84>
- [141] ECELECS (European Committee for Electrotechnique Standardization), "IEC 60825-1:2014 Safety of Laser products. Part I: Equipment classification and requirements." pp. 1–47, 2014.
- [142] M. A. Van Dam, "System Performance Characterization," in *Adaptive optics for vision science: Principles, Practices, Design and Applications*, 1st ed., J. Porter, H. M. Queener, J. E. Lin, K. Thorn, and A. Awwal, Eds. John Wiley & Sons, Inc., 2006, ch. System Per, pp. 189–202.
- [143] L. Noethe, "Chapter 1: Active optics in modern large optical telescopes," in *Progress in Optics 43*, 1st ed., E. Wolf, Ed. New York, USA: University of Rochester, 2002, ch. Chapter 1, pp. 1–70.
- [144] J. F. Alfonso, *Lentes intraoculares bifocales, multifocales y acomodativas en cirugía del cristalino*, 1st ed., Sociedad Española de Cirugía Ocular Implantanto-Refractiva, Ed. MAC LINE, S.L., 2007.
- [145] A. Giner, M. Arjona, F. Díaz-Doutón, M. Aldaba, C. E. García-Guerra, F. Sanabria, and J. Pujol, "New compact open-field double-pass system with asymmetric focus," *Optica Pura y Aplicada*, 2018.
- [146] Unkown, "A drawing of a section through the human eye with a schematic enlargement of the retina." [Online]. Available: <http://webvision.med.utah.edu/book/part-i-foundations/simple-anatomy-of-the-retina/>
- [147] D. Williams, "Imaging single cells in the living retina," *Vision Research*, vol. 51, pp. 1379–1396, 2011.

BIBLIOGRAPHY

- [148] H. Helmholtz, "Beschreibung eines Augen-Spiegels zur Untersuchung der Netzhaut im lebenden Auge (Description of an eye mirror for the investigation of the retina of the living eye)," *A Förstner'sche Verlagsbuchhandlung*, 1851.
- [149] A. Roorda, F. Romero-Borja, I. Donnelly, H. Queener, T. Hebert, and M. Campbell, "Adaptive optics scanning laser ophthalmoscopy," *Optics Express*, vol. 10, no. 9, pp. 405–412, 2002.
- [150] D. R. Williams, "Visibility of interference fringes near the resolution limit," *J. Opt. Soc. Am. A*, vol. 2, no. 7, pp. 1087–1093, 1985.
- [151] ———, "Topography of the foveal cone mosaic in the living human eye," *Vision Research*, vol. 28, no. 3, pp. 433–454, 1988.
- [152] R. Webb, G. Hughes, and O. Pomerantzeff, "Flying spot TV ophthalmoscope," *Applied Optics*, vol. 19, pp. 2991–2997, 1980.
- [153] A. Fercher, C. Hitzenberger, W. Drexler, G. Kamp, and H. Sattmann, "In vivo optical coherence tomography," *American Journal of Ophthalmology*, vol. 116, no. 1, pp. 113–114, 1993.
- [154] S. A. Shroff, J. R. Fienup, and D. R. Williams, "Estimation of Phase Shifts in Structured Illumination for High Resolution Imaging."
- [155] W. Lotmar, "Apparatus for the measurement of retinal visual acuity by Moire fringes," *Investigative Ophthalmology and Visual Science*, vol. 19, no. 4, pp. 393–400, 1980.